Defense Nuclear Agency
Alexandria, VA 22310-3398

DNA-TR-94-83

Experimental Data for Use in Constructing Material Models for Calculations of High Speed Ejecta

William R. Seebaugh
Science/Engrg Associates, Inc.
P.O. Box 3722
Albuquerque, NM 87190-3722

June 1995

Technical Report

CONTRACT No. DNA 001-92-C-0040

Approved for public release;
distribution is unlimited.

DTIC QUALITY INSPECTED 5

19950616 056

Destroy this report when it is no longer needed. Do not return to sender.

PLEASE NOTIFY THE DEFENSE NUCLEAR AGENCY, ATTN: CSTI, 6801 TELEGRAPH ROAD, ALEXANDRIA, VA 22310-3398, IF YOUR ADDRESS IS INCORRECT, IF YOU WISH IT DELETED FROM THE DISTRIBUTION LIST, OR IF THE ADDRESSEE IS NO LONGER EMPLOYED BY YOUR ORGANIZATION.

DNA PRINTING PLANT

REPORT DOCUMENTATION PAGE

Form Approved
OMB No. 0704-0188

Public reporting burden of this collection of information is estimated to average 1 hour per response, including the time for reviewing instructions, searching existing data sources, gathering and maintaining the data needed, and completing and reviewing the collection of information. Send comments regarding this burden estimate or any other aspect of this collection of information, including suggestions for reducing this burden, to Washington Headquarters Services, Directorate for Information Operations and Reports, 1215 Jefferson Davis Highway, Suite 1204, Arlington, VA 22202-4302, and to the Office of Management and Budget, Paperwork Reduction Project (0704-0188), Washington, DC 20503.

1. AGENCY USE ONLY *(Leave Blank)*	2. REPORT DATE	3. REPORT TYPE AND DATES COVERED
	950601	Technical 920408 - 940807

4. TITLE AND SUBTITLE

Experimental Data for Use in Constructing Material Models for Calculations of High Speed Ejecta

5. FUNDING NUMBERS

C - DNA 001-92-C-0040
PE - 62715H
PR - AC
TA - BD
WU - DH322350

6. AUTHOR(S)

William R. Seebaugh

7. PERFORMING ORGANIZATION NAME(S) AND ADDRESS(ES)

Science/Engrg Associates, Inc.
P.O. Box 3722
Albuquerque, NM 87190-3722

8. PERFORMING ORGANIZATION REPORT NUMBER

9. SPONSORING / MONITORING AGENCY NAME(S) AND ADDRESS(ES)

Defense Nuclear Agency
6801 Telegraph Road
Alexandria, VA 22310-3398
SPWE/Byers

10. SPONSORING / MONITORING AGENCY REPORT NUMBER

DNA-TR-94-83

11. SUPPLEMENTARY NOTES

This work was sponsored by the Defense Nuclear Agency under RDT&E RMC Code B4662D AC BD 00020 4400A 25904D.

12a. DISTRIBUTION / AVAILABILITY STATEMENT

Approved for public release; distribution is unlimited.

12b. DISTRIBUTION CODE

13. ABSTRACT *(Maximum 200 words)*

This report addresses the development and application of experimental methods for characterizing the soil behavior during the shock loading and subsequent unloading accompanying cratering detonations. The program was initiated to understand the behavior of the multiphase effective stress pore-air material model when used to predict the velocities of high speed ejecta (crater material which is ejected with sufficient velocity to become entrained into the rising fireball/dust cloud or form long-range ballistic ejecta fragments). The experiments were fielded on events DISTANT IMAGE and MINOR UNCLE, conducted on native soil at the White Sands Missile Range, and events HUSKY JAGUAR 1 and 2, conducted on a test bed backfilled with Socorro plaster sand. A small scale simulation of the HUSKY JAGUAR 2 experiment was conducted in the DNA halfspace facility.

14. SUBJECT TERMS

MINOR UNCLE
HUSKY JAGUAR
DISTANT IMAGE
Ejecta
Dilatancy
Material Model
Pore Air

15. NUMBER OF PAGES

146

16. PRICE CODE

17. SECURITY CLASSIFICATION OF REPORT	18. SECURITY CLASSIFICATION OF THIS PAGE	19. SECURITY CLASSIFICATION OF ABSTRACT	20. LIMITATION OF ABSTRACT
UNCLASSIFIED	UNCLASSIFIED	UNCLASSIFIED	SAR

NSN 7540-01-280-5500
Standard Form 298 (Rev. 2-89)
Prescribed by ANSI Std. 239-18
298-102

CLASSIFIED BY:

N/A since Unclassified.

DECLASSIFY ON:

N/A since Unclassified.

PREFACE

This final report was prepared by Science and Engineering Associates, Inc. (SEA) in compliance with the requirements of Defense Nuclear Agency Contract DNA001-92-C-0040. This contract was a Phase II award under DNA's Small Business Innovation Research (SBIR) Program. The program was sponsored by the Shock Physics Directorate of DNA and was performed during the period 8 April 1992 through 7 August 1994. Dr. Charles R. Gallaway (SPWE) and LTC Mark E. Byers (SPWE) were the Contracting Officer's Technical Representatives for the sponsor. Their guidance and assistance throughout the work are greatly appreciated. The technical effort at SEA was performed by Dr. W. R. Seebaugh. Data collection for field events was conducted by Mr. K. A. Benson and other employees of the New Mexico Engineering Research Institute (NMERI) under a subcontract to SEA, Dr. R. W. Henny of Field Command DNA, and Dr. Seebaugh. Laboratory analyses were conducted by Mr. R. G. McKeen, P.E., and Mr. L. R. Lenke, P.E., of NMERI. The data from the halfspace experiment were acquired by Mr. P. Roupas of NMERI; the film analysis was performed by Mr. R. C. Bair of NMERI.

Accession For
NTIS GRA&I ☑
DTIC TAB ☐
Unannounced ☑
Justification
By
Distribution/
Availability Codes
Dist | Avail and/or Special
A-1

CONVERSION TABLE

Conversion factors for U.S. Customary to metric (SI) units of measurement.

MULTIPLY → / TO GET ←	BY → / BY ←	TO GET / DIVIDE
angstrom	1.000 000 X E -10	meters (m)
atmosphere (normal)	1.013 25 X E +2	kilo pascal (kPa)
bar	1.000 000 X E +2	kilo pascal (kPa)
barn	1.000 000 X E -28	meter^2 (m^2
degree (angle)	1.745 329 X E -2	radian (rad)
degree Fahrenheit	t_k = (t°f + 459.67)/1.8	degree kelvin (K)
electron volt	1.602 19 X E -19	joule (J)
erg	1.000 000 X E -7	joule (J)
erg/second	1.000 000 x E -7	watt (W)
foot	3.048 000 X E -1	meter (m)
foot-pound-force	1.355 818	joule (J)
gallon (U.S. liquid)	3.785 412 X E -3	meter3 (m3)
inch	2.540 000 X E -2	meter (m)
kilotons	4.183	terajoules
kip (1000 lbf)	4.448 222 X E +3	newton (N)
kip/inch^2 (ksi)	6.894 757 X E +3	kilo pascal (kPa)
micron	1.000 000 X E -6	meter (m)
mil	2.540 000 X E -5	meter (m)
mile (international)	1.609 344 X E +3	meter (m)
ounce	2.834 952 X E -2	kilogram (kg)
pound-force (lbs avoirdupois)	4.448 222	newton (N)
pound-force inch	1.129 848 X E -1	newton-meter (N◊m)
pound-force/inch	1.751 268 X E +2	newton/meter (N/m)
pound-force/foot^2	4.788 026 X E -2	kilo pascal (kPa)
pound-force/inch^2 (psi)	6.894 757	kilo pascal (kPa)
pound-mass (lbm avoirdupois)	4.535 924 X E -1	kilogram (kg)
pound-mass/foot^3	1.601 846 X E +1	kilogram/meter^3 (kg/m^3)
slug	1.459 390 X E +1	kilogram (kg)
torr (mm Kg, 0° C)	1.333 22 X E -1	kilo pascal (kPa)

TABLE OF CONTENTS

TABLE OF CONTENTS (Continued)

FIGURES

FIGURES (Continued)

FIGURES (Continued)

FIGURES (Continued)

TABLES

TABLES

SECTION 1

INTRODUCTION

The primary technical objectives of the Phase II SBIR research program described in this report were to develop experimental methods for characterizing the soil behavior during the shock loading and subsequent unloading accompanying cratering detonations, to understand the behavior of the pore air and pore water during loading and unloading, and to provide an experimental data base for use in formulating and validating material property models for soils with relatively lower water content. A secondary objective was to increase the understanding of the soil conditions that form high speed ejecta (crater material which is ejected with sufficient velocity to become entrained into the rising fireball/ dust cloud or form long-range ballistic ejecta fragments).

1.1 MODELING ISSUES.

The Phase I program (Seebaugh 1991) investigated the experimental and theoretical bases for the multiphase effective stress pore-air material model (Koik 1988, Schuster 1989, and Koik, Schuster, and Hassig 1990), with emphasis placed on the ability of the model to predict the velocities of the high speed ejecta. The multiphase effective stress model was developed by California Research & Technology (CRT) for use in the California Research Arbitrary Lagrangian Eulerian two-dimensional finite difference code (CRALE2). Following the large yield high-explosive events MINOR SCALE and MISTY PICTURE it was clear that existing material models severely underestimated the experimentally observed ejection velocities. Several material models were developed to include the expansion effects of pore air in attempts to increase the calculated ejection velocities. The last of these was the multiphase effective stress model which provided the pneumatic push needed to increase the calculated velocities to the experimentally observed levels.

As discussed in detail by Seebaugh 1991, Lee (1989) challenged the conclusion that the release of pore air upon unloading could actually produce the calculated ejection velocities and further suggested that material expansion due to dilatancy could produce a similar result. CRT implemented a dilatancy model using a simple associated flow rule for dilatant behavior. This model produced essentially identical ejection velocities as the multiphase effective stress model; however, unlimited dilation occurred in some other regions of the crater. The modeling effort for MINOR SCALE and MISTY PICTURE was terminated at this point.

A review of the physics incorporated in the multiphase effective stress model was completed during the Phase I program (Seebaugh 1991). In this model the pore air was assumed to take up part of the applied load as the soil was compressed by the shock wave; upon unloading, the expansion of the highly compressed pore air caused the soil to expand greatly at low pressures. The evaluation of the physical principles used in the multiphase effective stress and dilatancy models culminated in a meeting (held in April 1991) between the author and representatives of the organization supporting each model to examine the physical bases for the models.

The majority of the meeting participants concluded that the multiphase effective stress model used incorrect physics and should be rejected. A major problem

with this model occurs at volume strains approaching soil lockup. The pore air pressure becomes so high that the air takes most of the load, leaving the soil skeleton essentially unloaded. This behavior near lockup is not physically correct. Two participants at the meeting asserted that a proper multiphase model would include three phases--the soil skeleton, pore air, and pore water. For some so-called dry soils, there is sufficient pore water in the soil to dissolve all of the pore air, resulting in saturation of the soil at lockup (the MINOR SCALE/MISTY PICTURE soil had a pore water content of about 8%).

The participants in the April 1991 meeting concluded that the dilatancy model using a simple associated flow rule was probably not sufficient since it allowed unlimited dilation to occur under certain unloading paths. Some control must be placed on this behavior. All of the meeting participants agreed that the MINOR SCALE/MISTY PICTURE soil exhibits dilatant behavior that must be properly modeled. There was a general consensus that both pore air and dilatancy effects occur in the MINOR SCALE/MISTY PICTURE soil in various regions and time regimes. The majority of the participants in the discussions concluded that the multiphase effective stress model should not be used in combination with the dilatancy model, but that a physically correct pore air model should be developed (an earlier pore air model in which the pore air is simply compressed during loading and allowed to expand during unloading, without the multiphase effective stress features, was endorsed).

Related work using the multiphase effective stress model was performed by CRT for the field events MIDNIGHT HOUR 2, HUSKY JAGUAR 1, and HUSKY JAGUAR 2. The purpose of these events was to evaluate the calculational methodology used to predict down-axis free-field ground shock and motion fields in the presence of strong surface rarefaction effects. The test bed for each of these experiments was Socorro plaster sand, a dry porous soil prepared to a water content of about 4%. The use of the multiphase effective stress model for these events was justified by improvements in predictions (versus experiment) of late time motions beneath the charge for event MIDNIGHT HOUR 2 when the material model was changed from one with no pore air effects to the full multiphase effective stress model. Models with intermediate pore air participation in the material behavior (as evaluated for MINOR SCALE and MISTY PICTURE) were apparently not considered. Socorro plaster sand is currently being used as a backfill medium for a number of test programs including additional events in the HUSKY JAGUAR series and the DIPOLE EAST Conventional Weapons Test Program. The multiphase effective stress model is used for Socorro plaster sand by CRT, who is the calculational contractor for these programs. It is important that a validated model be used for this backfill material; otherwise, some of the benefits of using a test bed material with known and reproducible properties may be lost. Sufficient data should be available from the HUSKY JAGUAR 1 and 2 events to test the modeling approach for various regions of the crater (ejecta region, crater lip region, and down axis region).

Related work using the small-strain/displacement finite element code SABRE for ground motion calculations for event MISERS GOLD was also performed by CRT (England *et al.* 1991). This work compared results calculated using four material models (non-dilatant, associated flow rule (fully dilatant), 40% dilatant, and 80% dilatant) to experimental ground motion data near the crater edge. Both the vertical and horizontal direct induced velocities were extremely sensitive to the dilatancy model, with factors of 5-10 differences in peak velocity between the non-dilatant (lowest velocity) and the 80% dilatant (highest velocity) models. The 40% dilatant flow model provided the best overall match to the

data, but no single model produced a good fit to all of the measurements. Late time crater related displacements also increased with dilatancy (same factor of 5-10), with 80% dilatancy giving the best comparisons to experimental data for the first several hundred milliseconds. None of the calculated later time motions continued as long as the measurements. The authors concluded that the lack of pore air effects in the model could be responsible for this result. Post-test calculations for event DISTANT IMAGE, which was conducted at the same site after backfilling the MISERS GOLD crater, required greater dilatancy than the pre-test calculations to obtain the proper direct-induced ground shock intensity (England and Choi (1993).

1.2 EXPERIMENTAL APPROACH.

The experimental program described in this report addressed the issue of soil behavior during the loading and subsequent unloading for two dry porous soils: (1) the native soil at the MINOR SCALE/MISTY PICTURE/MISERS GOLD site at the DNA Permanent High Explosive Test Site (PHETS), located in the northern region of the White Sands Missile Range, New Mexico (WSMR) and (2) Socorro plaster sand, a soil used for prepared test beds at the Phenomenology Test Bed (PTB) of PHETS. The explosive loading for the WSMR/PHETS soil was provided by two large high-explosive detonations, events DISTANT IMAGE and MINOR UNCLE. Socorro plaster sand was used as the test bed soil for two smaller field events, HUSKY JAGUAR 1 and HUSKY JAGUAR 2, and for a laboratory halfspace simulation of HUSKY JAGUAR 2.

Soil samples were collected pre- and post-test for the four field events. Three types of soil samples were collected for events DISTANT IMAGE and MINOR UNCLE: (1) the pre-test soil, (2) natural ejecta fragments which impacted at distances from the crater lip to the maximum ejecta range, and (3) soil contained in sealed aluminum cans emplaced pre-test at known locations in the test bed and collected post-test (event DISTANT IMAGE only). Two types of soil samples were collected for events HUSKY JAGUAR 1 and HUSKY JAGUAR 2: (1) the pre-test soil and (2) the soil contained in sealed aluminum cans emplaced pre-test at known locations in the test bed and recovered post-test (event HUSKY JAGUAR 1 only). The water content of each sample was determined in the field immediately following the sample collection activities. Dry densities were obtained by the immersion method after coating the samples with a sealant.

Laboratory tests performed on the pre-test WSMR/PHETS soil included hydrostatic compression with measurement of pore pressure as a function of applied stress, particle size distribution, specific gravity, and suction-water content relationship. Particle size distributions and specific gravities were also obtained for the post-test samples taken from the cans. Descriptions of the soil samples and the results of the laboratory tests for events DISTANT IMAGE and MINOR UNCLE are given in Section 2. The impact locations of the cans and other artificial ejecta implants are also discussed in Section 2.

Laboratory tests performed on the pre-test Socorro plaster sand included particle size distribution and specific gravity (HUSKY JAGUAR 1 only). Descriptions of the soil samples and the results of the laboratory tests are given in Section 3. Also discussed in Section 3 are the results of in-flight ejecta photography and the impact locations of various artificial ejecta implants.

The basic approach taken to evaluate the multiphase effective stress pore-air model was to subject samples of soil with known initial properties to compressive loading and subsequent unloading in the field test environment and in the

laboratory, to determine changes in properties that occurred during the loading/unloading process, and to compare the observed changes to those that would occur if the soil behaved as dictated by the model. The primary indicator of the material response was the degree of soil grain fracture that occurred during the various compression events. In the multiphase effective stress model, the individual soil grains must be fractured to reduce the residual air void volume to the small values consistent with the high pressures reached by the compressed pore air occupying that residual volume. The implications of the results of the experimental program for the multiphase effective stress model are discussed in Section 4. Additional laboratory testing coupled with cratering code calculations to aid in modeling the behavior of dilatant soils for strain paths related to high speed ejecta is also discussed in Section 4.

A scaled HUSKY JAGUAR 2 experiment was conducted in the halfspace facility (Roupas 1987 and 1988, Bair 1988). One of the ejecta experiments fielded on HUSKY JAGUAR 2 was also performed on the halfspace test using scaled artificial ejecta implants emplaced at scaled ranges in the test bed. The ejection velocities for both experiments were measured using high speed and high resolution photography. The results of the experiments are compared to pre-test predictions in Section 3 (full scale) and Section 5 (halfspace).

Overall conclusions and recommendations are given in Sections 6 and 7, respectively.

SECTION 2

EXPERIMENTAL PROGRAM FOR WSMR/PHETS SOIL

Laboratory tests of many materials indicate that the minimum porosities of dry granular soils are seldom below 20 percent, even under compressive stresses exceeding a kilobar (Lambe and Whitman 1969). Near-zero porosities during the loading process are inferred from the multiphase effective stress pore-air model. The major permanent result of this type of compression process is the fracturing of soil grains. An experimental program was fielded on the DISTANT IMAGE and MINOR UNCLE events to determine if significant soil grain fracture occurred in the soil ejected from the craters during these events. As detailed below, this was accomplished by inferring the soil behavior by comparing properties of four types of soil samples: pre-test control samples taken from the predicted region of maximum ejection velocity, post-test samples from soil filled cans emplaced pre-test in the test bed, pre-test samples compressed mechanically in a soils laboratory, and post-test samples of actual long-range ejecta fragments.

2.1 EXPERIMENTAL PROGRAM.

2.1.1 Event DISTANT IMAGE.

The test bed for DISTANT IMAGE was reconstituted by backfilling the crater from the MISERS GOLD event. The charge was a 35-ft (11 m) radius fiberglass hemisphere placed on the ground surface and filled with 2650 tons (2.4×10^6 kg) of ammonium nitrate and fuel oil (ANFO) in bulk form. DISTANT IMAGE was executed on 20 June 1991.

For all of the prior events at the WSMR/PHETS site, numerous discrete clumps of soil (hereinafter called natural ejecta fragments) were found post-test dispersed around the craters. The natural ejecta fragments that impacted at significant ranges constituted the ballistic ejecta portion of the high speed ejecta (Seebaugh 1987). Part of the post-test data recovery plan for DISTANT IMAGE was the collection of a selection of these ejecta fragments. This included limited sample analysis in the field for water content, which was determined prior to transportation and storage of the samples.

Research on instrumentation that could be used to supplement the basic soil property measurements for the DISTANT IMAGE event was conducted. Passive volumetric strain cans, which consisted of aluminum cans packed with soil at the *in situ* soil density and water content, were previously employed in some HEST test configurations by NMERI (Bell, Jarpe, and Aguilar 1988). It appeared that these cans could also serve as artificial ejecta implants which would subject soil samples from known locations to high shock stresses with the potential of recovery and post-test examination of the soil samples. This would eliminate the difficulty with natural ejecta fragments of inferring the pre-test location. These passive volumetric strain cans were implanted pre-test in the DISTANT IMAGE test bed.

NMERI conducted an extensive artificial ejecta implant program on DISTANT IMAGE (Benson and Henny 1992). The implants consisted of numbered aluminum cubes and disks, numbered concrete spheres, and a linear array of adobe bricks containing colored tracers. The positions of the individual implants were surveyed pre- and post-test to define crater profiles.

2.1.1.1 Pre-Test Activities. The pre-test soil samples were collected in two phases. Seven samples were obtained from the area to be occupied by the charge during the first phase (mid-February 1991). Near surface samples were obtained at 10, 20, and 25 ft (3, 6, and 8 m) from surface ground zero (SGZ) and to depths of about 6.5 ft (2 m) at the two larger ranges. The water content and dry density were determined for each sample except that nearest SGZ.

The second phase of pre-test data collection was accomplished during late April 1991, coincident with placement of the artificial ejecta in a trench excavated along a radial from the charge center. The samples were collected from the trench at ranges of 50, 60, 75, 105, and 150 ft (15, 18, 23, 32, and 46 m). Three samples were obtained at each range at depths of 1.5, 3.0, 4.5, and 6.0 ft (0.5, 0.9, 1.4, and 1.8 m), the first for determination of water content, the second for determination of dry density, and the third to be stored for later analysis. Surface measurements of water content and dry density were obtained using a nuclear densitometer. Attempts were also made to use this instrument within the trench; however, problems occurred because of the gypsum content of the soil. During the second phase 18 volumetric strain cans were emplaced in the trench as backfilling progressed from the bottom of the trench. The cans were filled with soil from the test bed which was compacted to a wet density of about 120 lb/ft^3 (1.92 g/cm^3).

2.1.1.2 Post-Test Activities. The initial post-test activities occurred on test day and began about 15 min after the test. The first activity was to block access to the ejecta radial to prevent destruction of natural and artificial ejecta by vehicular traffic. A brief reconnaissance of the ejecta field was then carried out. Sample collection began immediately thereafter (about 30 min after the test) in order to secure the water content samples before significant desiccation of the natural ejecta had occurred.

About 40 natural ejecta fragments were identified at ranges from just below the crater lip crest to about 2,460 ft (750 m) from SGZ. Four samples were collected from each fragment, one sample for determining water content (all fragments were visibly moist internally), two clumps for determining dry density (weighed and coated with a sealant on the test bed), and a bag of loose soil and clumps. The location of each sample collection activity was flagged for later survey, and photographs of the impact craters were obtained for the seven longest-range fragments.

The interiors of some of the natural ejecta fragments, including one composed of highly fractured rock recovered on the outer crater lip, were hot when the fragments were broken open. These fragments also released some water vapor, which condensed and then immediately dissipated.

Documentary photographs of all natural ejecta fragments collected on DISTANT IMAGE were taken in preparation for cutting samples from the fragments for detailed laboratory analysis. Several soil samples were sectioned for examination in an environmental scanning electron microscope.

Eight of the volumetric strain cans were recovered intact. Fragments of five additional cans which contained soil were also recovered. Additional artificial ejecta implants (part of NMERI's routine passive ejecta experiment) were recovered during the process of searching for suitable natural ejecta fragments. These implants were used to determine the actual contours of the ejected zone (Benson and Henny 1992).

2.1.2 Event MINOR UNCLE.

The test bed for MINOR UNCLE was reconstituted by backfilling the crater from the DISTANT IMAGE event. The MINOR UNCLE charge was a 35-ft (11 m) radius fiberglass hemisphere placed on the ground surface and filled with 2431 tons (2.2×10^6 kg) of ammonium nitrate and fuel oil (ANFO) in bulk form. The MINOR UNCLE event was executed on 10 June 1993.

The implants normally used on large field events are 2-in (5-cm) aluminum cubes. It is well known that the acoustic impedance of aluminum is much higher (by a factor of 8 to 12) than that of the test bed soil. The mismatch in acoustic impedance of an object surrounded by soil can affect the motion of the object relative to the soil. It was of interest to compare the impact ranges of implants with acoustic impedance more nearly matching that of the soil to the impact ranges of the aluminum cubes. Properties of a number of materials were compared with those of the test bed soil. The best match was an acetal plastic called Delrin which had an acoustic impedance 1.2-1.9 times that of the soil. This material was easily cut into cubes and appeared to be sufficiently strong to survive the process of ejection from the developing crater.

Both aluminum and plastic cubes were used as artificial ejecta implants on MINOR UNCLE. Other implants were fielded by NMERI. Natural ejecta fragments were also recovered on the MINOR UNCLE event.

2.1.2.1 Pre-Test Activities. Pre-test soil samples were collected from the bottom of a 2.5-ft (0.75-m) deep trench which was excavated along a radial from the edge of the charge to a range beyond the expected crater lip radius for installation of the artificial ejecta implants. Two soil samples for water content determination, several clumps of soil for dry density determination, and a bag of soil for laboratory testing were obtained at ranges of 38, 50, 60, 75, 90, 105, and 118 ft (12, 15, 18, 23, 27, 32, and 36 m).

The overall artificial ejecta implant program for MINOR UNCLE was substantially less ambitious than that fielded on DISTANT IMAGE. Two ejecta implant arrays were installed in the trench from just outside the charge to the expected crater lip radius. Seventy-nine 2-in (5-cm) aluminum cubes were placed at 1-ft (0.3-m) range intervals from 40 to 118 ft (12 to 36 m) at the 2.5-ft (0.75-m) depth below the test bed surface. Ten 2-in (5-cm) plastic cubes were placed at 5-ft (1.5-m) range intervals from 43 to 88 ft (13 to 27 m) at the same depth as the aluminum cubes. NMERI implanted numbered concrete spheres (metal fiber reinforced) and an array of rocks painted to identify their initial locations. The volumetric strain cans were not used on MINOR UNCLE.

2.1.2.2 Post-Test Activities. The initial post-test activities occurred on test day and began about 30 min after the test. Thirty seven natural ejecta fragments were identified at ranges from just below the crater lip crest to about 3,180 ft (970 m) from SGZ. Three samples were collected from each fragment, one sample for determining water content, one clump for determining dry density, and a bag of loose/clumped soil. The location of each natural ejecta fragment was flagged for later survey, and photographs of the fragments and their impact craters were obtained.

The aluminum and plastic cubes were recovered and their impact locations surveyed following the MINOR UNCLE event. Ninety percent of the plastic cubes and 84 percent of the aluminum cubes were recovered.

2.2 TEST BED SOIL CHARACTERIZATION.

Eight events have been conducted in the natural soil of interest at WSMR/PHETS; these are listed in Table 2-1. DIRECT COURSE was an air burst; the remaining events were cratering bursts. MINI-SCALE 1 and 2 were calibration events. MINOR SCALE and MISTY PICTURE were essentially identical events, except that MINOR SCALE was conducted at the same SGZ as DIRECT COURSE. The test bed in the vicinity of the GZ for MINOR SCALE was modified by the DIRECT COURSE event itself and site restoration activities following that event. DISTANT IMAGE was conducted at the same GZ as MISERS GOLD in a reconstituted test bed. DISTANT IMAGE was followed by MINOR UNCLE at the same GZ.

Table 2-1. Events conducted at WSMR/PHETS.

Event	Explosive(1) (tons ANFO)	Charge Configuration	Comment
DIRECT COURSE	600	CG 166 FT ABOVE SGZ	UNDISTURBED GZ
MINI-SCALE 1	22.6	SURFACE HEMISPHERE	UNDISTURBED GZ
MINI-SCALE 2(2)	22.8	SURFACE HEMISPHERE	MINI-SC. 1 GZ
MINOR SCALE(3)	4744	SURFACE HEMISPHERE	DIR. COURSE GZ
MISTY PICTURE	4685	SURFACE HEMISPHERE	UNDISTURBED GZ
MISERS GOLD	2445	SURFACE HEMISPHERE	UNDISTURBED GZ
DISTANT IMAGE(2)	2650	SURFACE HEMISPHERE	MISERS GOLD GZ
MINOR UNCLE (2)	2431	SURFACE HEMISPHERE	MISERS GOLD GZ

(1) Ammonium nitrate and fuel oil.
(2) Test bed reconstituted following prior event at same GZ.
(3) Surface layer modified by pre-test operations.

Much of the available soil data for the events listed above was obtained using samples collected prior to DIRECT COURSE (Phillips 1986). The measured profiles were used to derive a generalized geologic profile for MINOR SCALE cratering calculations (Phillips 1985). The properties for this profile are given in Table 2-2.

The DIRECT COURSE event itself, backfilling of the compression crater formed by DIRECT COURSE, and preparations for the MINOR SCALE event modified the soil properties under and near the 44-ft (13-m) radius ANFO charge used in MINOR SCALE. It has been estimated that the soil was compacted to a depth of up to 13 ft (4 m) out to a range of about 100 ft (30 m) (Koik and Schuster 1987). The data for the soil layer labeled C-1A in Table 2-2 give the least dense and most dense conditions for this layer (see footnote to Table 2-2).

Table 2-2. Generalized DIRECT COURSE geologic profile, seismic velocity, and composition property estimates for use in MINOR SCALE cratering and ejecta calculations.

Layer	Depth to Bottom of Layer, m	Water Content w, %	Wet Density γ, g/cm^3	Dry Density γ_d, g/cm^3	Specific Gravity G_s	Air Voids Content V_a, %	Shear Wave Velocity V_s, m/s	Compr. Wave Velocity V_p, m/s
C-1	4	7.5	1.630	1.515	2.82	35.6	400	700
C-1A LD*	4	7.5	1.630	1.515	2.82	35.6	400	700
C-1A MD*	4	7.5	1.990	1.850	2.82	20.5	500	850
C-2	10	9.3	1.705	1.860	2.84	30.6	500	900
C-3	18	13.6	1.710	1.505	2.78	25.4	650	1300
C-4	51	11.9	1.900	1.700	2.72	17.3	500	900
C-5	78	7.4	1.810	1.685	2.71	25.4	500	750
C-6	>78	22.5	2.065	1.685	2.71	0.0	550	2050

*LD and MD indicate the values corresponding to the least dense and most dense conditions, respectively, for the fill material.

Similar compaction occurred prior to MISERS GOLD, which was conducted on native soil, and the subsequent events DISTANT IMAGE and MINOR UNCLE, which were conducted on a successively reconstituted test bed at the same GZ. Before events DISTANT IMAGE and MINOR UNCLE the crater from each previous event was backfilled in lifts with the soil excavated during the previous event. Additional soil was scraped from borrow pits near the GZ and added, as required, to bring the test bed surface to the desired height. For both events, the strata present in the undisturbed native soil at PHETS were completely missing in the reconstituted test beds. Additional compaction of the surface layers occurred as a result of the vehicular traffic and the frequent application of water to control blowing dust during charge construction.

The properties of the pre-test soil samples for DISTANT IMAGE are given in Table 2-3. The properties determined with the nuclear densitometer were used for the surface point at each range; the values from the excavated soil samples were used for the points below the surface. As indicated in Section 2.1.1.1, samples were obtained at several depths below the test bed surface for this event.

The pre-test soil properties for MINOR UNCLE are given in Table 2-4 (the measurements are described in detail in Appendix A). All of the pre-test soil samples for this event were obtained at the same depth below the test bed surface.

The longest-range and therefore highest-velocity ejecta fragments originated in the top meter of soil (scaled to the DISTANT IMAGE yield) for the cratering events listed in Table 2-1. As indicated above, this layer was compacted by pre-test operations. The three soil parameters of primary interest for this soil layer are the wet density, water content, and air voids content or air porosity (the definitions of these and other standard soil parameters are given in Table 2-5, abstracted from Lambe and Whitman 1969).

Table 2-6 compares the pre-test soil properties for the compacted surface layer for four of the five large cratering events (no data were available for MISTY PICTURE). The DISTANT IMAGE data for the 150-ft (45.73-m) range were obtained in compacted natural soil and not in the reconstituted portion of the test bed (this range was beyond the crater lip crest for MISERS GOLD, which was conducted at the same GZ).

The specific gravity of the soil grains and the water content of the soil affect the air voids content (Table 2-5), with air voids content increasing with increasing specific gravity and decreasing water content. Table 2-6 includes two values of the specific gravity for DISTANT IMAGE and MINOR UNCLE: the value reported by Zelasko (1991) for DISTANT IMAGE (2.725) and the values obtained by NMERI (Appendix A) for DISTANT IMAGE and MINOR UNCLE (2.646 and 2.603, respectively). England and Choi (1993) used the specific gravity given by Zelasko (1991) for DISTANT IMAGE calculations.

Except for the significantly higher water content and its effect on the wet density, the mean properties for MISERS GOLD are very close to those for MINOR SCALE layer C-1A LD. England, *et al.* (1991) used the standard deviations given in Table 2-6 for MISERS GOLD in sensitivity studies. The values for DISTANT IMAGE for the region beyond the reconstituted portion of the test bed fall within the range of properties for MINOR SCALE and MISTY PICTURE.

The contrasts between the properties for MINOR SCALE and MISERS GOLD and those obtained for the reconstituted test beds for DISTANT IMAGE and MINOR UNCLE are

Table 2-3. DISTANT IMAGE soil property measurements.

Sample Number	Range From SGZ, m	Depth to Sample, m	Water Content w, %	Wet Density γ, g/cm^3	Dry Density γ_d, g/cm^3	Notes
1A	3.05	0.51	11.5			1
2A	6.10	0-0.51	11.0	1.859	1.675	2
3A	6.10	0.76-1.42	11.7	1.867	1.671	2
4A	6.10	1.42-1.93	10.3	2.068	1.875	2
5A	7.62	0-0.66	10.5	2.021	1.829	2
6A	7.62	0.66-1.40	12.8	1.818	1.612	2
7A	7.62	1.40-2.03	9.7	1.695	1.545	2
Surface	15.24	0	7.0	1.977	1.848	3
1	15.85	0.46	9.7	1.913	1.744	4
2	15.85	0.91	8.8	2.080	1.912	4
3	15.85	1.37	11.0	2.222	2.002	4
4	15.85	1.83	6.8	2.090	1.957	4
Surface	18.29	0	6.5	2.072	1.946	3
5	18.29	0.46	9.8	2.106	1.918	4
6	18.29	0.91	7.7	2.122	1.970	4
7	18.29	1.37	6.4	2.160	2.030	4
8	18.29	1.83	8.3	2.164	1.998	4
Surface	22.87	0	5.8	2.074	1.960	3
9	22.87	0.46	9.5	2.060	1.881	4
10	22.87	0.91	9.9	1.997	1.817	4
11	22.87	1.37	9.2	1.989	1.821	4
12	22.87	1.83	8.6	2.123	1.955	4

(1) Taken off auger bit into can.
(2) Taken from core tube in auger; moisture values from can samples; dry density from tube sample.
(3) Nuclear densitometer readings.
(4) Moisture values from can samples; dry densities from soil clump.

Table 2-3. DISTANT IMAGE soil property measurements (Continued).

Sample Number	Range From SGZ, m	Depth to Sample, m	Water Content w, %	Wet Density γ, g/cm^3	Dry Density γ_d, g/cm^3	Notes
Surface	32.01	0	6.2	2.053	1.933	3
13	32.01	0.46	10.2	2.139	1.941	4
14	32.01	0.91	9.3	1.977	1.809	4
15	32.01	1.37	9.0	2.189	2.008	4
16	32.01	1.83	8.2	2.155	1.992	4
Surface	45.73	0	6.5	1.878	1.763	3
17	45.73	0.46	7.1	1.806	1.686	4
18	45.73	0.91	6.1	1.808	1.704	4
19	45.73	1.37	8.9	1.868	1.715	4
20	45.73	1.83	6.5	1.677	1.575	4

(3) Nuclear densitometer readings.
(4) Moisture values from can samples; dry densities from soil clump.

Table 2-4. MINOR UNCLE soil property measurements.

Sample Number	Range From SGZ, m	Depth to Sample, m	Water Content w, %	Wet Density γ, g/cm^3	Dry Density γ_d, g/cm^3
38	11.6	0.75	14	2.09	1.83
38	11.6	0.75	13	2.12	1.88
38	11.6	0.75	12	2.11	1.88
50	15.2	0.75	12	2.02	1.80
50	15.2	0.75	9	1.92	1.76
50	15.2	0.75	13	2.02	1.79
50	18.3	0.75	9	1.91	1.75
60	18.3	0.75	9	1.93	1.77
60	18.3	0.75	9	2.01	1.84
75	22.9	0.75	7	1.99	1.86
75	22.9	0.75	12	2.09	1.87
90	27.4	0.75	12	2.08	1.86
90	27.4	0.75	9	1.96	1.80
90	27.4	0.75	10	2.04	1.85
105	32.0	0.75	11	1.93	1.74
105	32.0	0.75	11	2.03	1.83
105	32.0	0.75	11	1.94	1.75
118	36.0	0.75	8	1.92	1.81
118	36.0	0.75	12	1.99	1.78
118	36.0	0.75	14	2.05	1.80

Table 2-5. Relationships between soil parameters.

DEFINITIONS:

V = Total volume of soil element
V_S = Volume of solid mineral particles
V_V = Volume of voids
V_W = Volume of pore water
V_g = Volume of gas (air)
W = Total weight of soil element
W_S = Weight of solid mineral particles
W_W = Weight of water
W_g = Weight of gas (air)--negligible

Total Unit Weight	$\gamma = W/V$
Dry unit weight (dry density)	$\gamma_d = W_S/V$
Water Content (expressed in %)	$w = W_W/W_S$
Porosity	$n = V_V/V$
Specific Gravity	$G_S = W_S/V_S/\gamma_o$

(where γ_o = Unit Weight of Water at 4°C)

Air Voids Content (expressed in %)	$V_a = V_g/V$

(note does not equal porosity)

RELATIONSHIPS BETWEEN QUANTITIES:

$V = V_S + V_V = V_S + V_W + V_g$

$W = W_S + W_W$

$n = 1 - \gamma_d/G_S\gamma_o$

$V_a = n - w\gamma_d$ (expressed in %)

Table 2-6. Comparison of soil properties for MINOR SCALE, MISERS GOLD, DISTANT IMAGE, and MINOR UNCLE.

Event	Range From SGZ, m	Top and Bottom of Layer, m	Water Content w, %	Wet Density γ, g/cm^3	Dry Density γ_d, g/cm^3	Specific Gravity G_s	Air Voids Content V_a, %	Notes
MINOR SCALE	All	0-4 (C-1A LD)	7.5	1.630	1.515	2.82(1)	36	
	All	0-4 (C-1A MD)	7.5	1.990	1.850	2.82(1)	20	
MISERS GOLD	All	0-2.3	14.6±6.3	1.73±0.11	1.51±0.13	2.75(2)	23±7	
DISTANT IMAGE	15.24-32.01	0-1	8.4	2.049	1.890	2.725(3)	14.8	Mean of 12

(1) Phillips (1985).
(2) England, *et al.* (1991).
(3) Zelasko (1991).

Table 2-6. Comparison of soil properties for MINOR SCALE, MISERS GOLD, DISTANT IMAGE, and MINOR UNCLE (Continued).

Event	Range From SGZ, m	Top and Bottom of Layer, m	Water Content w, %	Wet Density γ, g/cm^3	Dry Density γ_d, g/cm^3	Specific Gravity G_s	Air Voids Content V_a, %	Notes
DISTANT IMAGE	45.73	0-1	6.6	1.831	1.718	2.725(3)	25.6	Mean of 3
	15.24-32.01	0-1	8.4	2.049	1.890	2.646(4)	12.5	Mean of 12
MINOR UNCLE	All	0-0.75	10.8	2.09	1.89	2.725(3)	10.2	
	All	0-0.75	10.8	2.09	1.89	2.603(4)	7.0	

(3) Zelasko (1991).
(4) Mean values of samples tested in 1994 (Appendix A).

immediately evident. The backfilling and other pre-test operations resulted in higher wet density and lower air voids content for DISTANT IMAGE and MINOR UNCLE than for the most compacted layer for MINOR SCALE (layer C-1A MD). The air voids content for MINOR UNCLE was less than one-third of the air voids content of the undisturbed soil and less than one-half of the air voids content of the most dense layer for MINOR SCALE. These variations in air voids content can have significant effects on the soil response calculated using the material models discussed in Section 1.

2.3 NATURAL EJECTA.

Properties for the natural ejecta samples from DISTANT IMAGE are presented in Table 2-7. The impact locations of the ejecta fragments are also given. The mean values of the wet density and water content for the natural ejecta samples are 2.06 g/cm^3 and 8.2 percent, respectively. These values are nearly identical to those for the pre-test samples (wet density of 2.05 g/cm^3 and water content of 8.4 percent). The water contents of the ejecta fragments vary over a wider range than for the pre-test samples.

Table 2-8 gives the properties and impact locations for the natural ejecta samples from MINOR UNCLE. The column "Test Day Water Content" gives the values of water content obtained in the field on the day of the test. The mean water content for the natural ejecta samples was 10.3 percent, which was very close to to the mean of 10.8 percent for the pre-test samples. The remainder of the analysis of the properties of the natural ejecta samples was performed during June 1994 (two columns headed "6/94"). As indicated in Appendix A, the water contents decreased and the dry densities increased during storage (apparently some shrinkage of the samples occurred). The 6/94 density measurements are not considered valid. In the future, all measurements on natural ejecta samples should be performed immediately following collection of the samples (the procedure used for DISTANT IMAGE).

2.4 ARTIFICIAL EJECTA IMPLANTS.

The impact locations of the recovered volumetric strain cans from DISTANT IMAGE were surveyed and the cans were weighed and photographed. The pre- and post-test data for the cans are summarized in Table 2-9 (data from Benson and Henny 1992). Cans 13 and 14 were entered in the field book as undamaged; however, these cans were missing from the inventory when the samples were returned to the laboratory for analysis. The four cans (numbers 11, 12, 17, and 18) installed at the 1.5-ft (0.5-m) and 3.0-ft (0.9-m) depths at a range of 105 ft (32 m) were not damaged. Can number 20, which was installed at the 1.5-ft (0.5-m) depth at a range of 165 ft (50 m), was also undamaged. The remaining intact can (number 4), installed at the 6-ft (1.8 m) depth at a range of 75 ft (23 m), was slightly deformed. The recovered can fragments represented from 15 to 50 percent of the initial volume of the cans. All identified fragments were from cans installed at the 75-ft (23-m) and 105-ft (32-m) ranges. The soil contained in these can fragments, although desiccated, was suitable for determining dry density and the degree of fracture of the soil particles.

The surveyed impact locations of the aluminum and plastic cubes for MINOR UNCLE are compared in Table 2-10. The plastic cube installed at a range of 53 ft (16 m) and the aluminum cubes installed at ranges of 63 and 73 ft (19 and 22 m) were not recovered. For the latter cases, the impact ranges for the nearest aluminum cubes are given. In all cases, the impact ranges for the aluminum cubes were

Table 2-7. Natural ejecta data for DISTANT IMAGE.

Sample Number	Range From SGZ, m	Azimuth, deg	Water Content w, %	Wet Density γ, g/cm^3	Dry Density γ_d, g/cm^3
A1-1	191	30.7	8.5	2.165	1.995
A2-1	197	30.3	8.9	2.165	1.989
A3-1	356	25.9	8.0	2.046	1.896
A3-2	356	25.9	8.0	2.135	1.976
A4-1	341	26.6	10.0	2.071	1.881
A4-2	341	26.6	10.0	2.160	1.963
A5-1	305	26.3	10.2	2.010	1.824
A5-2	305	26.3	10.2	1.982	1.800
A6-1	315	25.5	9.2	2.135	1.955
A6-2	315	25.5	9.2	2.239	2.050
A7-1	287	26.0	8.0	2.146	1.989
A8-1	297	25.6	8.4	2.104	1.941
A8-2	297	25.6	8.4	2.167	1.998
A9-1	274	25.6	8.2	2.050	1.894
A9-2	274	25.6	8.2	2.183	2.018
A10-1	251	27.6	9.6	2.386	2.176
A10-2	251	27.6	9.6	2.000	1.825
A11-1	(1)	(1)	8.8	2.122	1.949
A11-2			8.8	2.147	1.973
A12-1	62.9	29.6	9.9	2.099	1.910
A14-1	79.0	29.8	10.2	2.162	1.962
A14-2	79.0	29.8	10.2	2.131	1.934
A15-1	77.0	30.0	12.4	2.000	1.779
A15-2	77.0	30.0	12.4	2.131	1.897
A16-1	105	27.2	0.3	2.101	2.093
A19-1	117	23.1	6.7	2.079	1.949
A19-2	117	23.1	6.7	1.995	1.870
A20-1	123	23.5	4.5	2.050	1.962
A20-2	123	23.5	4.5	1.962	1.877
A21-1	134	24.2	7.2	2.077	1.937

(1) If no entry in this column, this fragment was not surveyed.

Table 2-7. Natural ejecta data for DISTANT IMAGE (Continued).

Sample Number	Range From SGZ, m	Azimuth, deg	Water Content w, %	Wet Density γ, g/cm^3	Dry Density γ_d, g/cm^3
A21-2	134	24.2	7.2	2.029	1.893
A22-1	420	25.6	7.2	2.050	1.912
A22-2	420	25.6	7.2	2.024	1.888
A23-1	433	25.4	5.1	2.035	1.936
A23-2	433	25.4	5.1	2.010	1.912
A24-1	478	27.6	9.3	2.093	1.915
A24-2	478	25.4	9.3	2.136	1.954
A29-1	121	26.5	9.4	2.103	1.921
A29-2	121	26.5	9.4	2.112	1.929
A30-1	126	27.0	9.3	2.032	1.861
A30-2	126	27.0	9.3	2.112	1.933
A32-1	142	22.8	8.8	2.008	1.846
A33-1	165	23.2	7.5	2.144	1.994
A33-2	165	23.2	7.5	2.037	1.894
A35-1	211	26.2	9.2	2.175	1.990
A35-2	211	26.2	9.2	1.970	1.804
A37-1	198	28.3	7.7	1.971	1.830
B1-1	728	25.6	10.3	2.003	1.817
B1-2	728	25.6	10.3	1.923	1.744
B3-1	731	25.5	5.2	2.082	1.981
B3-2	731	25.5	5.2	2.066	1.965
B4-1	739	25.3	6.8	2.062	1.931
B5-1	(1)	(1)	8.1	1.929	1.785
B5-2			8.1	1.700	1.569
B6-1			8.4	2.128	1.965
B7-1	749	25.2	8.9	2.059	1.891
B7-2	749	25.2	8.9	2.077	1.907
B8-1	736	25.0	8.6	1.864	1.716
B8-2	736	25.0	8.6	1.974	1.817
B9-1			6.9	1.962	1.835

(1) If no entry in this column, this fragment was not surveyed.

Table 2-7. Natural ejecta data for DISTANT IMAGE (Continued).

Sample Number	Range From SGZ, m	Azimuth, deg	Water Content w, %	Wet Density γ, g/cm^3	Dry Density γ_d, g/cm^3
B9-2	(1)	(1)	6.9	1.840	1.720
B10-1	710	25.5	5.0	1.926	1.835
B10-2	710	25.5	5.0	1.947	1.854

(1) If no entry in this column, this fragment was not surveyed.

Table 2-8. Natural ejecta data for MINOR UNCLE.

Sample Number	Range From SGZ, m	Azimuth, deg	Test Day Water Content w, %	6/94 Water Content w, %	6/94 Dry Density γ_d, g/cm^3
Y 01	518	(1)	12.1	3.6	2.02
Y 02	626	24	8.1	4.1	1.99
Y 03	579		16.0	4.9	1.94
Y 04	483	25	12.1	3.8	2.07
Y 05	460	25	10.4	4.6	2.07
Y 06	416	26	10.3	3.4	2.03
Y 07	293	26	8.7	4.1	2.02
Y 08	363	27	11.1	2.7	2.04
Y 09	336	27	10.2	2.3	2.07
Y 10	307	25	10.3	2.2	2.05
Y 11	269	25	9.1	5.5	2.06
Y 12	244	26	8.4	3.4	2.00
Y 13	223	27	12.4	3.1	2.07
Y 14	190	22	14.4	4.0	2.02
Y 15	165	31	10.9	6.0	1.96
Y 16	140	33	11.0	3.4	2.12
Y 17	111	35	11.0	3.1	2.08
Y 18	87	33	11.3	4.6	2.07
Y 19	60	38	15.8	4.7	2.02
Y 20	60	38	11.2	(2)	
Y 21	49	42	13.5	4.5	2.09
Y 22	49	42	8.7		
Y 23	52	38	11.7	3.3	2.13
Z 01	610		8.5	4.8	2.01
Z 02	610		11.5		
Z 03	610		11.0	4.4	1.96

(1) If no entry in this column, this fragment was not surveyed; range was determined by walking from nearest survey marker.
(2) If no entry in this column, sample was damaged or was too small to make measurements.

Table 2-8. Natural ejecta data for MINOR UNCLE (Continued).

Sample Number	Range From SGZ, m	Azimuth, deg	Test Day Water Content w, %	6/94 Water Content w, %	6/94 Dry Density γ_d, g/cm^3
Z 04	667	25	(3)	3.4	2.13
Z 05	705	25		4.7	2.05
Z 06	733	26	13.5	4.5	1.96
Z 07	756	26	4.8	1.5	2.06
Z 08	798	22	2.1	(2)	
Z 09	823	(1)	4.5	1.4	2.08
Z 10	840	25	9.8	2.8	2.05
Z 12	883	24	5.6	0.5	2.13
Z 13	935	24	10.3	3.9	2.03
Z 14	968	25	3.6	0.7	2.13
Z 15	833	25	7.2		

(1) If no entry in this column, this fragment was not surveyed; range was determined by walking from nearest survey marker.
(2) If no entry in this column, sample was damaged or was too small to make measurements.
(3) If no entry in this column, no value was recorded.

Table 2-9. Volumetric strain can ejecta implants for DISTANT IMAGE.

Can Number	Mass of Soil in Can, kg	Soil Density kg/m^3	Pre-Test Location Range m	Pre-Test Location Depth m	Post-Test Condition	Post-Test Range m
1	0.725	1.92	15.2	1.8	Missing	
2	0.724	1.92	15.2	1.8	Missing	
3	0.723	1.91	22.9	1.8	Bot. 20%	147
4	0.731	1.93	22.9	1.8	Whole	109
5	0.745	1.97	32.0	1.8	Missing	
6	0.728	1.93	32.0	1.8	Bot. 15%	269
7	0.723	1.91	15.2	0.9	Missing	
8	0.725	1.92	15.2	0.9	Missing	
9	0.723	1.92	22.9	0.9	Bot. 20%	52
10	0.723	1.91	22.9	0.9	Bot. 50%	147
11	0.726	1.92	32.0	0.9	Whole	101
12	0.729	1.93	32.0	0.9	Whole	101
13	0.726	1.92	15.2	0.5	Whole	679
14	0.730	1.93	15.2	0.5	Whole	696
15	0.725	1.92	22.9	0.5	Missing	
16	0.724	1.92	22.9	0.5	Broken	324
17	0.724	1.92	32.0	0.5	Whole	113
18	0.722	1.91	32.0	0.5	Whole	113
19	0.724	1.92	50.3	0.5	Missing	56
20	0.722	1.91	50.3	0.5	Whole	
			Unidentified top 25% of can			561

Table 2-10. Impact locations of aluminum and plastic cubes for MINOR UNCLE.

Initial Range, m	Aluminum Cubes Final Range, m	Plastic Cubes Final Range, m
13.1	799	516
14.6	762	585
16.2	671	(1)
17.7	613	508
18.9	559	(2)
19.2	(1)	389
19.5	575	(2)
20.7	432	349
22.0	433	(2)
22.3	(1)	221
22.6	419	(2)
23.8	398	353
25.3	130	112
26.8	193	131

(1) Not recovered.
(2) No plastic cube implanted at this range; data for aluminum cubes adjacent to missing cube given for range comparison.

greater than for the corresponding plastic cubes. Ratios of the impact ranges are from 1.16 to 1.95 (aluminum to plastic). Both higher ejection velocities (resulting from the greater acoustic impedance) and the higher density of the aluminum cubes will produce greater impact ranges for the aluminum cubes. Since predictions of the ejection velocities were not available for MINOR UNCLE, it was not possible to compute the impact ranges for the artificial ejecta implants for this event. This issue is explored further in Section 3.2 for event HUSKY JAGUAR 2.

2.5 LABORATORY TESTING.

Three types of soil samples were available from events DISTANT IMAGE and MINOR UNCLE:

1. Pre-test soil samples taken from the predicted ejecta region. These samples were placed in mason jars and plastic bags for long term storage.

2. Post-test samples of natural ejecta fragments. These samples were of four types: clumps of soil from the ejecta fragments coated with sealant, clumps of soil placed in mason jars and sealed, soil remaining in cans already used to determine water content, and residual parts of ejecta fragments placed in plastic bags and sealed.

3. Post-test soil samples contained in volumetric strain cans (DISTANT IMAGE only). The cans were sealed in plastic bags.

Laboratory tests performed on the DISTANT IMAGE and MINOR UNCLE pre-test soil samples included hydrostatic compression with measurements of pore pressure as functions of applied stress, particle size distribution, specific gravity, and suction-water content relationship. Particle size distributions and specific gravities were also obtained for the natural ejecta fragments, the post-test samples taken from the volumetric strain cans, and the pre-test soil samples which were subjected to hydrostatic compression testing. Limited examination of a pre-test soil clump and a natural ejecta fragment was performed using an environmental scanning electron microscope.

2.5.1 Hydrostatic Compression with Pore Pressure.

Hydrostatic compression tests are tests in which the specimen is subjected to an all-around confining pressure during axial loading. The confining pressure and the height and diameter changes of the specimen are measured. NMERI used an existing triaxial test cell for these tests (Appendix B).

Hydrostatic compression tests were performed on the DISTANT IMAGE pre-test soil. The test samples were prepared to a dry density of 1.9 g/cm^3 and a water content of 8.5 percent. The specific gravity of the soil grains was 2.625, giving a calculated air voids content of 11.5 percent. The two successful tests produced lockup at 3,000 and 6,000 psi (0.2 and 0.4 kbar). The difference in total stress required to produce lockup was probably caused by differences in the water contents of the two samples. The pore pressures exceeded 7,000 psi (0.48 kbar) for both samples, with the pore fluid taking up most of the total loading as lockup was approached. It is clear that the pore pressure response at the higher loadings was due to pore water and not pore air. The detailed test procedures and results are given in Appendix B.

2.5.2 Particle Size Distribution.

The particle size distributions were determined as indicated in Table A-1. As explained in Appendix A, some material was removed from some of the samples before obtaining the size distributions. The results presented in Appendix A compare distributions on a consistent basis.

Four sets of particle size distributions were obtained for event DISTANT IMAGE: (1) pre-test soil from individual storage jars, (2) pre-test soil from a blend-prepared as indicated in Appendix A, (3) blended pre-test soil after hydrostatic compression tests, and (4) post-test soil from the volumetric strain cans. As shown in Figure A-1 for the whole samples of types (1) and (2), there were some differences in size distributions among the various pre-test samples and the blended soil. The most important comparison for evaluation of the multiphase effective stress pore-air model is shown in Figure A-3: hydrostatic compression to 10,000 psi (0.7 kbar) produced no observable effect on the particle size distribution for the DISTANT IMAGE soil (Figure A-2 also shows that the initial compression to produce the sample for the hydrostatic compression tests did not affect the size distribution). The samples in the strain cans were either unchanged or lost fines (Figures A-5 through A-10).

Two sets of size distributions were obtained for event MINOR UNCLE: (1) pre-test soil from one location in the trench from which the pre-test samples were obtained and (2) post-test natural ejecta fragments. The results presented in Figures A-11 through A-16 show that the process of ejection from the crater produced no increase in fines; one sample (Z14) exhibited a loss of fines.

A total of 20 particle size distributions were obtained for events DISTANT IMAGE and MINOR UNCLE. Although there are differences among the distributions obtained for each event, there is no evidence of an increase in fine particles as a result of the compression events.

2.5.3 Specific Gravity.

The standard for the determination of the specific gravity of the soil grains and the results obtained for events DISTANT IMAGE and MINOR UNCLE are given in Appendix A. As discussed in Section 2.2, the specific gravity of the upper layer of the test bed soil decreased over the sequence of events from MINOR SCALE through MINOR UNCLE (Table 2-6). This could be due to the use of different sources of soil to bring the test beds to their final levels or to differences in testing methods.

The specific gravity is important because it is used in determining the air voids content. The values of this parameter for the pre-test soil samples are given in Table 2-6. These values are compared to the air voids content of the natural ejecta samples in Table A-5. The air voids contents for the pre-test soil and natural ejecta were equal for DISTANT IMAGE when the same value of specific gravity was used in determining the air voids content. This indicates that any changes that occurred during loading were reversed during unloading. This issue is discussed further in Section 4.

2.5.4 Suction-Water Content Relationship.

The suction-water content relationship is used in civil engineering practice to characterize the behavior of expansive soils (Appendix A). The total suction is

made up of a matrix component, due to the attraction of water to the soil particle surfaces, and an osmotic component, due to dissolved salts or other solutes in the pore water. Levels of suction are associated with the physical behavior of soils.

As discussed in Appendix A, the suction-water content relationship for WSMR/PHETS soil indicates that the soil is granular with a high dissolved salt content. The latter characteristic can cause the soil to hold together due to the tension in the pore water.

2.5.5 Soil Morphology Observations.

Soil morphology observations were made in an environmental scanning electron microscope. A pre-test clump sample from the DISTANT IMAGE test bed and a post-test natural ejecta sample were prepared by impregnation with a stabilizing agent which hardened sufficiently to permit sectioning and polishing. This allowed observation of the soil particles in the same proximity to each other as in the undisturbed sample. No distinguishing features could be delineated for either sample and this approach was discontinued.

SECTION 3

EXPERIMENTAL PROGRAM FOR SOCORRO PLASTER SAND

This section addresses the experimental determination of the dynamics of high speed ejecta from cratering detonations in Socorro plaster sand. The primary objective of this component of the experimental program was to field experiments to determine the ejection velocities of the high speed ejecta fragments. A secondary objective was to investigate any changes in the properties of the soil that formed those fragments.

The ejecta experiments in Socorro plaster sand were fielded on events HUSKY JAGUAR 1 and 2, which were 1,000-lb (454 kg) detonations conducted at the same site at the PTB. The experiments were simplified relative to those for the WSMR/PHETS soil because of several factors: (1) the test bed and ejecta field for a 1,000-lb (454 kg) detonation were much smaller than for the large detonations at WSMR/PHETS, simplifying the post-test search for artificial ejecta implants, (2) no long-range natural ejecta fragments were anticipated for Socorro plaster sand due to its low cohesiveness, so the entire process of processing natural ejecta fragments was eliminated, (3) the relatively small test bed and the anticipated lack of a background of large natural ejecta fragments were conducive to the use of high resolution motion picture photography to obtain trajectory data for in-flight artificial ejecta implants, and (4) the test bed was well characterized by the U.S. Army Engineer Waterways Experiment Station (WES), eliminating the requirement for an extensive independent analysis of the pre-test soil.

3.1 EXPERIMENTAL PROGRAM.

3.1.1 Event HUSKY JAGUAR 1.

The HUSKY JAGUAR 1 charge was a half-buried 3-ft (0.92-m) diameter sphere containing 1,000 lb (454 kg) of nitromethane. The test bed was a 26-ft (8-m) radius hemisphere of Socorro plaster sand centered on the spherical charge. HUSKY JAGUAR 1 event was conducted on 6 August 1992. Five experiments related to ejecta phenomenology were fielded on this event.

The first experiment used volumetric strain cans placed pre-test within and beneath the expected ejecta region of the crater to measure the effects of the ground shock on the properties of the soil. The pre- and post-test locations of the cans were surveyed. For the cans that were ejected from the crater, high resolution photography was used to determine the trajectories (see Section 3.2.1).

The second experiment was an attempt to determine the maximum ejection velocity of the soil near the test bed surface. The ejecta spires observed on many near-surface cratering events were of particular interest because the material in the spires was believed to be the highest velocity ejecta. The spires are typically made up of small particles which do not reach large ranges due to aerodynamic drag effects; much of this material actually ends up in the rising dust cloud. For near-surface events, this material is believed to originate within a few charge radii of the charge center as surface spall (Wisotski 1977). The velocities of this spalled material are not available from cratering codes since the depth of the spall layer is a small fraction of the height of the surface cells

in a calculation; therefore, the ejection velocities of this material must be determined experimentally. The spall experiment, in which several 2-in (5-cm) aluminum cubes were placed flush with the test bed surface in the expected ejecta region, provided relatively large objects with known initial locations that could be photographed to determine their ejection velocities.

The third experiment included high resolution (70-mm, 20 frames/second) and high-speed (16-mm, 400 frames/second) photography of the in-flight ejecta and the fireball development for HUSKY JAGUAR 1. A camera plan was designed by SEA and the Denver Research Institute (DRI). Photography was required to obtain in-flight trajectory information to permit determination of ejection velocities (speed and angle), information that could not be obtained from initial and final locations of the ejected objects. The in-flight ejecta objects included the volumetric strain cans, the aluminum cubes, and clumps of Socorro plaster sand. DRI performed the photographic data reduction (described in a separate DRI report, Lynch, Wisotski, and Samaras 1992). SEA correlated the photographic results with the post-test survey locations of individual objects (see Section 3.2.1).

The fourth experiment, fielded by NMERI, was a passive Cratering and Related Effects (CARE) experiment to characterize the crater and net ground displacement. Horizontal colored layers of the Socorro plaster sand backfill were placed at several depths in the test bed. Numbered implants (disks and 1-in (2.5-cm) aluminum cubes) were placed within each colored layer. Surface displacement pins (large nails) were driven into the test bed surface. The positions of the colored layers, the individual implants, and the pins were surveyed pre- and post-test to define crater profiles and net displacements (Benson 1993).

The fifth experiment was designed and fielded by WES to support the ejecta experiments. The WES gage plan for the free-field ground motion and stress measurements included velocity measurements at seven radii from the charge center along a radial depressed 8 degrees from the horizontal. These gauges and the resulting waveforms are described in separate WES reports.

CRT provided calculational support in the form of predicted ejection velocities and strain paths for Lagrangian tracer points included in the pre-test prediction for HUSKY JAGUAR 1. The initial locations of these tracer points are included in the HUSKY JAGUAR 1 Program Plan (Wesevich 1992).

3.1.1.1 Pre-Test Activities. A representative bulk sample of Socorro plaster sand of sufficient size to prepare 50 volumetric strain cans was obtained from the supply during the construction of the test bed. An additional 50 lb (23 kg) was stored for later use in the laboratory test program.

Forty-eight volumetric strain cans were filled with Socorro plaster sand, which was packed into the cans at a wet density of 115 pcf (1.84 g/cm^3); 40 of these were implanted in the test bed and 8 were set aside as controls. An additional 8 cans were filled with backfill material taken from the test bed of the prior event DISTANT IMAGE to supplement the samples recovered from that event. Six of these cans were implanted in the HUSKY JAGUAR 1 test bed and 2 were retained as controls.

All implants, including the 1-in (2.5-cm) cubes installed by NMERI to determine the ejecta volume, the volumetric strain cans, and the 2-in (5-cm) aluminum

spall implants, were emplaced during backfilling of the test bed as part of NMERI's passive ejecta program. The pre-test locations of the implants are given in Table 3-1 (the coordinate system is positive X to the east, positive Y to the north, and positive Z upward).

3.1.1.2 Post-Test Activities. The initial post-test activities occurred immediately following the event. The first activity was a reconnaissance of the access road prior to general reentry of the test bed for artificial ejecta implants and interesting natural ejecta fragments. The area from the crater lip to about 500 ft (150 m) from SGZ along the east radial and to about 1,000 ft (300 m) along the west radial was searched for cans, cubes, and natural ejecta clumps. The final locations of these objects were marked with flags and the objects were recovered. Only a few small natural ejecta fragments, which were small clumps of sand from the colored layers in the test bed, were found; none was recovered. A complete survey of all objects found on the test bed surface was conducted within two days of the test. Further searches for cubes were conducted along the west radial on an intermittent basis over a period of several months. As part of its CARE program, NMERI completely excavated the HUSKY JAGUAR 1 crater and surveyed the final locations of the artificial ejecta implants that were not ejected from the crater.

A summary of the recovered implants is given in Table 3-1. Five of the six 2-in (2.5-cm) cubes and 18 of the 25 1-in (2.5-cm) cubes implanted in the layer nearest the surface were recovered. Soil samples were recovered in 30 of the 46 volumetric strain cans fielded on HUSKY JAGUAR 1. The post-test condition of the cans is summarized in Table 3-1. Photographic records of the recovered cans were obtained.

All event cameras obtained film records. The original films taken during HUSKY JAGUAR 1 were sent to DRI for analysis. Seven of the eight high resolution (70-mm) films contained trackable ejecta fragments. The eighth film contained no fragments. DRI obtained trajectories for 20 objects from the high resolution films of the event (Lynch, Wisotski, and Samaras 1992).

3.1.2 Event HUSKY JAGUAR 2.

The HUSKY JAGUAR 2 charge was a 3-ft (0.92-m) diameter sphere containing 1,000 lb (454 kg) of nitromethane with its center located at a depth of 8.2 ft (2.5 m) below the test bed surface. The test bed was a 26-ft (8-m) radius hemisphere of Socorro plaster sand centered at SGZ. A 9.8-ft (3-m) thick layer of concrete was placed with its top surface 16.4 ft (5 m) below the test bed surface. This event was conducted on 29 July 1993. Three experiments related to ejecta phenomenology were fielded on this event.

The first experiment on HUSKY JAGUAR 2 was similar to the spall experiment conducted on HUSKY JAGUAR 1, except that both aluminum and plastic cubes were placed flush with the top of the test bed surface. Additional aluminum cubes were implanted between the test bed surface and the charge. The HUSKY JAGUAR program provided a unique opportunity to address the issue of yield scaling of ejection velocities. This experiment was repeated in the halfspace facility using scaled surface implants emplaced at scaled ranges in the test bed. The halfspace experiment is discussed in Section 5.

The second experiment included high resolution (70-mm, 20 frames/second) and high-speed (16-mm, 400 frames/second) photography of the in-flight ejecta and

Table 3-1. Volumetric strain can and aluminum cube ejecta implants for HUSKY JAGUAR 1.

Implant Number	Pre-test location X m	Y m	Z m	Post-test location X m	Y m	Z m	Condition
EI-101	1.50	0.26	-0.08				2 parts--metal only
EI-102	1.22	-0.23	-0.17				Top--metal only
EI-103	-1.98	0.22	-0.21	-5.52	0.77	0.09	Unchanged
EI-104	-1.96	-0.21	-0.25	-5.52	-0.85	-0.28	Unchanged
EI-105	-2.36	0.24	-0.28	-3.83	0.44	0.21	Unchanged
EI-106	-2.36	-0.23	-0.30	-3.93	-0.55	0.25	Unchanged
EI-107	2.78	0.25	-0.33	3.80	0.44	0.05	Unchanged
EI-108	2.79	-0.23	-0.28	4.00	-0.29	0.25	Unchanged
EI-109	-3.16	0.23	-0.38	-3.76	0.29	-0.21	Unchanged
EI-110	-3.18	-0.24	-0.42	-3.69	-0.29	0.20	Unchanged
EI-111	-0.88	0.23	0.00				Missing
EI-112	-0.91	-0.23	0.00				Top--metal only
EI-113	-1.20	0.23	0.00				2 parts--metal only
EI-114	-1.52	0.26	0.01	-132.36	6.00	-1.29	Top--metal only
EI-115	-1.49	-0.22	0.00				Top--metal only
EI-116	-1.82	0.25	0.00	-87.96	13.42	-1.34	Intact/no soil
EI-117	-2.44	0.25	0.00	-30.48	1.62	-0.70	Unchanged
EI-118	-3.07	0.24	-0.00	-6.44	0.57	0.10	Unchanged
EI-119	0.91	0.24	-0.11				Missing

EI-101-119 were volumetric strain cans filled with Socorro plaster sand, except 112 and 115, which were filled with DISTANT IMAGE test bed soil.

Table 3-1. Volumetric strain can and aluminum cube ejecta implants for HUSKY JAGUAR 1 (Continued).

Implant Number	Pre-test location X m	Y m	Z m	Post-test location X m	Y m	Z m	Condition
EI-120	0.90	-0.24	-0.14				Missing
EI-121	-0.88	0.24	-0.12				Missing
EI-122	-0.89	-0.23	-0.15				Missing
EI-123	1.21	0.25	-0.11				Top--metal only
EI-124	1.52	-0.24	-0.14	19.70	-2.89	-0.08	Top/bottom--soil inside
EI-125	-1.52	0.25	-0.11	-33.07	8.89	-0.27	3 parts--soil inside
EI-126	-1.52	-0.25	-0.14				Top found--soil inside
EI-127	1.86	0.27	-0.11	23.69	1.83	0.00	Top--soil inside
EI-127				13.89	0.89	-0.04	Bottom--soil inside
EI-128	1.85	-0.24	-0.14	14.83	-1.41	-0.09	Unchanged
EI-129	2.45	0.29	-0.12	10.98	1.31	0.09	Unchanged
EI-130	2.45	-0.23	-0.14	9.92	-0.67	0.04	Unchanged
EI-131	3.07	0.27	-0.12	5.03	0.54	0.18	Unchanged
EI-132	3.08	-0.24	-0.14	5.32	-0.34	0.16	Top--metal only
EI-133	0.91	0.23	-0.31				In crater--metal only
EI-134	0.91	-0.22	-0.34	2.85	-0.80	-0.36	Several small pieces
EI-135	1.23	0.25	-0.31				Broken open
EI-136	1.22	-0.22	-0.34	2.55	-0.55	-0.58	Split/shortened
EI-137	1.82	0.22	-0.31	3.61	0.48	0.12	Unchanged

EI-120-137 were volumetric strain cans filled with Socorro plaster sand, except 121, 122, 125, and 126, which were filled with DISTANT IMAGE test bed soil.

Table 3-1. Volumetric strain can and aluminum cube ejecta implants for HUSKY JAGUAR (Continued).

Implant Number	Pre-test location X m	Y m	Z m	Post-test location X m	Y m	Z m	Condition
EI-138	1.83	-0.22	-0.34	3.52	-0.30	0.07	Unchanged
EI-139	0.91	0.23	-0.50	2.64	0.65	-0.39	2 large pieces
EI-140	0.91	-0.23	-0.52	2.59	-0.53	-0.41	Shortened
EI-141	1.20	0.23	-0.49	2.39	0.63	-0.54	One end angled
EI-142	1.21	-0.23	-0.53	2.59	-0.75	-0.39	Shortened
EI-143	0.91	0.24	-0.69				Slightly shortened
EI-144	0.89	-0.19	-0.72	1.16	-0.30	-0.98	Small soil fragment
EI-145	0.90	0.22	-0.88	1.13	0.29	-1.14	Bottom--metal only
EI-146	0.94	-0.23	-0.91	1.17	-0.34	-1.11	Shortened
EI-147	-0.92	0.00	0.00				Not recovered
EI-148	-1.21	0.01	0.00	-310.09	13.39	-1.92	
EI-149	-1.51	-0.01	0.00	-208.96	7.40	-1.81	
EI-150	-1.84	0.01	0.00	-115.62	4.85	-1.48	
EI-151	-2.44	-0.02	0.00	-37.30	0.14	-0.70	
EI-152	-3.04	0.00	0.00	-8.86	0.10	0.06	
T10	-2.20	0.42	-0.14	-17.54	3.58	-0.33	
T11	-1.88	0.42	-0.14				Not recovered
T12	-1.58	0.42	-0.14	-34.47	9.78	-0.52	
T13	-1.28	0.42	-0.14	-53.91	22.67	-0.73	

EI-138-146 were volumetric strain cans filled with Socorro plaster sand; EI-147-152 were 2-in (5.1-cm) aluminum cubes; T10-T13 were 1-in (2.5-cm) aluminum cubes.

Table 3-1. Volumetric strain can and aluminum cube ejecta implants for HUSKY JAGUAR 1 (Continued).

Implant Number	Pre-test location X m	Y m	Z m	Post-test location X m	Y m	Z m	Condition
T14	-0.97	0.42	-0.14				Not recovered
T15	0.88	0.41	-0.16				Not recovered
T16	1.18	0.41	-0.15	106.51	45.26	0.87	
T17	1.48	0.41	-0.15				Not recovered
T38	2.09	-0.04	-0.17	15.29	0.93	-0.04	
T39	1.78	-0.03	-0.16	20.21	1.35	-.03	
T40	1.17	-0.04	-0.15	123.50	-0.30	0.92	
T41	0.86	-0.04	0.15				Not recovered
T42	-0.96	-0.04	-0.1	-81.90	-1.83	-1.28	
T43	-1.27	-0.04	-0.14	-76.52	5.81	-1.15	
T44	-1.58	-0.03	-0.14	-60.25	4.49	-0.94	
T45	-1.88	-0.03	-0.13				Not recovered
T46	-2.18	-0.04	-0.14	-16.88	0.83	-0.37	
T47	-2.49	-0.03	-0.13	-15.72	-0.57	-0.32	
T66	-2.15	-0.50	-0.14	-16.56	-4.54	-0.43	
T67	-1.85	-0.49	-0.13	-18.70	-6.75	-0.56	
T68	-1.55	-0.49	-0.13	-41.58	-10.73	-0.79	
T69	-1.24	-0.49	-0.14				Not recovered
T70	-0.94	-0.49	-0.14	-100.38	-48.72	-1.46	
T71	0.89	-0.49	0.16	103.89	-58.96	0.69	

T14-T71 were 1-in (2.5-cm) aluminum cubes.

Table 3-1. Volumetric strain can and aluminum cube ejecta implants for HUSKY JAGUAR 1 (Continued).

Implant Number	Pre-test location X m	Y m	Z m	Post-test location X m	Y m	Z m	Condition
T72	1.20	-0.49	-0.16	107.64	-51.01	0.67	

T72 was a 1-in (2.5-cm) aluminum cube.

the fireball development for HUSKY JAGUAR 2. The camera plan was similar to that used on HUSKY JAGUAR 1, except that the number of 70-mm cameras was reduced to two. These cameras were located west of SGZ to film the trajectories of the 2-in (5-cm) aluminum cubes. Applied Research Associates, Inc. (ARA) performed the photographic data reduction (described in a separate ARA report, Seebaugh 1994). SEA correlated the photographic results with the post-test survey locations of individual objects and compared the trajectories obtained from the films with calculated trajectories (see Section 3.2.2).

The third experiment, fielded by NMERI, was a passive CARE experiment similar to that fielded on HUSKY JAGUAR 1. No volumetric strain cans were used on HUSKY JAGUAR 2.

3.1.2.1 Pre-Test Activities. SEA and NMERI installed an array of implants, including 31 2-in (5-cm) aluminum and 14 2-in (5-cm) plastic cubes, on HUSKY JAGUAR 2. The implant locations, given in Table 3-2, were determined following a review of the pre-test calculation performed by CRT. The initial ranges were from 1 to 15 ft (0.3 to 4.6 m) from SGZ. All implants, including the 2-in (5-cm) aluminum cubes and the 1-in (2.5-cm) cubes installed by NMERI to determine the ejecta volume, were emplaced during backfilling of the test bed as part of NMERI's passive ejecta program.

3.1.2.2 Post-Test Activities. The initial post-test activities were essentially the same as those conducted following HUSKY JAGUAR 1. A more intensive search for natural ejecta fragments was conducted for HUSKY JAGUAR 2. Only small fragments which shattered upon impact were found; none was recovered. Extensive searches for cubes were conducted along the west radial.

Forty of the 45 2-in (5-cm) cubes were recovered, including 9 of the 10 plastic cubes (Table 3-2). NMERI completely excavated the HUSKY JAGUAR 2 crater and surveyed the final locations of the recovered artificial ejecta implants.

All cameras operated on HUSKY JAGUAR 2 and the quality of the high resolution films was excellent. One film did not have timing marks; the frame rate was estimated using the dress rehearsal film from the same camera. ARA obtained trajectories for 27 objects from the high resolution film with the field of view including the SGZ and the cleared area along the west radial (Seebaugh 1994).

3.2 ARTIFICIAL EJECTA IMPLANTS.

3.2.1 Event HUSKY JAGUAR 1.

Table 3-1 gives the post-test locations of the volumetric strain cans. Only two cans with soil samples remaining inside were found at significant ranges from SGZ: EI-117 (30.5 m west, unchanged condition) and EI-125 (33 m west, broken apart). The latter can contained soil from the DISTANT IMAGE test bed; the post-test particle size distribution for this can was discussed in Section 2.5.2.

As shown in Table 3-1, five of the six 2-in (5-cm) cubes were recovered on HUSKY JAGUAR 1. These cubes were found at ranges that varied inversely with their pre-test ranges from SGZ, that is, the cube initially at the greatest distance from SGZ was found closest to SGZ, etc. The longest range for the recovered cubes (number EI-148) was 1018 ft (310 m). Cube EI-149, which has not been recovered, should be at a significantly greater range.

Table 3-2. Aluminum and plastic cube ejecta implants for HUSKY JAGUAR 2.

Implant Number	Pre-test location X m	Y m	Z m	Post-test location X m	Y m	Z m	Description
HJ2 11	-0.29	0.00	2.50	-281.32	-64.99	0.33	Aluminum, at surface
HJ2 13	-0.28	0.09	0.60				Removed before test
HJ2 14	-0.60	0.09	0.60	-100.67	27.92	1.49	Aluminum
HJ2 17	-0.90	0.09	0.60	-63.55	32.12	1.83	Aluminum
HJ2 18	-0.45	0.13	0.95	-178.59	53.82	1.26	Aluminum
HJ2 22	-0.91	0.12	0.96	-180.12	-38.24	0.46	Aluminum
HJ2 23	-0.59	-0.01	2.50	-268.99	5.55	0.50	Aluminum, at surface
HJ2 28	-1.36	0.09	0.97	-41.54	3.45	1.95	Aluminum
HJ2 34	-0.89	0.00	2.50	-250.03	-30.27	0.41	Aluminum, at surface
HJ2 35	-0.30	0.10	1.61	Not recovered			Aluminum
HJ2 36	-0.90	0.09	1.62	-225.54	33.29	0.82	Aluminum
HJ2 40	-1.51	0.10	1.62	-121.52	16.20	1.29	Aluminum
HJ2 41	-1.19	-0.01	2.51	-201.43	-4.71	0.53	Aluminum, at surface
HJ2 42	-1.50	-0.02	2.50	Not recovered			Aluminum, at surface
HJ2 43	-2.11	0.10	1.62	-42.94	5.69	1.92	Aluminum
HJ2 48	-2.71	0.10	1.61	-28.95	6.89	2.38	Aluminum
HJ2 49	-1.80	-0.01	2.50	-199.33	14.19	0.70	Aluminum, at surface
HJ2 50	-2.11	-0.01	2.50	Not recovered			Aluminum, at surface
HJ2 51	-0.46	0.10	2.20	-222.80	69.13	0.74	Aluminum

Z denotes the height above the center of the charge, which was 2.50 m below the surface of the test bed.

Table 3-2. Aluminum and plastic cube ejecta implants for HUSKY JAGUAR 2 (Continued).

Implant Number	Pre-test location X m	Y m	Z m	Post-test location X m	Y m	Z m	Description
HJ2 52	-2.41	-0.02	2.49	-128.09	5.40	1.09	Aluminum, at surface
HJ2 53	-2.71	0.00	2.51	Not recovered			Aluminum, at surface
HJ2 54	-3.03	-0.02	2.50	-67.49	-0.01	1.54	Aluminum, at surface
HJ2 56	-3.33	-0.01	2.51	-63.81	1.52	1.55	Aluminum, at surface
HJ2 59	-1.37	0.11	2.20	-219.76	37.17	0.75	Aluminum
HJ2 60	-2.29	0.12	2.20	-112.37	2.88	1.05	Aluminum
HJ2 64	-3.16	0.12	2.19	-47.32	3.04	1.89	Aluminum
HJ2 66	-3.63	-0.01	2.50	-46.13	-1.21	2.02	Aluminum, at surface
HJ2 67	-3.93	-0.01	2.51	-36.46	-1.56	2.14	Aluminum, at surface
HJ2 68	-4.12	0.11	2.20	-18.20	1.90	2.53	Aluminum
HJ2 70	-4.54	-0.01	2.52	-15.18	0.14	2.54	Aluminum, at surface
HJ2 72	-5.14	0.01	2.52	-12.41	0.64	2.59	Aluminum, at surface
D01	0.33	-0.01	2.49	Not recovered			Plastic, at surface
D04	0.63	-0.01	2.49	181.34	30.90	3.84	Plastic, at surface
D05	0.95	-0.01	2.51	178.27	3.25	3.85	Plastic, at surface
D06	1.27	-0.02	2.51	182.23	-0.36	3.90	Plastic, at surface
D07	1.54	-0.01	2.51	129.39	13.19	3.51	Plastic, at surface
D08	1.85	0.00	2.52	130.33	29.75	3.51	Plastic, at surface
D09	2.16	0.00	2.52	120.55	1.95	3.42	Plastic, at surface

Z denotes the height above the center of the charge, which was 2.50 m below the surface of the test bed.

Table 3-2. Aluminum and plastic cube ejecta implants for HUSKY JAGUAR 2 (Continued).

Implant Number	Pre-test location X m	Y m	Z m	Post-test location X m	Y m	Z m	Description
D10	2.46	0.00	2.52	106.32	-3.81	3.25	Plastic, at surface
D11	2.79	0.01	2.51	73.41	-1.78	3.19	Plastic, at surface
D12	3.08	0.02	2.52	59.34	0.18	3.14	Plastic, at surface
D13	3.40	0.03	2.51	44.79	0.76	2.88	Plastic, at surface
D14	3.69	0.01	2.51	31.75	-1.00	2.67	Plastic, at surface
D15	4.00	0.03	2.51	13.06	0.25	2.64	Plastic, at surface
D16	4.61	0.04	2.48	19.30	-0.56	2.63	Plastic, at surface

Z denotes the height above the center of the charge, which was 2.50 m below the surface of the test bed.

Twenty-five 1-in (2.5-cm) aluminum cubes (numbers T10 through T72) were emplaced by NMERI within the ejecta zone in the upper colored sand layer at pre-test depths from the surface of 0.43 to 0.56 ft (0.13 to 0.17 m) on HUSKY JAGUAR 1. As shown in Table 3-1, 18 of these cubes were recovered. The longest range for the 1-in (2.5-cm) cubes that were recovered was 407 ft (124 m).

The camera plan for the high resolution photography for HUSKY JAGUAR 1 was designed to permit resolution of the larger implants (volumetric strain cans and 2-in (5-cm) cubes) at velocities on the order of 300 ft/s (90 m/s). Smaller objects (the 1-in (2.5-cm) NMERI cubes) traveling at such high velocities would blur; however, the same cubes traveling at lower velocities would be resolved. The larger implants were distributed along the east and west radials to provide the maximum separation of the individual objects on the films.

DRI tracked 20 objects on the high resolution film records of HUSKY JAGUAR 1 (Lynch, Wisotski, and Samaras 1992). Eight trajectories included time intervals during which the fragments were visible on two overlapping films, giving "stereo" views of portions of these trajectories (the separation distance between the two cameras was much greater than for normal stereo photography). Analysis of these trajectories produced both coordinates (X,Y) of the impact points. The remaining trajectories were each recorded by only one camera; only one coordinate was determined for each impact point (X) for these objects since it was necessary to assume that each trajectory was in the plane normal to the camera axis (Y=0). Table 3-3 gives the trajectory identification numbers assigned by DRI, the ejection velocities and angles, and the impact locations (left side of table) for 18 tracked objects (the number of data points for the two remaining trajectories was not sufficient to permit the projection of their impact locations). The detailed results of the trajectory analysis are given in the DRI report (Lynch, Wisotski, and Samaras 1992).

Thirteen of the film trajectories for HUSKY JAGUAR 1 were matched with objects from the NMERI ground survey results (Table 3-3). Nine impact locations projected from the film trajectories were uniquely associated with implants recovered post-test (trajectories T2, T3, T4, T7, T8, L1C, L2D, L3A, and L4A), 3 impact locations from the film trajectories were associated with 2 implants recovered post-test (trajectories T1, T6, and L1D), and 1 impact location from the film trajectories was associated with 3 implants recovered post-test (trajectory L1A). The implant numbers associated with the trajectories are listed on the right side of Table 3-3. The first of each group of multiple entries is considered to be the best match (for example, implant EI-126 is considered to be the best match for trajectory T1). The 5 remaining impact locations projected from the film trajectories were not sufficiently close to recovered implants to make any associations. Only one specific object, volumetric strain can EI-116, was positively identified on the films. The projected impact location for this can from the films was X = -245 ft (-75 m), Y = 51 ft (16 m); the impact location from the survey was X = -289 ft (-88 m), Y = 44 ft (13 m). It was observed that the can rolled after initial impact (during which the cap separated from the can and the contents spilled onto the test bed surface), so this result seemed reasonable.

This part of the analysis was more difficult than anticipated because many more natural ejecta fragments were produced than expected for the Socorro plaster sand and their presence on the films complicated identification of the ejecta implants. Also, seven small cubes that were not recovered should have impacted in the regions covered by the films.

Table 3-3. Impact locations from films and survey for HUSKY JAGUAR 1.

Film Traj. Number	Ejection Vel. m/s	Ejection Angle deg	X m	Y m	Implant Number	X m	Y m
T1	28.2	52.7	-77.13	-1.22	EI-126	-78.99	-6.68
					T42	-81.90	-1.83
T2	25.6	54.1	-74.70	15.55	EI-116	-87.96	13.42
T3	22.7	61.5	-58.23	26.22	T13	-53.91	22.67
T4	31.6	54.9	-95.12	-10.98	T70	-100.38	-48.72
T5	30.7	56.2	89.02	8.84			
T6	38.6	51.3	96.04	-25.30	T72	107.64	-51.01
					T71	103.89	-58.96
T7	30.8	50.6	102.13	19.51	T16	106.51	45.28
T8	38.4	47.5	121.34	0.91	T40	123.50	-0.30
L1A	17.6	48.9	-35.67	0.00	T12	-34.47	9.78
					EI-125	-33.07	8.89
					EI-151	-37.30	0.14
L1B	15.1	56.7	-26.52	0.00			
L1C	16.2	57.4	-30.18	0.00	EI-117	-30.48	1.62
L1D	18.1	59.5	-34.76	0.00	EI-125	-33.07	8.89
					EI-151	-37.30	0.14
L2D	25.3	63.4	-66.16	0.00	T44	-60.25	4.49
L2E	28.3	63.1	-74.39	0.00			
L2G	31.2	60.0	-92.07	0.00			
L2H	24.2	68.3	-98.78	0.00			
L3A	20.7	70.3	-105.79	0.00	EI-150	-115.62	4.85
L4A	52.3	70.4	-171.95	0.00	EI-149	-208.96	7.40

The maximum impact range determined from the film analysis was 565 ft (172 m); this object (EI-149) had an ejection velocity of 172 ft/s (52.3 m/s). Ejection velocities in excess of 330 ft/s (100 m/s) were predicted for this event (Rocco 1991). Comparisons of the velocities given in Table 3-3 (from the film measurements) to the predicted velocities were inconclusive. There was not a good match between the initial locations of the tracer points in the calculation and the actual pre-test locations of the ejecta implants (the calculation was performed before the implant locations were finalized). Also, the predicted velocity gradients were extremely high. These factors precluded the determination of predicted ejection velocities for specific implants. The predicted high velocities appear credible since the impact range of one implant (EI-148) was over 1,000 ft (310 m) and the missing implant (EI-147) apparently impacted at a greater range. These high speed objects were not tracked on the films, either because they were blurred or were not in the fields of view of the cameras for a sufficient distance to establish their trajectories.

3.2.2 Event HUSKY JAGUAR 2.

The artificial ejecta experiments fielded on event HUSKY JAGUAR 2 represented an improvement over those conducted on HUSKY JAGUAR 1 in several areas:

1. The actual implant locations were in much better agreement with the initial locations of the tracer points in the HUSKY JAGUAR 2 pre-test prediction performed by CRT (Rocco 1993) than for HUSKY JAGUAR 1. This greatly facilitated comparisons of ejecta implant ranges calculated using the ejection velocities from the pre-test predictions with the actual ranges measured during the experiment.

2. Because of the depth of burial of the charge for HUSKY JAGUAR 2, the material ejected from the near-surface layer of the test bed (including the surface implants) did not traverse the fireball, simplifying the determination of the effects of aerodynamic drag on the impact ranges for specified ejection velocities.

3. The plastic cubes prepared for the MINOR UNCLE event to investigate the effects of the mismatch in acoustic impedance of the implants and the surrounding soil were available for use on HUSKY JAGUAR 2.

The results of the ejecta experiments are presented in this section in the following order: (1) comparison of the impact ranges of the aluminum and plastic cubes, (2) comparison of the ejecta trajectories calculated using the experimental ejection velocities to the trajectories from the films (to determine the drag coefficient for the cubes), (3) comparison of the impact ranges of the aluminum and plastic cubes calculated using the ejection velocities from the pre-test predictions, and (4) comparison of the impact ranges calculated using the ejection velocities from the pre-test predictions with the actual impact ranges of the aluminum and plastic cubes.

Table 3-2 gives the pre- and post-test locations of the entire array of 2-in (5-cm) cubes implanted in the HUSKY JAGUAR 2 test bed. Twenty-six of the 30 aluminum cubes and 13 of the 14 plastic cubes were recovered. The impact ranges for the aluminum and plastic cubes implanted at the surface are given in Table 3-4. In all cases except one, the impact ranges for the aluminum cubes were greater than for the corresponding plastic cubes. Ratios of the impact ranges were from 0.79 to 2.79 (aluminum to plastic).

Table 3-4. Impact locations of aluminum and plastic cubes for HUSKY JAGUAR 2.

Aluminum Cubes			Plastic Cubes		
Implant Number	Initial Range m	Final Range m	Implant Number	Initial Range m	Final Range m
HJ2 11	0.29	288.7	D01	0.33	(1)
HJ2 23	0.59	269.0	D04	0.63	183.8
HJ2 34	0.89	251.9	D05	0.95	178.4
HJ2 41	1.19	201.5	D06	1.27	182.3
HJ2 42	1.50	(1)	D07	1.54	130.2
HJ2 49	1.80	199.8	D08	1.85	133.5
HJ2 50	2.11	(1)	D09	2.16	120.6
HJ2 52	2.41	128.2	D10	2.46	106.4
HJ2 53	2.71	(1)	D11	2.79	73.5
HJ2 54	3.03	67.5	D12	3.08	59.5
HJ2 56	3.33	63.8	D13	3.40	44.8
HJ2 66	3.63	46.2	D14	3.69	31.8
HJ2 67	3.93	36.6	D15	4.00	13.1
HJ2 70	4.54	15.3	D16	4.61	19.3

(1) Not recovered.

Three factors can affect the relative impact ranges of the aluminum and plastic cubes: (1) the higher acoustic impedance of the aluminum cubes could produce higher ejection velocities relative to the plastic cubes (this was the premise on which the experiment was based), (2) the greater masses of the aluminum cubes would result in greater impact ranges for equal ejection velocities, and (3) the aluminum cubes were implanted slightly closer to the SGZ than the corresponding plastic cubes, resulting in higher ejection velocities for the aluminum cubes. It was necessary to perform a number of trajectory calculations to understand the relative importance of these factors

The aerodynamic drag of a blunt object such as a cube depends primarily on its shape; for this reason, the drag coefficients of the aluminum and plastic cubes should be essentially identical. The drag coefficient was derived using the results of the ARA analysis of the in-flight ejecta for HUSKY JAGUAR 2 (Seebaugh 1994). Eight trajectories with 10 or more data points defining each trajectory were examined. The ejection velocities determined from the film analysis for these objects were from approximately 50 to 200 m/s. Trajectory 25 (the number assigned by Seebaugh 1994), which was tracked to its impact on the surface, was used as the baseline case.

Using the ejection conditions obtained from the film analysis for trajectory 25, the trajectory was calculated for still air at the atmospheric pressure and temperature from HUSKY JAGUAR 2. The drag coefficient was varied until the calculated impact range was equal to the measured value. The calculated trajectory is compared to the trajectory measured from the film in Figure 3-1. The resulting drag coefficient was 0.81, a reasonable value for an object such as a cube (Hoerner 1965). The impact ranges for 7 additional trajectories were calculated using this drag coefficient; the results are given in Table 3-5. As shown, there is some scatter in the ratio of the calculated range to the range from the film analysis. Figures 3-2 and 3-3 show two additional comparisons of full trajectories.

Table 3-5. Impact ranges for drag coefficient determination for HUSKY JAGUAR 2.

Film Traj. Number	R Film m	R Calc. m	R Calc./ R Film
25	53.66	53.66	1.00
6	334.13	278.65	0.83
16	194.26	179.17	0.92
18	71.40	69.82	0.98
20	113.77	106.83	0.94
28	132.02	155.87	1.18
39	66.76	63.50	0.95
40	67.25	67.95	1.01
		Mean	0.98

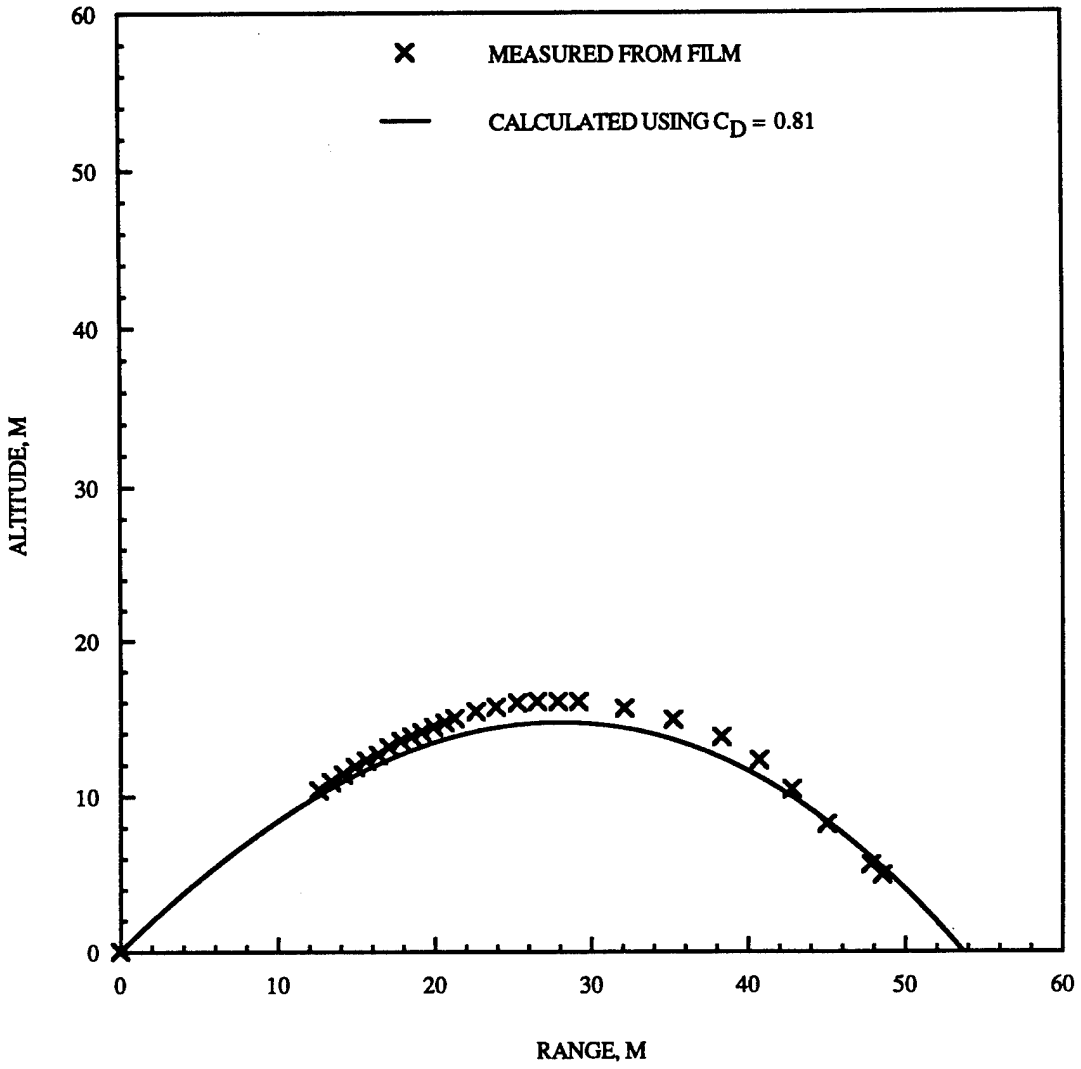

Figure 3-1. Comparison of calculated trajectory with trajectory 25 from film analysis for HUSKY JAGUAR 2.

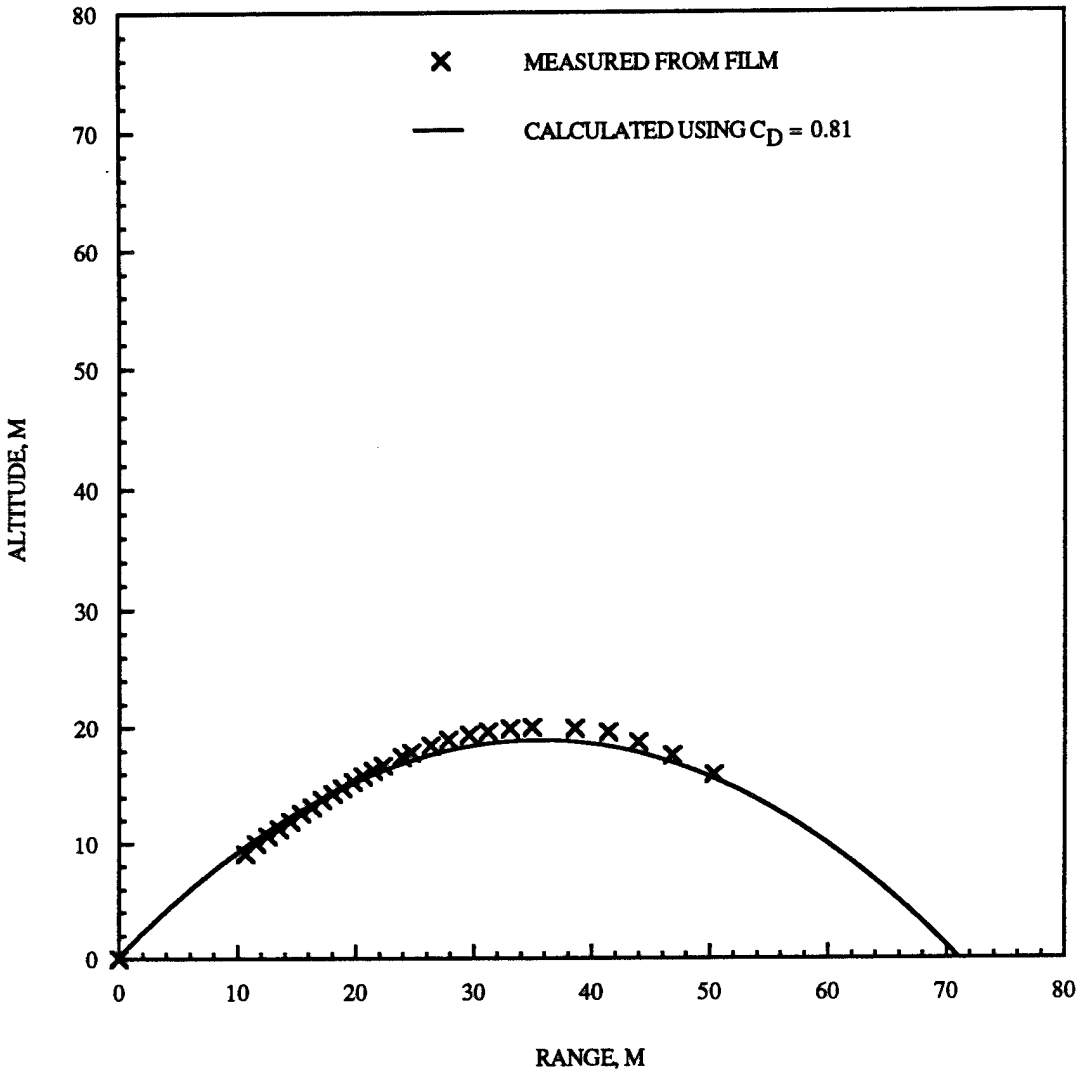

Figure 3-2. Comparison of calculated trajectory with trajectory 18 from film analysis for HUSKY JAGUAR 2.

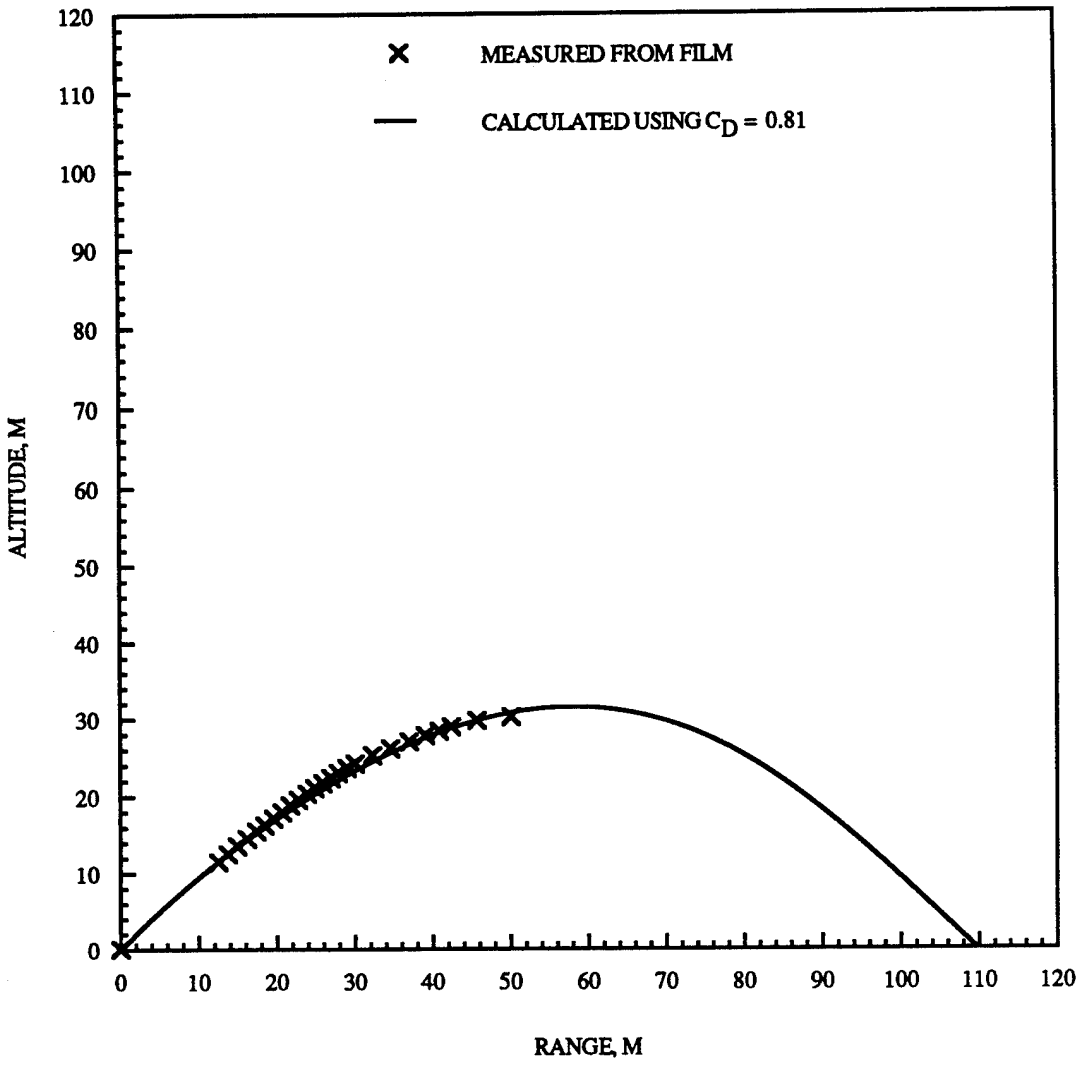

Figure 3-3. Comparison of calculated trajectory with trajectory 20 from film analysis for HUSKY JAGUAR 2.

The identities of the objects tracked on the films could not be positively determined and it was not possible to associate the ejection velocities and the impact ranges with the origins of the objects in the crater (Seebaugh 1994). Additional information relating these parameters was obtained from the pre-test predictions (Rocco 1993). The trajectories of the 29 surface implants were calculated using the predicted ejection velocities and a drag coefficient equal to 0.81. Since HUSKY JAGUAR 2 was a deeply buried detonation, the shock wave and the expanding detonation products pushed the soil above the charge upward and outward. The calculated ejection velocities were taken to be the maximum velocities that tracer points in the calculation reached as the soil was ejected; the locations where the maximum velocities occurred were above the original surface of the test bed (the usual definition of ejection velocity for a near-surface burst is the velocity of the tracer point as it crosses the original ground surface). The vertical and horizontal velocity components of the top layer of soil in the calculation are given by the "x" and "+" symbols in Figure 3-4. Fifth order polynomials (solid lines in Figure 3-4) were fit to the points to permit interpolation of the velocity components as functions of the initial range from SGZ.

The trajectory of each surface implant was calculated using the ejection velocity components from Figure 3-4 and a drag coefficient of 0.81. The resulting impact ranges are given in Table 3-6 (third column) and Figures 3-5 (aluminum cubes) and 3-6 (plastic cubes). Figure 3-5 shows that the predicted impact ranges were greater for the aluminum cubes (solid curve) than for plastic cubes (dashed curve) with equal ejection velocities for initial ranges less than about 3.7 m. This was a result of the greater masses of the aluminum cubes compared to the plastic cubes. For greater initial ranges, the calculated impact ranges were essentially identical for both types of cubes at same ejection velocities. The differences noted in Table 3-6 for comparable cubes (HJ2 56 versus D13, HJ2 66 versus D14, HJ2 67 versus D15, and HJ2 70 versus D16) were caused by the slightly greater ejection velocities for the aluminum cubes.

It was initially anticipated that the ratios of impact ranges for the aluminum cubes to those for the plastic cubes would provide the information required to determine any effect of the impedance mismatch between the artificial ejecta implants and the test bed soil on the ejection velocity. The calculations discussed above show that these ratios were determined primarily by the greater masses of the aluminum cubes; therefore, this approach was inconclusive.

An alternative approach was then attempted--examination of the ratios of the actual ranges to the predicted ranges for the aluminum cubes and plastic cubes, respectively. These ratios were larger for the aluminum cubes for initial ranges between about 3 and 4 m (Table 3-6); there was no trend for the smaller or greater initial ranges. This approach was also inconclusive

With no conclusive information on the effects of the impedance mismatch between the implants and the soil available from the impact ranges of the implants, evidence on the possible differences in ejection velocities between the aluminum cubes and the test bed soil was sought from the high resolution film (the plastic cubes were all implanted on the opposite side of the test bed and were not visible on the film). On the first frame in which each object identified as an ejecta implant was visible, the object was slightly ahead of the nearby soil mass. Before that time, the object was obscured by the soil. The velocity of the soil mass was decreasing faster than the velocity of the object, indicating that the motion of the soil was affected more by aerodynamic drag than that of

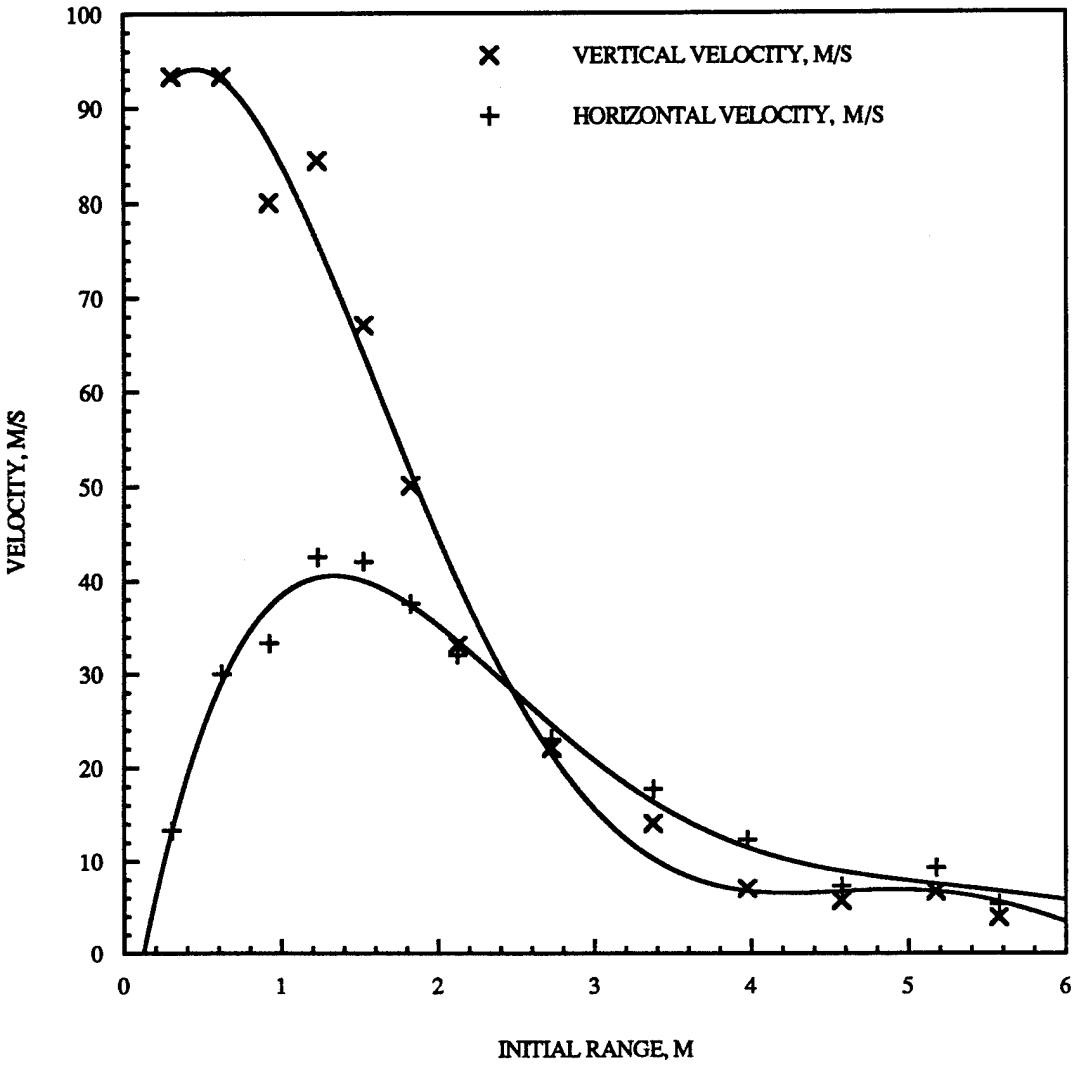

Figure 3-4. Ejection velocity components from pre-test prediction for surface soil layer for HUSKY JAGUAR 2.

Table 3-6. Comparison of calculated and measured impact ranges for HUSKY JAGUAR 2.

Implant Number	R Initial m	R Calc. m	R Exper. m	R Exper./ R Calc.
HJ2 11	0.29	66.4	288.7	4.35
HJ2 23	0.59	140.6	269.0	1.91
HJ2 34	0.89	179.3	251.9	1.40
HJ2 41	1.19	201.9	201.5	1.00
HJ2 42	1.50	201.4	(1)	
HJ2 49	1.80	176.4	199.8	1.13
HJ2 50	2.11	149.8	(1)	
HJ2 52	2.41	117.7	128.2	1.09
HJ2 53	2.71	84.8	(1)	
HJ2 54	3.03	55.6	67.5	1.21
HJ2 56	3.33	36.6	63.8	1.74
HJ2 66	3.63	25.3	46.2	1.83
HJ2 67	3.93	19.6	36.6	1.86
HJ2 70	4.54	16.4	15.3	0.93
D01	0.33	49.4	(1)	
D04	0.63	92.9	183.8	1.98
D05	0.95	116.8	178.4	1.53
D06	1.27	127.4	182.3	1.43
D07	1.54	127.1	130.2	1.02
D08	1.85	120.2	133.5	1.11
D09	2.16	105.8	120.6	1.14
D10	2.46	87.5	106.4	1.22
D11	2.79	64.6	73.5	1.14
D12	3.08	45.7	59.5	1.30
D13	3.40	31.0	44.8	1.45
D14	3.69	22.7	31.8	1.40
D15	4.00	18.3	13.1	0.72
D16	4.61	15.9	19.5	1.21

(1) Not recovered.

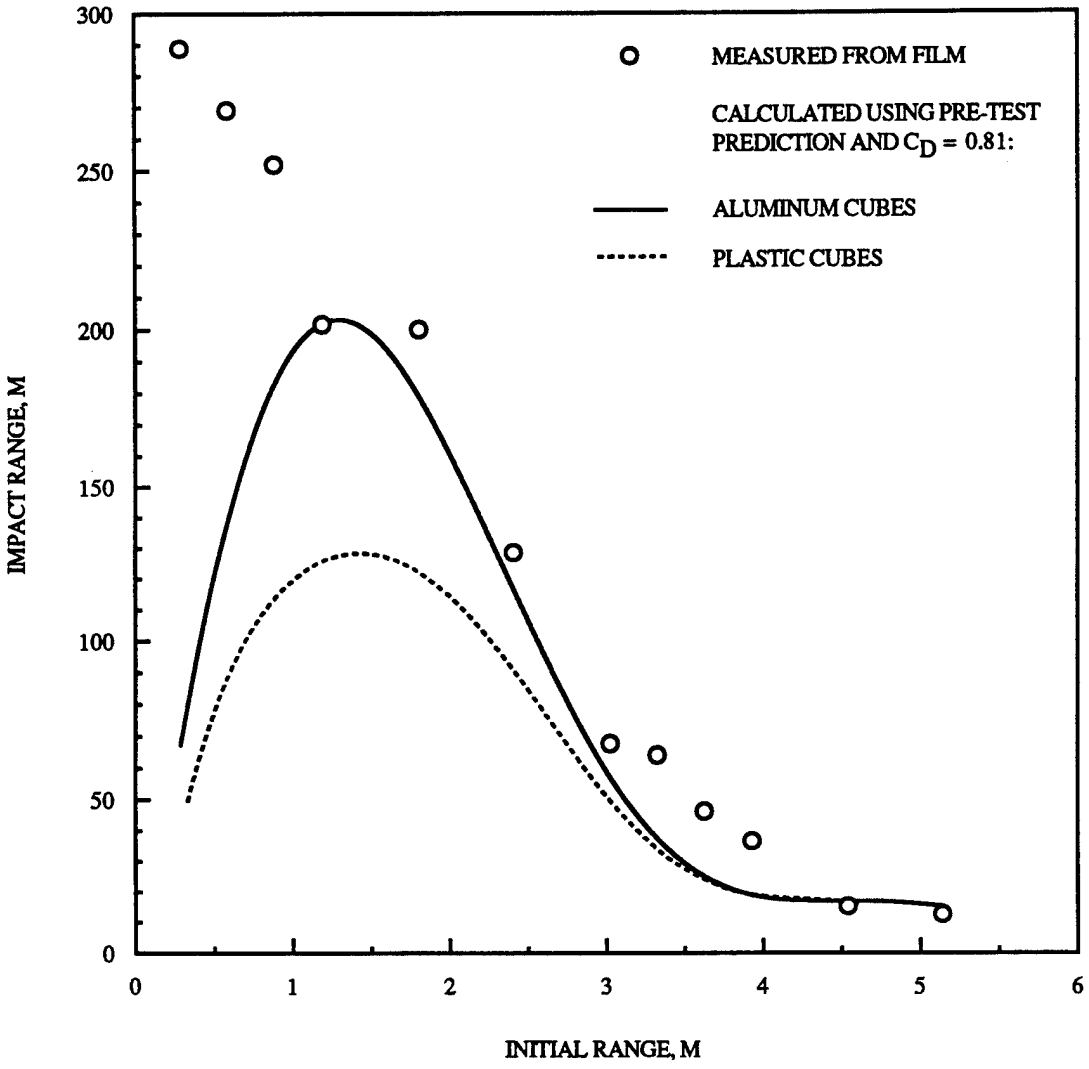

Figure 3-5. Comparison of calculated and measured impact ranges for aluminum implants on HUSKY JAGUAR 2.

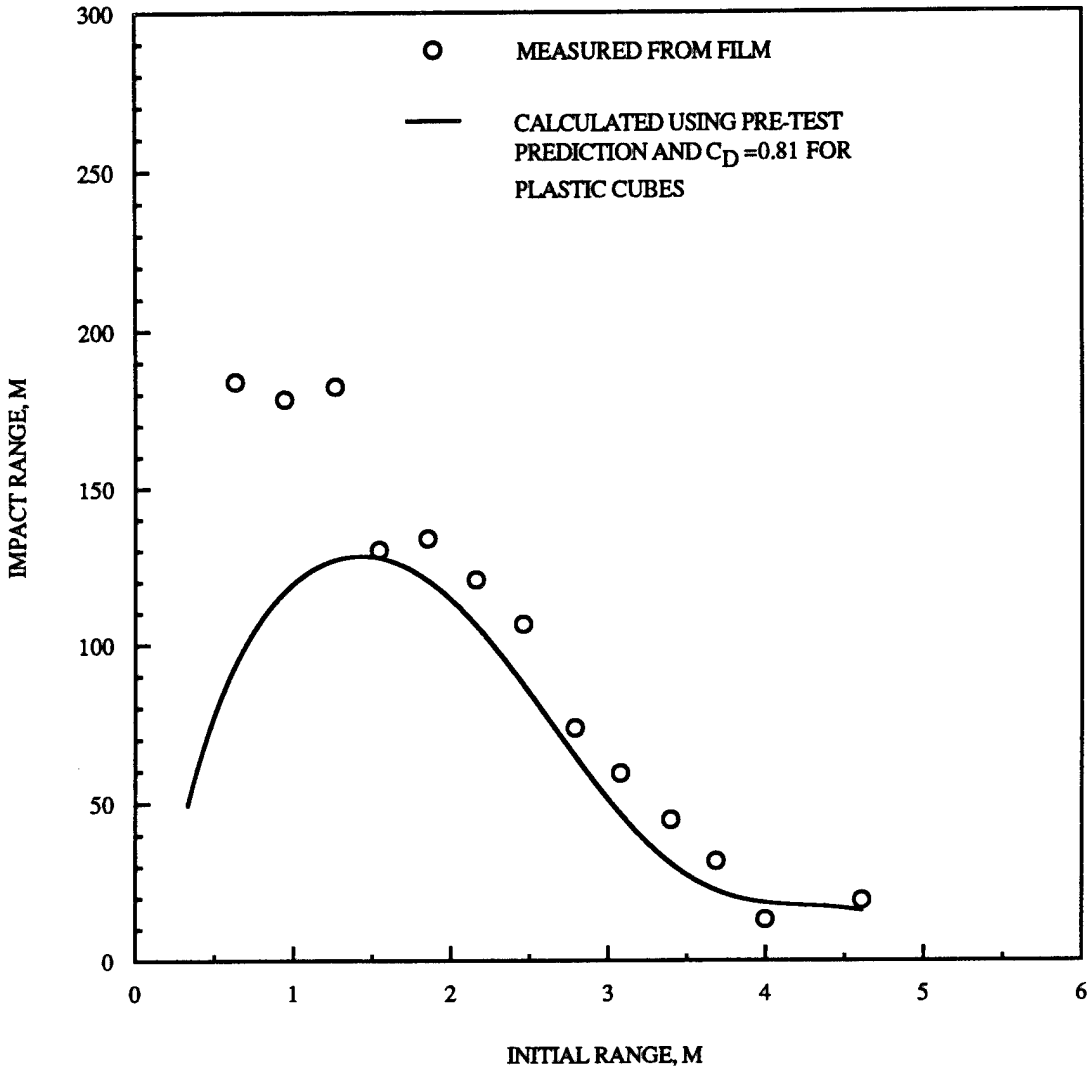

Figure 3-6. Comparison of calculated and measured impact ranges for plastic implants on HUSKY JAGUAR 2.

the aluminum cube. The conclusion from these observations was that the ejection velocities of the cubes and the soil were not significantly different.

None of the results of the artificial ejecta experiments for HUSKY JAGUAR 2 suggest that the ejection velocities of the artificial ejecta implants were higher than the velocities of the adjacent soil. We therefore conclude that the ejection velocities of artificial ejecta implants, which can be determined much more readily than the ejection velocities of the test bed soil, can be considered to represent the soil velocities within the accuracy of the experiments.

The final comparison for HUSKY JAGUAR 2 was between the impact ranges calculated using the ejection velocities from the pre-test predictions and the actual impact ranges of the aluminum and plastic cubes. The experimental ranges for the cubes implanted closest to the SGZ were considerably greater than the predicted values, with the opposite trend with decreasing initial range (Figures 3-5 and 3-6). This result is believed to be due to the presence of the fill pipe for the buried nitromethane charge which extended from the charge container through the sand layer to the test bed surface. The pipe was ejected upward at a velocity exceeding 300 m/s (Seebaugh 1994), resulting in almost immediate venting. This anomaly caused an outward expansion that was not predicted (the pre-test prediction did not include any effects of the pipe and the flange that attached it to the charge container).

Figures 3-5 and 3-6 show that the predicted impact ranges were too low for initial implant ranges between about 3 and 4 m. It is shown in Section 5 that this is a result of the underprediction of the vertical velocity component.

No conclusions can be drawn from the ejecta experiments fielded on HUSKY JAGUAR 2 regarding the validity of the multiphase effective stress pore-air model. The predicted maximum stresses in the ejecta region were less than 1 kbar (Rocco 1993). Significant pore pressures would not be developed in Socorro plaster sand at these low stress levels.

More information could have been obtained from the artificial ejecta experiments if it had been possible to positively identify the implants on the high resolution films. It is necessary to identify every implant to remove all ambiguities from the data analysis. This can be accomplished by using a smaller number (five to ten) of larger implants. This approach was used successfully on the halfspace simulation of event HUSKY JAGUAR 2 (Section 5).

3.3 LABORATORY TESTING.

The soil properties for Socorro plaster sand were summarized in the mechanical property recommendations for event MIDNIGHT HOUR 2, which was the event before HUSKY JAGUAR 1 (Phillips 1991). The recommended properties were: dry density, 1.78 g/cm^3; water content, 4 percent; specific gravity, 2.69; and air voids content, 26.7 percent. Ten particle size distributions were also included in the recommended properties. NMERI measured the specific gravity and particle size distribution for several pre-test samples of Socorro plaster sand obtained during the construction of the HUSKY JAGUAR 1 and 2 test beds. The results for the upper layers of the test beds which contained the ejecta implants were similar to the recommended properties for MIDNIGHT HOUR 2 (Phillips 1991).

A laboratory test program similar to that described in Section 2.5 for WSMR/PHETS soil was initially planned for Socorro plaster sand. This program would

compare soil samples after hydrostatic compression to pre-test soil and soil samples from volumetric strain cans to determine changes in the particle size distribution. It was obvious after completing the hydrostatic compression tests on the WSMR/PHETS soil (Appendix B) that similar testing of the Socorro plaster sand used for the HUSKY JAGUAR 1 and 2 test beds would produce the same result, that is, no observable change in particle size distribution following compression to 10,000 psi (0.7 kbar). The stress required to produce lockup for Socorro plaster sand was about 7.5 kbar (Phillips 1991), so that it was considered unlikely that measurable pore pressures would be present in this material at a stress of 0.7 kbar (the maximum level attainable in the available test cell). Also, none of the volumetric strain cans implanted in the region of maximum ejection velocity for HUSKY JAGUAR 1 survived the detonation, and no intact natural ejecta fragments were found following either event. With no post-test samples available, the laboratory test program for Socorro plaster sand was terminated.

We anticipate that hydrostatic compression of samples of Socorro plaster sand to stresses sufficient to produce lockup would provide data that could be used in developing new material models, especially if the pore pressure can be measured during the tests. We recommend that such tests be performed at WES.

SECTION 4

EVALUATION OF MULTIPHASE EFFECTIVE STRESS PORE-AIR MODEL

At the conclusion of the calculational effort that followed the MINOR SCALE and MISTY PICTURE events (Section 1), we had two very dissimilar material models giving nearly identical results. The question was: which material model was correct? It is possible that pore air and dilatancy effects were both operative simultaneously under certain loading conditions. Finding the answer to this question was the driving force for the Phase II research program.

The peak stress calculated for the region of the test bed from which the high speed ejecta fragments originated for MINOR SCALE was about 0.3 to 2.0 kbar (Koik, Schuster, and Hassig 1990). For WSMR/PHETS soil the stress at lockup was about 0.3 kbar for the most dense layer for MINOR SCALE (estimated properties given by Phillips 1985); the range of stress at lockup for the DISTANT IMAGE pre-test soil was 0.2 to 0.4 kbar. Assuming that the actual stresses imposed on the ejected material were similar to the calculated values, it is reasonable to conclude that the soil which formed the high speed ejecta fragments reached lockup conditions.

The two phases in the multiphase effective stress pore-air model are the soil skeleton and air. The pore air is assumed to be compressed adiabatically during the compression event. In order to provide any significant pneumatic push to the soil during unloading, the pore air must reach high pressures. For the most dense surface layer for MINOR SCALE with an air voids content of 20 percent (Table 2-6) an air volume reduction to about 0.15 percent is required to produce a pore air pressure of 0.1 kbar. For a dry soil (the model assumes zero water content) significant fracturing of soil grains would accompany a volume reduction of this magnitude.

The experimental program described in Section 2 was undertaken to determine if significant soil grain fracture occurred in the soil ejected from the craters during events DISTANT IMAGE and MINOR UNCLE. No measurable increase in the fraction of fine particles occurred for: (1) pre-test DISTANT IMAGE soil samples compressed hydrostatically to 10,000 psi (0.7 kbar), (2) soil in aluminum cans emplaced pre-test in the DISTANT IMAGE test bed, and (3) actual long-range ejecta fragments for MINOR UNCLE.

The WSMR/PHETS soil is not dry, but has a water content of 7 percent or higher. The pore air and pore water are distributed within the soil skeleton, forming a three phase system. The pore water occupies a volume comparable to that of the pore air. The effects of this relatively large volume of pore water are ignored in the multiphase effective stress pore-air model. For quasi-static loading conditions, it is likely that the pore air is dissolved into the pore water as lockup is approached (Appendix B), forming a two phase system with water as the second phase rather than air as assumed in the multiphase effective stress pore-air model. Upon unloading, the air comes out of solution and the three phase system is restored. A pneumatic push comparable to that obtained with an earlier pore air model (Koik and Schuster 1987; Koik, Schuster, and Hassig 1990) is the probable result. Dynamic testing must be performed to determine if these phenomena occur in very rapid compression events (Appendix B).

At the initiation of the program described in this report, the existing experimental evidence for volume expansion due to dilatancy was very strong (Lee 1989). Quoting the relevant paragraph: "The fact that dry soil dilates (i.e., expands due to shear) is common knowledge among soil engineers. In the field of cratering and ground shock, much has been learned in recent years about how geomaterials dilate. First, the sand column data of the NSS event (1983) indicted no permanent compaction of the material in the vicinity of the crater. Second, the velocity-time history data of the MILL YARD event (1985) indicated a rapid volume recovery upon unloading for Yuma soil. Third, we noted a lack of significant depression of the crater bench (just outside the crater) in the DRY CARES event (1986), as well as the DRY CARES sand column data that showed no permanent compaction. Fourth, the laboratory data from both WES and Terra Tech that followed MILL YARD strain paths also showed dilatant behavior."

The same behavior was observed for the natural ejecta fragments from the DISTANT IMAGE event--the mean density of the recovered ejecta fragments was essentially identical to the density of the pre-test soil. The laboratory tests showed that the air voids were removed by loading pre-test samples to 0.2 to 0.4 kbar, which is the lower end of the predicted maximum stress levels for the high speed ejecta. It appears that the natural ejecta fragments from DISTANT IMAGE were subjected to a compression event sufficient to cause lockup, followed by complete volume recovery.

The meeting held in April 1991 to review the physics incorporated into the multiphase effective stress model was reviewed in Section 1. Subsequently, Lee (1993) reviewed the crush curves for Yuma soil and two Socorro plaster sands. He concluded that the air pressure in the material being ejected from the crater was only a few bars, which was not sufficient to drive the high speed ejecta. In a reply, Rosenblatt (1993) asserted that "the high speed ejecta is driven by the nature of the release paths down to low stresses for both the ejected material and the material subjected to higher stresses which acts to accelerate the ejecta...Both dilatancy and pore air can keep the stresses/pressures sufficiently high during unloading to produce high ejecta velocities in agreement with experimental data. If the dilatancy is sufficiently high in both the ejecta and higher peak stress regions, then pore pressure effects can be negligibly small...dilatancy alone does not explain many aspects of cratering, ejecta or ground motion phenomenology...we recommend using a constitutive model which includes both dilatancy and pore air effects--they do both occur! This is the approach being taken in future CRT cratering and ground motion calculations. It appears to be the only prudent, and the most physically realistic, approach because it is not possible to assess the relative importance of dilatancy vs. pore air prior to doing the calculations."

The statements quoted above are in essential agreement with the conclusions of the April 1991 meeting (Seebaugh 1991). Unfortunately, the suggested approach was not implemented in the CRALE2 code for the pre-test predictions for events HUSKY JAGUAR 1 and 2 and the multiphase effective stress pore-air model was the only model used for those calculations.

The material properties included in the models were derived for very simple strain paths. In order to determine the degree of dilatant behavior of any soil under specific strain paths (such as those associated with the high speed ejecta and the soil subjected to higher stresses that provides some of the push) it is necessary to define a range of strain paths for the region of interest and perform laboratory tests for these strain paths.

The following procedure was recommended at the April 1991 meeting for obtaining the dilatant behavior of WSMR/PHETS soil using the soil samples obtained from the compacted near surface region prior to DISTANT IMAGE (Seebaugh 1991): (1) determine the strain paths from the existing CRALE2 calculations, (2) determine the soil response in the laboratory for the calculated strain paths, and (3) rerun the calculations to determine which effect dominates (probably using a material model which includes both pore air and dilatancy effects). Unfortunately, this procedure could not be carried out for DISTANT IMAGE using existing calculational results because the needed information was not saved.

While performing the pre-test predictions for HUSKY JAGUAR 1, Rocco (1991) determined the (calculated) strain paths for a number of target points from the ejecta region of the test bed. These strain paths are available to be used as a guide for strain path testing of reconstituted specimens of Socorro plaster sand from the HUSKY JAGUAR 1 test bed. WES has the testing equipment required to perform these tests and also has considerable experience with Socorro plaster sand. Strain path tests (including pore pressure measurements until saturated soil behavior was obtained) on HUSKY JAGUAR 1 soil samples were requested by SEA as Government Furnished Information, but were not provided during the period of performance of the current research program.

SECTION 5

EJECTA SCALING EXPERIMENT

The goal of this experiment was to obtain data for two scaled events to determine the scaling relationship for the velocity of the high speed ejecta. The surface implant experiment conducted on event HUSKY JAGUAR 2 was discussed in Section 3. A scaled HUSKY JAGUAR 2 experiment (DHS-93-021) was conducted in the halfspace facility on 20 June 1993. The linear scale factor (full scale/halfspace) was 36.5. The surface ejecta experiment was performed on the halfspace test using scaled artificial ejecta implants emplaced at scaled ranges in the test bed.

Figure 5-1 (Roupas 1993) shows the halfspace facility as arranged for an earlier HUSKY JAGUAR 2 test (AHS-92-018). The facility (Roupas 1987 and 1988, Bair 1988) consists of an 8-ft (2.4-m) diameter steel vessel with a vertical transparent window mounted with one vertical surface placed along a diameter of the vessel. The test bed is constructed in half of the vessel; the other half is open to permit unobstructed viewing through the transparent window. A hemispherical charge was mounted at the scaled depth of burst on a metal sabot with the base of the charge flush with the halfspace side of the window. A grout slab was located at the appropriate depth to simulate the concrete layer in HUSKY JAGUAR 2. The test bed was Socorro plaster sand placed with the prescribed density and water content for the full scale HUSKY JAGUAR 2 event. The rectangles A, B, and C in Figure 5-1 delineate the locations of soil density measurements performed using a nuclear densitometer.

The surface ejecta implants used on the actual HUSKY JAGUAR 2 event, 2-in (5-cm) aluminum and plastic cubes, performed satisfactorily on that event (except that they were too small to positively identify on the film). Using cubes as scaled implants, exact scaling gave 0.12-in (0.3-cm) cubes. These were considered to be too small to photograph at the anticipated ejection velocities; therefore, 0.25-in (0.64 cm) cubes (aluminum and plastic) were implanted in the halfspace test bed at the same scaled distances from SGZ as in the actual HUSKY JAGUAR 2 event. The locations are shown in Figure 5-2.

The film from halfspace test DHS-93-021, which was exposed at a rate of 983 frames per second, contained trackable images of the closer of the two arrays of 10 ejecta implants; the cubes in the second array were apparently directly behind the visible cubes and could not be identified on the film. The film analysis was performed using a Vanguard Motion Analysis System.

The results of the film measurements are given in Table 5-1. The implants are numbered in order of increasing initial range (Figure 5-2). The second column in Table 5-1 gives the time interval over which each implant was actually tracked. The same zero time was assumed for all fragments. The horizontal and vertical coordinates of the first ten points (including the initial range at the zero time) were fitted with straight lines using the least squares method. Even though the time after detonation of the first tracked point (the second point on each trajectory) increased substantially for the higher numbered implants, all of the coordinates were extremely close to the linear fits. The curvefit coefficients are given in Table 5-1 for the form

$$X \text{ (or } Z) \text{ in m/s} = A + B \times \text{Time in s}$$

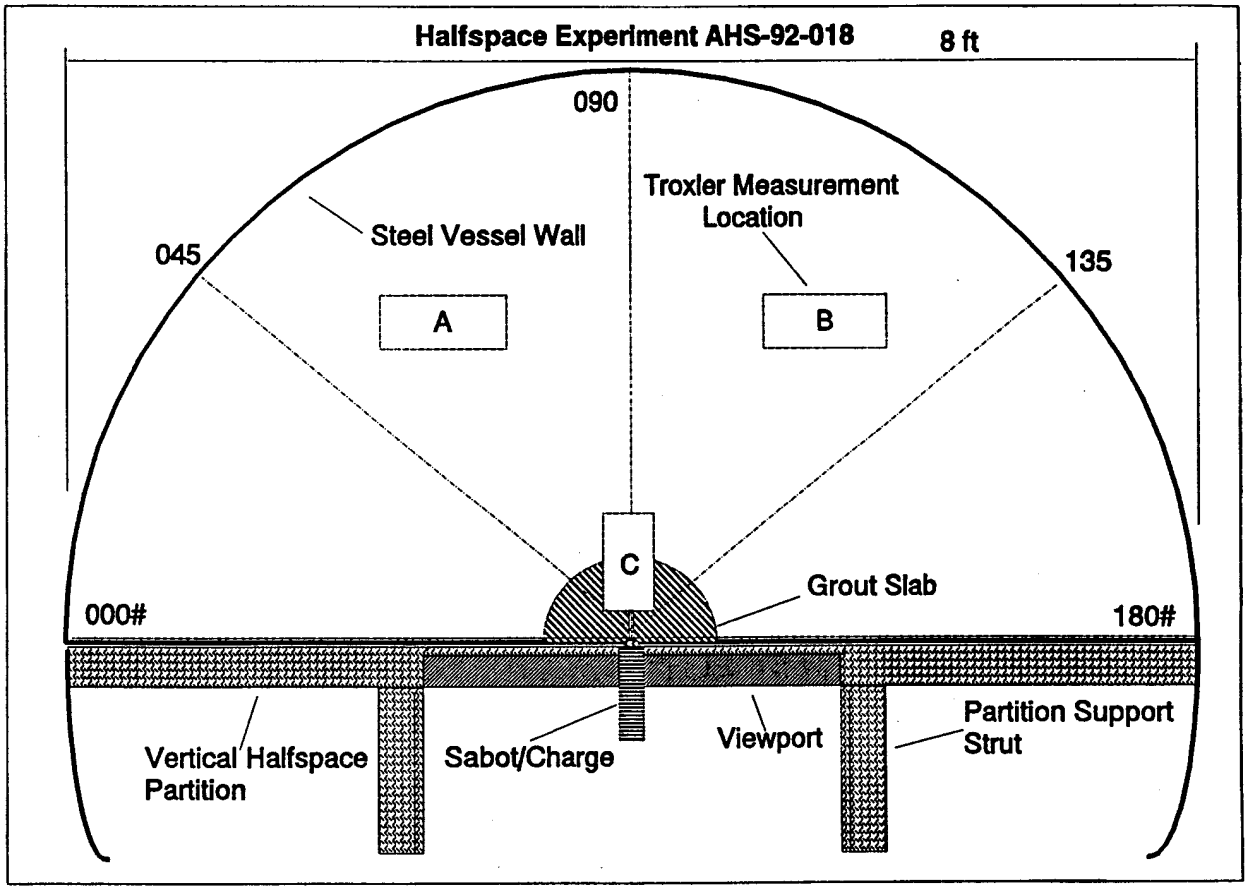

Figure 5-1. Plan view of halfspace facility.

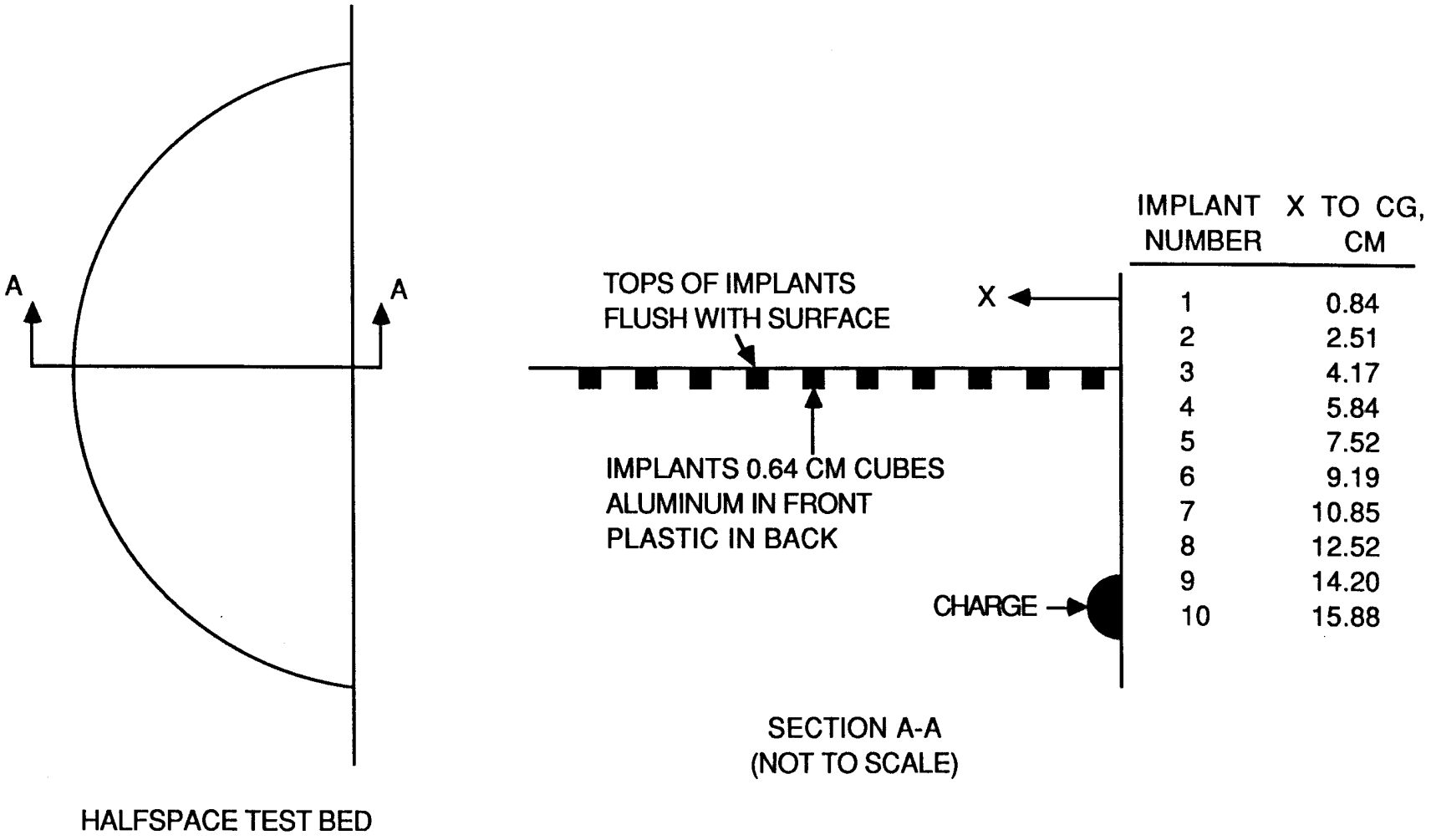

Figure 5-2. Ejecta implant array for halfspace simulation of event HUSKY JAGUAR 2.

Table 5-1. Film analysis results for HUSKY JAGUAR 2 halfspace test.

Implant Number	Start/ Stop ms	X Velocity Coefficients A	X Velocity Coefficients B	Z Velocity Coefficients A	Z Velocity Coefficients B	Vel. m/s	Angle deg.
HS 1	6.10 14.24	3.4857E-3	1.6247E+1	-2.8938E-2	1.0996E+2	111.2	81.6
HS 2	8.14 17.29	1.5430E-2	3.5478E+1	-8.4732E-3	8.6152E+1	93.2	67.6
HS 3	11.19 25.42	3.6965E-2	4.1033E+1	-1.4206E-3	5.9394E+1	72.2	55.4
HS 4	10.17 40.68	5.1889E-2	3.2170E+1	-5.2026E-3	3.7926E+1	49.7	49.7
HS 5	10.17 56.95	7.0375E-2	2.3665E+1	-4.3671E-3	2.6673E+1	35.7	48.4
HS 6	11.19 85.42	8.5799E-2	1.6172E+1	-5.4715E-3	1.8359E+1	24.5	48.6
HS 7	26.44 117.97	1.0594E-1	1.1543E+1	-4.8732E-4	1.3484E+1	17.8	49.4
HS 8	34.58 414.92	1.2210E-1	9.0746E00	5.8651E-4	1.0012E+1	13.5	47.8
HS 9	48.81 219.66	1.3745E-1	7.0598E00	-9.5176E-4	7.2857E00	10.2	45.9
HS 10	69.15 284.75	1.5767E-1	5.3402E00	3.1302E-3	4.9221E00	7.3	42.7

so that the velocity components in m/s are equal to the B coefficients. The resultant velocities and ejection angles (relative to the horizontal) are also given in Table 5-1.

The measured velocity components for the halfspace test are compared to the full scale pre-test prediction for HUSKY JAGUAR 2 (Rocco 1993) in Figures 5-3 and 5-4. The horizontal axis on each graph is the full scale initial implant range. The ability to compare individual velocity components rather than a composite parameter such as the final range (as for the full scale test in Section 3.2.2) precisely delineates the two areas of disagreement between the pre-test prediction and the halfspace data. The first is the region near the charge, where the vertical velocity for the first implant (Figure 5-4) is about 25 percent higher than the predicted value. This is probably an artifact of the method of obtaining the velocities from the output of the cratering calculation (Rocco 1993) and is not considered significant. The second is the region from about 2.5 to 5 m initial implant range (full scale), where the predicted vertical velocity components are substantially below the halfspace measurements. This disagreement also occurred for the full scale HUSKY JAGUAR 2 results for the initial range interval of about 3 to 4 m (Section 3.2.2).

As discussed in Section 3.2.2, it was impossible to positively associate the film measurements for the full scale HUSKY JAGUAR 2 event with individual ejecta implants. This was not a problem on the halfspace event since the entire array of 10 implants was discernible on the film. If the opportunity occurs to perform a similar experiment at full scale and in the halfspace facility, a smaller number of larger implants should be used on the full scale event to increase the probability of positively identifying all of the ejecta implants on the films of both events.

Using the theory of dimensional analysis, Housen, *et al.* (1983) and Mazzola and Lee (1989) observed that in the strength regime the velocity of material ejected from the region inward from the crater rim is invariant at geometrically scaled locations. The agreement between the impact ranges calculated using the pre-test predictions for the full scale HUSKY JAGUAR 2 event and the measured impact ranges (Figures 3-5 and 3-6) and the agreement between the calculated ejection velocities from the full scale pre-test predictions and the measured ejection velocities for the halfspace simulation (Figures 5-3 and 5-4) were quite good. When these results were considered together, the only possible conclusion is that the ejection velocities for the surface soil layer for the two events were invariant at geometrically scaled locations.

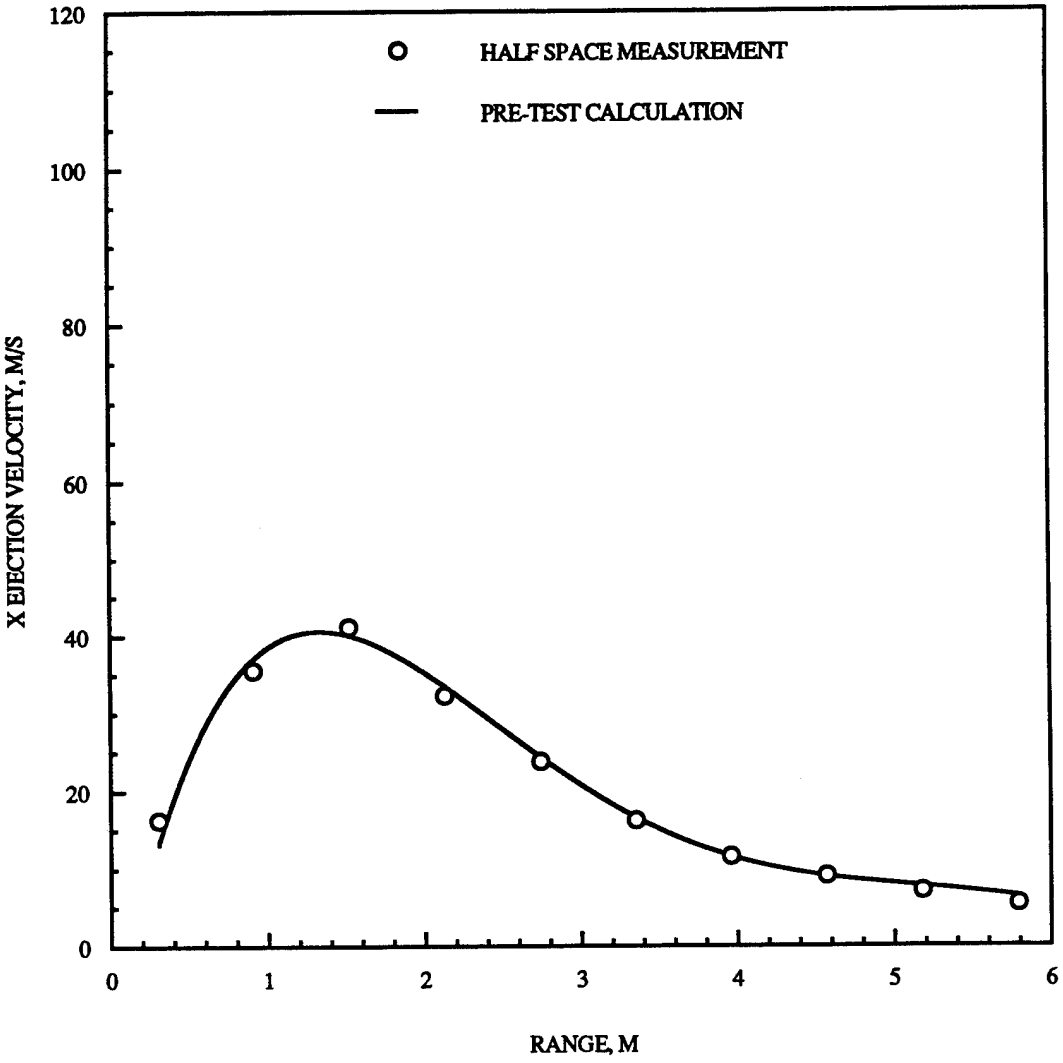

Figure 5-3. Comparison of horizontal velocity component from pre-test calculation to measurements from halfspace test for HUSKY JAGUAR 2.

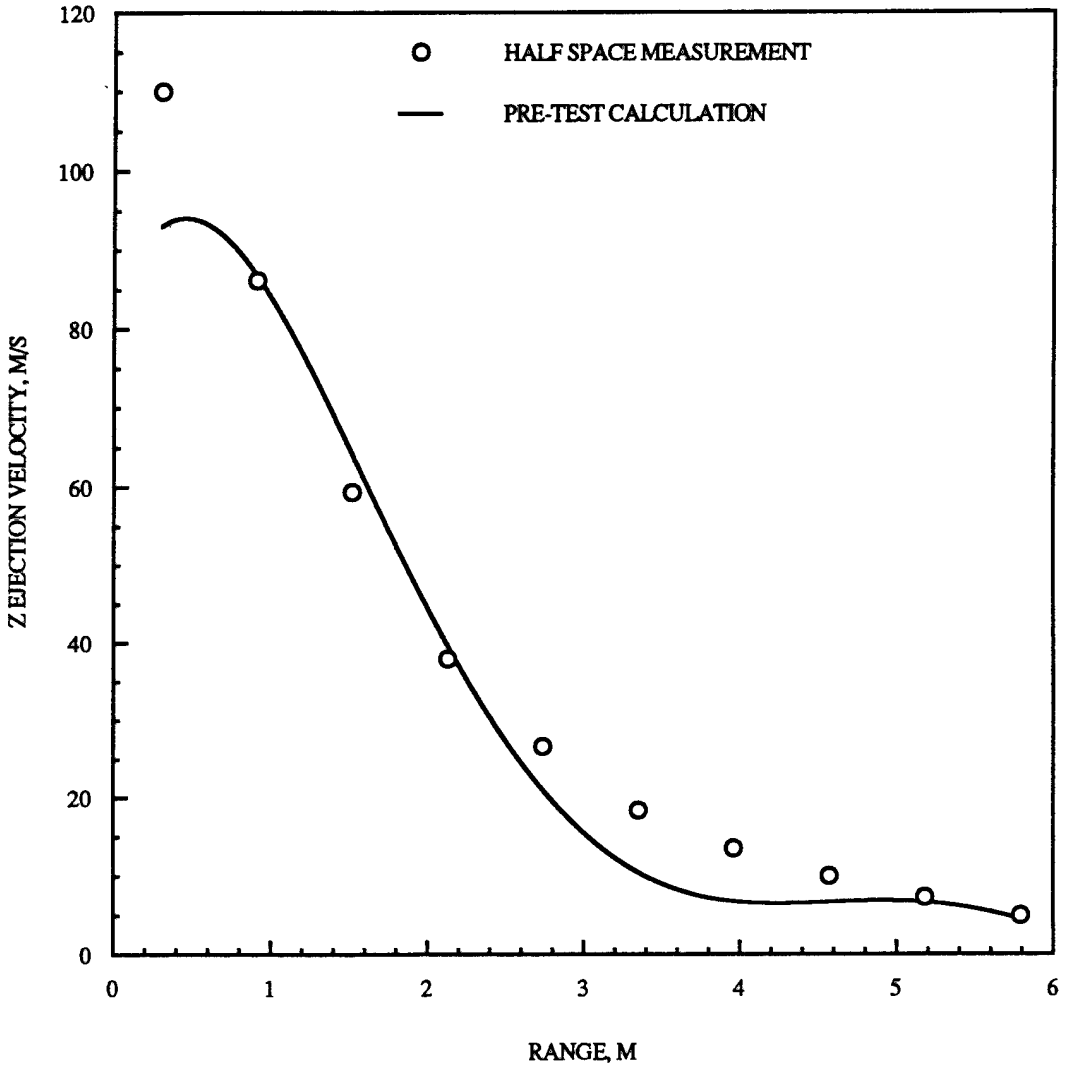

Figure 5-4. Comparison of vertical velocity component from pre-test calculation to measurements from halfspace test for HUSKY JAGUAR 2.

SECTION 6

CONCLUSIONS

This section presents key conclusions and describes observations drawn from the results of this Phase II research program.

1. The objectives of the program (delineated in Section 1) were satisfied.

2. The multiphase effective stress pore-air model, which was the first material model to enable cratering codes to predict the high ejection velocities observed experimentally for the WSMR/PHETS soil, uses incorrect physics and should be rejected. The model permits the pore air pressure to increase to unreasonably high levels at volume strains approaching lockup. It is this high pore air pressure that provides the added push to increase the ejection velocities in the multiphase effective stress pore-air model. For a dry soil (the model assumes zero water content) significant fracturing of soil grains would accompany a volume reduction of this magnitude. In the experimental program described in this report no measurable increase in the fraction of fine particles occurred for: (1) pre-test DISTANT IMAGE soil samples compressed hydrostatically beyond lockup, (2) soil in aluminum cans emplaced pre-event in the DISTANT IMAGE test bed, and (3) actual long-range ejecta fragments for MINOR UNCLE. In the DISTANT IMAGE event, the mean post-test density of the natural ejecta fragments was equal to the pre-test soil density in the test bed. These fragments were subjected to a compression event sufficient to cause lockup and exhibited complete volume recovery, a typical dilatant response.

2. Dilatancy is an important soil response that must be considered in cratering calculations that attempt to predict the initial conditions for high speed ejecta for the WSMR/PHETS soil and other similar soils. The behavior of the pore water at loading conditions approaching lockup must also be considered.

3. Strain path testing of dilatant soils in the laboratory will provide a valuable input to material modeling for these soils.

4. The suction-water content relationship for WSMR/PHETS soil indicated that the soil was granular with a high dissolved salt content. The latter characteristic can cause the soil to hold together due to the tension in the pore water. This conclusion is consistent with the tendency of this soil to form large natural ejecta fragments.

5. High resolution photography of artificial ejecta objects implanted in the test bed provided data for comparisons with the results of code calculations on the ejection velocities for two 1,000 lb (454 kg) events conducted in Socorro plaster sand. Good agreement was obtained between the impact ranges calculated using the pre-test predictions for ejection velocities and the experimental impact ranges for the surface soil layer for event HUSKY JAGUAR 2. Due to the small size of the ejecta implants it was not possible to positively identify individual implants and thus permit an unambiguous association of the trajectories extracted from the films with specific implants. This association should be possible using the same camera plan with a smaller number of larger implants.

6. High speed photography of artificial ejecta implants in the test bed of the DNA halfspace facility was highly successful and provided data on ejection

velocities for direct comparison with the results of code calculations. Excellent agreement was obtained between the ejection velocities calculated for the surface soil layer for the full scale HUSKY JAGUAR 2 event and the experimental measurements except for the vertical velocity component in the region from about 5 to 9 charge radii.

7. The ejection velocities for the surface soil layer for the full scale HUSKY JAGUAR 2 event and the halfspace simulation were invariant at geometrically scaled locations in the test bed for the scale factor of 36.5.

SECTION 7

RECOMMENDATIONS

Additional laboratory results at higher confining pressures than SEA/NMERI could achieve with the available laboratory apparatus would be useful in implementing an alternative material model that properly includes dilatancy and pore air and pore water effects. These tests should be conducted at WES on WSMR/PHETS soil and Socorro plaster sand. Further modeling and calculational effort will also be required to develop this model.

It is important to perform a representative number of standard laboratory mechanical property tests on specimens of the reconstituted test bed soil for events DISTANT IMAGE, MINOR UNCLE, and any future tests conducted at the same SGZ to obtain a data base for the reconstituted soil, which has been determined to have different properties (especially the air voids content) than the native soil. This testing program should include measurements of the pore pressure build-up as the air voids close and the soil behavior under saturated conditions. This is necessary to experimentally determine the behavior of the soil in the loading regime where the multiphase effective stress pore-air model encountered problems.

A major component of the recommended program is the determination of the soil behavior under strain paths representative of those occurring in the near surface region away from the charge. These tests can be performed using standard laboratory mechanical property test devices. The results of these tests will provide data that are currently unavailable for use in developing material models for code calculations. There may be some difficulty in determining the strain paths; sources of information include the free field ground motion data for events MISERS GOLD and DISTANT IMAGE and prior code calculations for various WSMR events. New code calculations, carried out to times of about 100 ms to capture the ejecta history, may have to be performed for this purpose. New material models that correctly represent the dilatant behavior of the WSMR/PHETS soil should be developed if existing models cannot do so. Follow-up code calculations should be performed to ensure that the modified codes reproduce the measured ejecta velocities.

The experimental approach demonstrated on events DISTANT IMAGE and MINOR UNCLE should be applied on future events which have the potential of producing significant high-speed ejecta contributions to the resulting dust clouds for geologies of interest. This should be done both to continue compilation of a data base for different soils and to enhance the predictive capabilities of cratering/ejecta codes.

The experimental approach demonstrated on events HUSKY JAGUAR 1 and 2 should be applied on future events conducted at the PTB and on scaled events conducted in the halfspace facility. A smaller number of larger artificial ejecta implants should be used to permit positive identification of the objects on high resolution films. The information gained from these tests should be applied to the DNA Conventional Weapons Test Program.

SECTION 8

REFERENCES

Bair, R., "Digitization of High-Speed Cinema for the Air Force Halfspace Facility," (U) New Mexico Engineering Research Institute, Albuquerque, NM, Report NMER-WA8, 1988. (UNCLASSIFIED)

Bell, K.G., J.S. Jarpe, and H.J. Aguilar, "HEST and BLEST Developments for the ASH/ISST Test Program," (U) New Mexico Engineering Research Institute, Albuquerque, NM, AFWL TR 87-33, January 1988. (UNCLASSIFIED)

Benson, K. A., and R.W. Henny, "DISTANT IMAGE Cratering and Related Effects, New Mexico Engineering Research Institute," (U) Albuquerque, NM, NMERI SS 4.07 (6), November 1992. (UNCLASSIFIED)

Benson, K. A., "Test Bed Displacements HUSKY JAGUAR 1, MIDNIGHT HOUR 2, MISTY PORT 3," (U) New Mexico Engineering Research Institute, Albuquerque, NM, in Minutes of HUSKY JAGUAR 1 Results and HJ2-3 Planning Meeting, Field Command, Defense Nuclear Agency, Albuquerque, NM, February 1993. (UNCLASSIFIED)

Black, D.K., and K.L. Lee, "Saturating Laboratory Samples by Back Pressure," (U) *Journal of Soil Mechanics and Foundations Division*, Vol. 99, No. SM1, pp. 75-93, American Society of Civil Engineers, 1973. (UNCLASSIFIED)

England, R.H., S.B. Choi, V.E. Koik, and Y. Muki, "Ground Motion Calculations," (U) California Research & Technology, Inc., Chatsworth, CA, in *MISERS GOLD Symposium Report*, Volume II, POR 7352-2, May 1991. (UNCLASSIFIED)

England, R.H., and S.B. Choi, "DISTANT IMAGE Ground Motion Calculations," (U) California Research & Technology, Div., The Titan Corp., Chatsworth, CA, in *DISTANT IMAGE Symposium Report*, Volume 2, POR 7379-2, April 1993. (UNCLASSIFIED)

Fredlund, D.G., and H. Raharjdo, *Soil Mechanics for Unsaturated Soils*, (U) John Wiley & Sons, New York, NY, 1993. (UNCLASSIFIED)

Hoerner, S.F., *Fluid-Dynamic Drag*, (U) Published by the Author, 1965. (UNCLASSIFIED)

Housen, K.R., R.M. Schmidt, and K.A. Holsapple, "Crater Ejecta Scaling Laws: Fundamental Forms Based On Dimensional Analysis," (U) *J. Geophys. Res., 88,* 2485-2499, 1983. (UNCLASSIFIED)

Koik, V.E., "Multiburst Environments and Fratricide Effects, Task 5, Ejecta Fields, MINOR SCALE/MISTY PICTURE Numerical Simulation of Ejecta Physics," (U) California Research & Technology, Inc., Chatsworth, CA, CRT0988-06PM, October 1988. (UNCLASSIFIED)

Koik, V.E., and S.H. Schuster, "MINOR SCALE Cratering & Ejecta Predictions," (U) California Research & Technology, Inc., Chatsworth, CA, DNA-TR-87-64, 1987. (UNCLASSIFIED)

Koik, V., S. Schuster, and P. Hassig, "Large H.E. Event Ejecta Calculations MINOR SCALE/MISTY PICTURE," (U) California Research & Technology, Inc., Chatsworth, CA, CRT039-09PM, March 1990. (UNCLASSIFIED)

Lambe, T.W., and R.V. Whitman, *Soil Mechanics*, (U) Wiley, New York, 1969. (UNCLASSIFIED)

Lee, C.K.B., Logicon RDA, Los Angeles, CA, Letter to Dr. C. Gallaway, DNA/SPWE, (U) 7 March 1989. (UNCLASSIFIED)

Lee, C.K.B., Logicon RDA, Los Angeles, CA, Letter to M. Rosenblatt, California Research & Technology, Inc., Chatsworth, CA, (U) 19 February 1993. (UNCLASSIFIED)

Lee, C.K.B., and T.A. Mazzola, "Ejecta Scaling Laws for Craters in Dry Alluvial Sites," (U) *J. Geophys. Res., 94,* 17,595-17,605, 1989. (UNCLASSIFIED)

Lowe, T., and T.C. Johnson, "Use of Backpressure to Increase Degree of Saturation of Triaxial Test Specimens," (U) *Shear Strength of Cohesive Soils*, p. 819, American Society of Civil Engineers, 1960. (UNCLASSIFIED)

Lynch, R., J. Wisotski, and T. Samaras, "In-Flight Ejecta Analysis for HUSKY JAGUAR 1," (U) Denver Research Institute, Denver CO, December 1992. (UNCLASSIFIED)

McKeen, R.G., "A Model for Predicting Expansive Soil Behavior," (U) *Proceedings 7th International Conference on Expansive Soils*, American Society of Civil Engineers, August 1992. (UNCLASSIFIED)

Phillips, B.R., "Generalized DIRECT COURSE Profile and Mechanical Property Estimates for use in MINOR SCALE Cratering and Ejecta Calculations," (U) U.S. Army Engineer Waterways Experiment Station, Vicksburg, MS, January 1985. (UNCLASSIFIED)

Phillips, B.R., R.E. Wahl, and J.R. Curro, Jr., "Geotechnical Investigation for DIRECT COURSE and Related Events, Report 1: Results from Subsurface Exploration Programs," (U) U.S. Army Engineer Waterways Experiment Station, Vicksburg, MS, Technical Report S-86-18, September 1986. (UNCLASSIFIED)

Phillips, B.R., "Geotechnical Investigation for DIRECT COURSE: Geologic Profile and Material Property Recommendations, Report 2: Laboratory Test Results," (U) U.S. Army Engineer Waterways Experiment Station, Vicksburg, MS, Technical Report SL-86-18, September 1986. (UNCLASSIFIED)

Phillips, B.R., "Geotechnical Investigation for DIRECT COURSE: Geologic Profile and Material Property Recommendations, Report 3: Geologic Profile and Material Property Recommendations," (U) U.S. Army Engineer Waterways Experiment Station, Vicksburg, MS, Technical Report SL-86-18, September 1986. (UNCLASSIFIED)

Phillips, B.R., "Mechanical Property Recommendations for Posttest Evaluation of the MIDNIGHT HOUR 2 Test," (U) U.S. Army Engineer Waterways Experiment Station, Vicksburg, MS, July 1991. (UNCLASSIFIED)

Phillips, B.R., U.S. Army Engineer Waterways Experiment Station, Vicksburg, MS, Personal Communication, (U) July 1991. (UNCLASSIFIED)

Rocco, J., California Research & Technology, Inc., Albuquerque, NM, Letter to W.R. Seebaugh, (U) University of Denver, Denver, CO, 27 November 1991. (UNCLASSIFIED)

Rocco, J., California Research & Technology, Inc., Albuquerque, NM, Personal Communication, (U) 1993. (UNCLASSIFIED)

Rosenblatt, M., California Research & Technology, Inc., Chatsworth, CA, Letter to C.K.B. Lee, (U) Logicon RDA, Los Angeles, CA, 24 February 1993. (UNCLASSIFIED)

Roupas, P., "Air Force Halfspace Facility Design Report," (U) New Mexico Engineering Research Institute, Albuquerque, NM, Report NMER-WA8-51, 1987. (UNCLASSIFIED)

Roupas, P., "Operation of the Air Force Halfspace Facility," (U) New Mexico Engineering Research Institute, Albuquerque, NM, Report NMER-WA8-69, 1988. (UNCLASSIFIED)

Roupas, P., "Preliminary Report Halfspace Experiment AHS-92-018 HUSKY JAGUAR 2 Developmental Event #1," (U) New Mexico Engineering Research Institute, Albuquerque, NM, Report NMER SS 7.22(1), January 1993. (UNCLASSIFIED)

Schuster, S., Presentation at Ejecta Status Review, (U) Logicon RDA, Los Angeles, CA, 6 December 1989. (UNCLASSIFIED)

SCS, "Soil Survey Laboratory Methods and Procedures for Collecting Soil Samples," (U) *Soil Survey Investigations Report No. 1*, Soil Conservation Service, U.S. Separtment of Agriculture, Washington, DC, 1972. (UNCLASSIFIED)

Seebaugh, W.R., "Ejecta-Fireball Interaction Modeling," (U) Science and Engineering Associates, Inc., Englewood, CO, DNA-TR-87-238, January 1987. (UNCLASSIFIED)

Seebaugh, W.R., "Acquisition of Experimental Data for Use in Constructing Material Models for Calculation of High Speed Ejecta," (U) Science and Engineering Associates, Inc., Albuquerque, NM, July 1991. (UNCLASSIFIED)

Seebaugh, W.R., "In-Flight Ejecta Analysis for HUSKY JAGUAR 2," (U) Applied Research Associates, Inc., Albuquerque, NM, September 1994. (UNCLASSIFIED)

Skempton, A.W., "The Pore Pressure Coefficients A and B," (U) *Geotechnique*, Vol. IV, pp. 143-147, 1954. (UNCLASSIFIED)

Wesevich, J.W., "HUSKY JAGUAR 1 Program Plan," (U) Karagozian & Case, Glendale CA, June 1992. (UNCLASSIFIED)

Wisotski, J., "Dynamic Ejecta Parameters from High-Explosive Detonations," (U) in Roddy, D.J., Pepin, R.O., and Merrill, R.B., eds., *Impact and Explosion Cratering*, Pergamon, New York, pp. 1101-1121, 1977. (UNCLASSIFIED)

Zelasko, J.Z., "DISTANT IMAGE Backfill Properties," (U) U.S. Army Engineer Waterways Experiment Station, Vicksburg, MS, Letter to R.H. England, California Research & Technology, Inc., dated 16 May 1991. (UNCLASSIFIED)

APPENDIX A

LABORATORY SOIL TESTING

A.1 INTRODUCTION.

The New Mexico Engineering Research Institute (NMERI), The University of New Mexico, performed evaluations of soil characteristics and behavior through several types of laboratory testing. This work was performed by R. Gordon McKeen, P. E., and Ken Martinez, both on the NMERI staff. Some high pressure testing was also performed by NMERI and is reported in Appendix B. That work was performed by Lary R. Lenke, P. E., and Thomas Escobedo, also from NMERI. The samples and tests are summarized in Table A-1 and discussed below. Samples were received and tests performed over the period 1 July 1992 through 14 August 1994. Work was performed in the NMERI laboratory facilities located on The University of New Mexico campus in Albuquerque.

Table A-1. Summary of soil samples and tests.

Sample	Sp.Gr.	Suction	Gradation	Density	Hi Pressure
Distant Image-Pre	X	X	X		X
Distant Image-Ejecta	X		X		
Minor Uncle-Pre	X	X	X	X	
Minor Uncle-Ejecta	X		X	X	
Husky Jaguar 1	X		X		

In Table A-1 Sp. Gr. indicates the determination of specific gravity using ASTM D 854, which involves the soils that pass the 4.75 mm (#4) sieve by means of a pycnometer. These data represent the density of individual solid particles in the soil.

Suction refers to the determination of suction and water content at various points for the purpose of defining the suction-water content characteristic curve for the soil (Table A-1). Suction measurements were made using the filter paper method, ASTM D 5298. Gravimetric water contents were determined using ASTM D 2216 procedures. The suction water content determination is an indicator of the existing moisture condition of the soil. The condition is measured in terms of the negative pressure (energy) of the soil water. In addition to the moisture condition at the time of test, the slope of the moisture suction curve is indicative of the soil capability to absorb and hold water, which is an important characteristic.

In Table A-1 gradation is the grain size distribution curve for the soil obtained by ASTM D 422. In some cases these tests included the fine sieve analysis only, on other samples a hydrometer analysis was performed in addition to the fine sieve analysis. The two methods involve different mechanisms for the determination of particle sizes. The fine sieve measures particle size as the size square opening through which the particles pass. The hydrometer measures the particle size by calculating the equivalent spherical diameter using Darcy's

Law and measurements of the specific gravity versus time for the soil-water fluid during the test.

Density tests were made on samples of pre-test soil and post-test natural ejecta fragments from MINOR UNCLE using procedures derived from the Coefficient of Linear Extensibility (COLE) test routinely used by the Soil Conservation Service (SCS 1972) in performing soil survey investigations (Table A-1). These samples were coated with Saran resin which forms a semi-permeable membrane to permit measurement of density by water displacement.

Hi Pressure in Table A-1 refers to high pressure tests performed in a test chamber operated by NMERI to a pressure of 10,000 psi hydrostatic compression. These tests were conducted to determine the lock-up characteristics of the samples and whether grain crushing occurred during hydrostatic tests to 10,000 psi. The samples tested were prepared by blending materials from several pre-test samples. These tests are discussed in Appendix B.

A.2 DISCUSSION OF RESULTS.

Table A-2 summarizes the specific gravity and the particle size (percent less than the #200 sieve) data. Samples identified as Pre-Test are individual samples previously reported (Benson and Henny 1992). Blend Pre is the soil obtained by combining samples 1, 2, 4, 6, 7, 9, 13, and 14 previously reported. Comp Blend are samples of the blend compacted statically to determine if the compaction caused grain crushing. Strain cans were individual samples from strain cans obtained after the test. Note that the samples used for the hydrometer analysis were sieved through a 2 mm (#10) sieve prior to the analysis; this changed the size distribution in relation to the original whole sample size distribution. Comparisons of size distribution must be made on the basis of similar initial samples. For example, the percent less than the #200 sieve for MINOR UNCLE sample 60A, 47.78 versus 10.44, is due to the removal of the portion greater than the 2 mm (#10) sieve from the hydrometer test sample.

A.2.1 Particle Size Analysis.

Gradation curves for DISTANT IMAGE soil samples are shown in Figures A-1 through A-10. Figure A-1 shows the data from three individual samples numbered 1, 3, and 4 (these are identified in a previous report, Benson and Henny 1992). Also shown is a blend made by combining samples numbered 1 (52), 2 (52), 4 (52), 6 (60), 7 (60), 9 (75), 13 (105), and 14 (105). The numbers in parentheses are the ranges from ground zero to the sampling point. Whole samples were tested to produce the data shown in Figure A-1. Based on the data shown in Figure A-1, the blended sample is slightly finer (higher percent passing) than the three individual samples. Figure A-2 shows the gradations of the blend after the material greater than the 4.76 mm (#4) sieve and 2 mm (#10) sieve was removed. Another sample of the < 2 mm (< #10 sieve) soil was subjected to static compression to verify the compaction procedure for the high pressure test samples. The gradation identified as Comp in Figure A-2 was performed on a sample after static compaction. There is no indication of a change in gradation as a result of the static compaction. The < 4.76 mm (< #4 sieve) sample is shown because the samples used in the high pressure tests were made of the soil blend passed through a 4.76 mm (#4) sieve.

The sample gradations after high pressure testing (Hi Press #4 and #6) are compared those for the whole sample and the < 4.76 mm (< #4 sieve) portion of the

Table A-2. Summary of specific gravity and fines data.

Test Date	Sample	Specific Gravity	<#200 (%)	Notes/Remarks
DISTANT IMAGE				
2/1/94	Pre-test #1	2.666	11.20	
2/1/94	Pre-test #2		5.81	
2/1/94	Pre-test #3		8.81	
2/1/94	Pre-test #4		5.92	
3/4/94	Blend Pre	2.625	48.80	hyd sample, -#10 only
3/4/94	Blend Pre		12.15	-#4 only
3/10/94	Comp Blend		49.27	hyd sample, -#10 only
3/2/94	Comp Blend		24.32	whole sample
7/15/94	Blend #4		11.10	
7/15/94	Blend #6		11.56	
7/12/94	Strain Can #3	2.689	49.69	hyd sample, -#10 only
7/13/94	Strain Can #10	2.662	48.59	hyd sample, -#10 only
7/13/94	Strain Can #16	2.638	46.91	hyd sample, -#10 only
7/13/94	Strain Can 125B	2.674	52.12	hyd sample, -#10 only
7/13/94	Strain Can #144	2.655	43.17	hyd sample, -#10 only
MINOR UNCLE				
2/1/94	#60	2.764		
2/1/94	#60	2.758		
3/4/94	#60A		47.78	hyd sample, -#10 only
3/2/94	#60A		10.44	whole sample
7/1/394	Y08	2.581*	55.82	ejecta fragment
7/1/394	Y10	2.610*	47.74	ejecta fragment
7/13/94	Y21	2.574*	50.60	ejecta fragment
7/1/394	Z10	2.601*	59.18	ejecta fragment
7/13/94	Z14	2.651*	44.87	ejecta fragment
HUSKY JAGUAR 1				
7/15/94	Old Plaster Sand	2.678		

*Fragment samples were small (about 20 g) which may have affected test results.

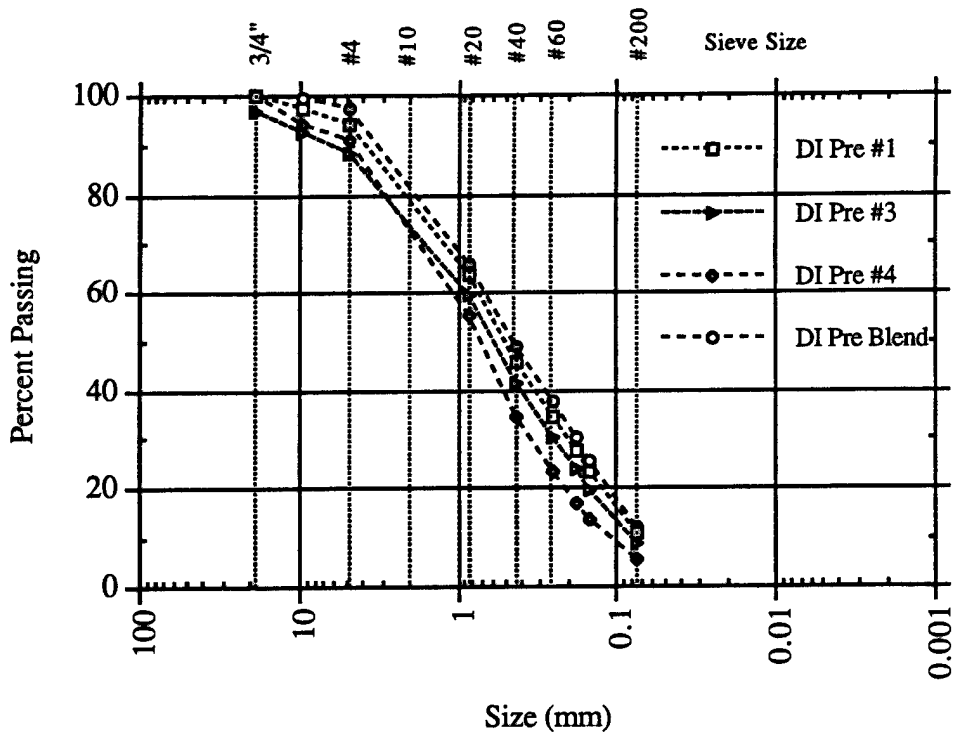

Figure A-1. DISTANT IMAGE pre-test and blend sample gradations.

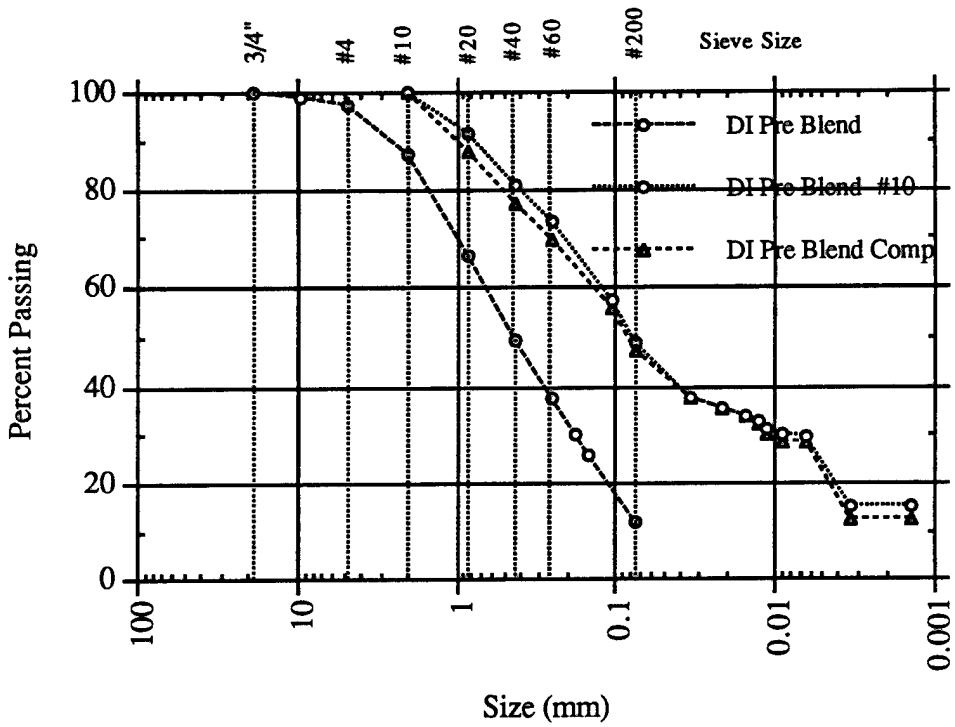

Figure A-2. DISTANT IMAGE pre-test and compacted sample gradations.

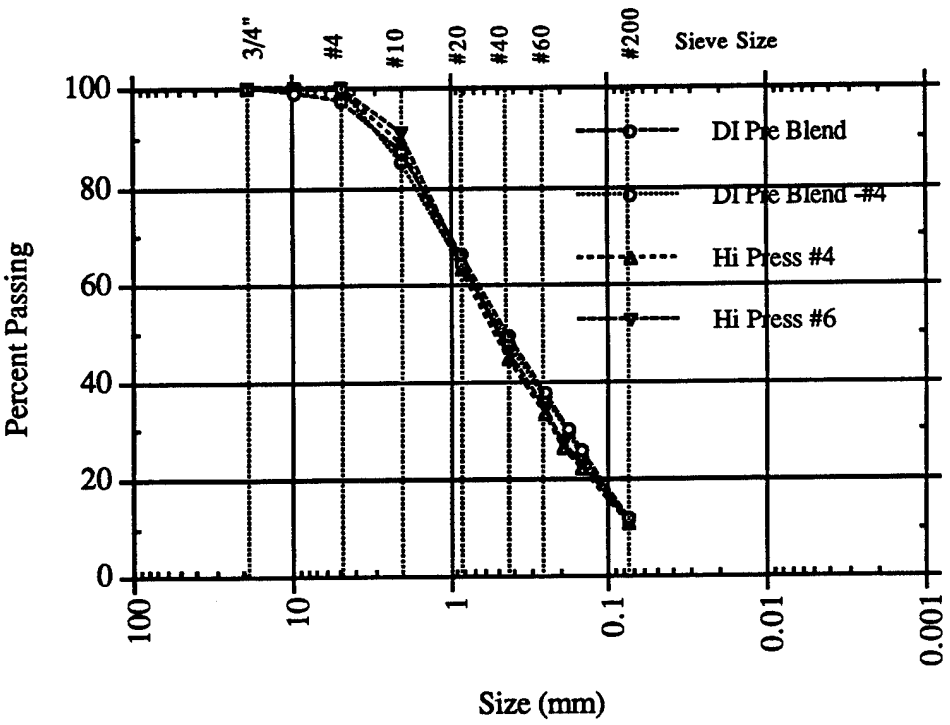

Figure A-3. DISTANT IMAGE pre blend and high pressure test sample gradations.

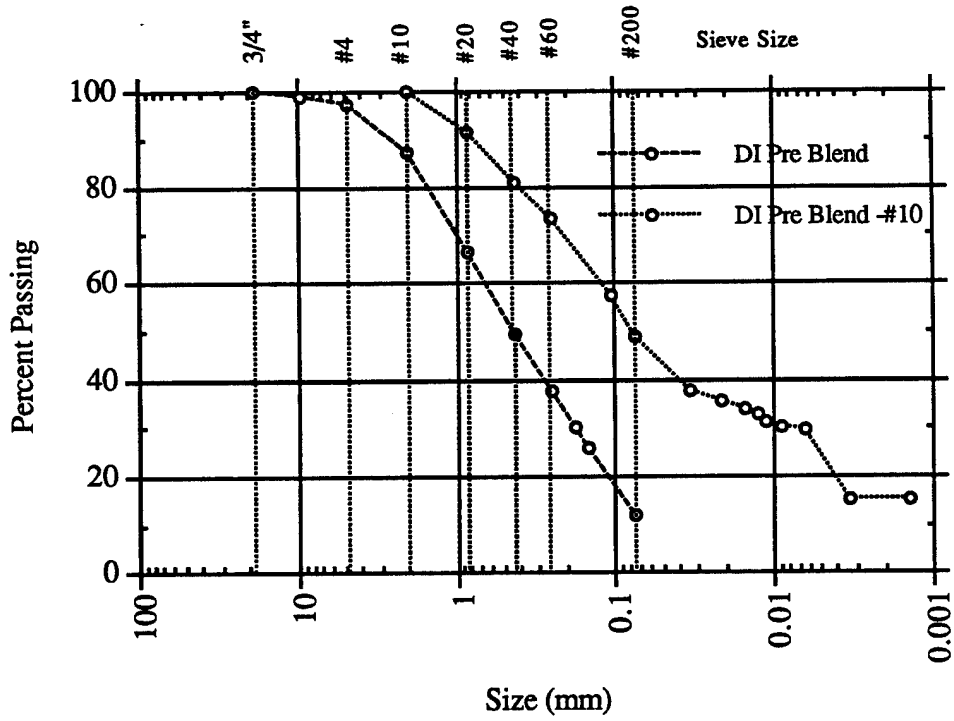

Figure A-4. DISTANT IMAGE pre blend whole and hydrometer sample gradations.

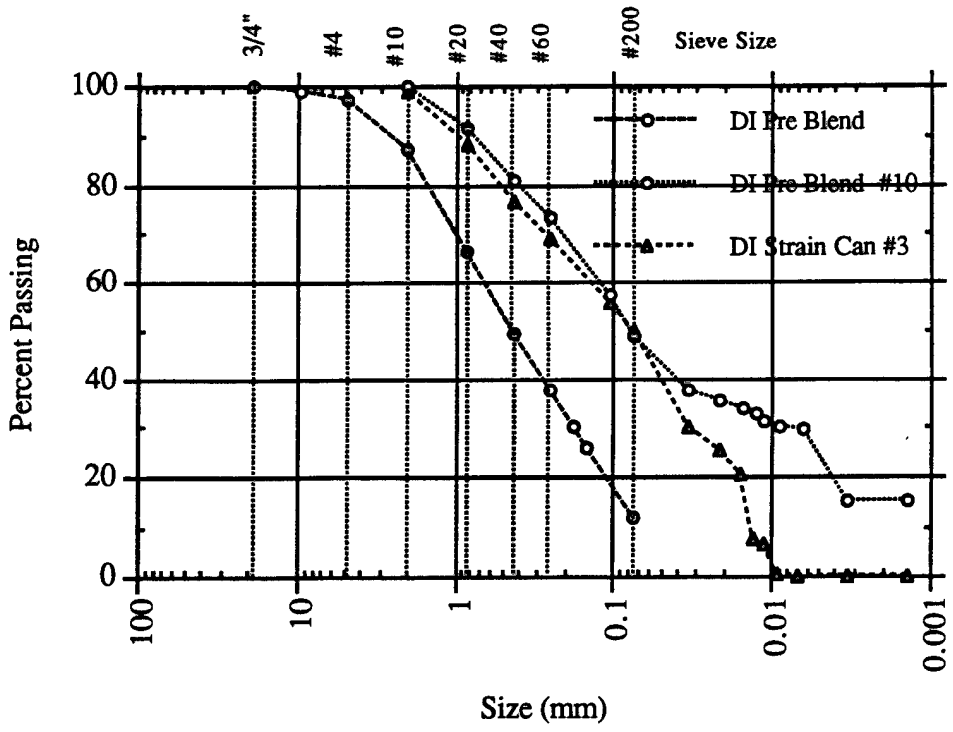

Figure A-5. DISTANT IMAGE pre blend and Strain Can 3 gradations.

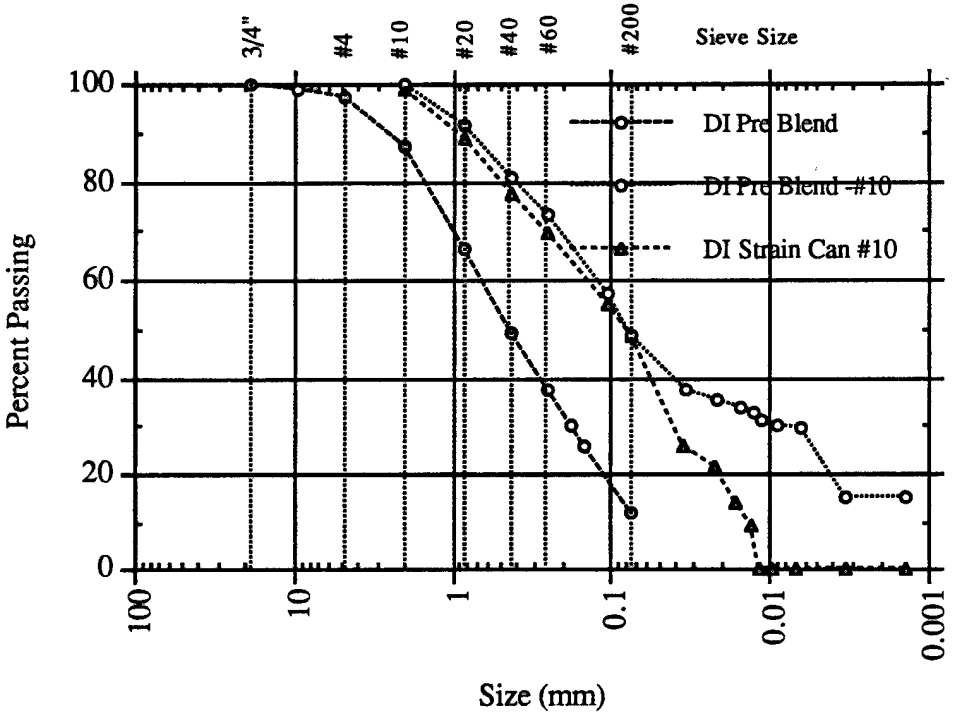

Figure A-6. DISTANT IMAGE pre blend and Strain Can 10 gradations.

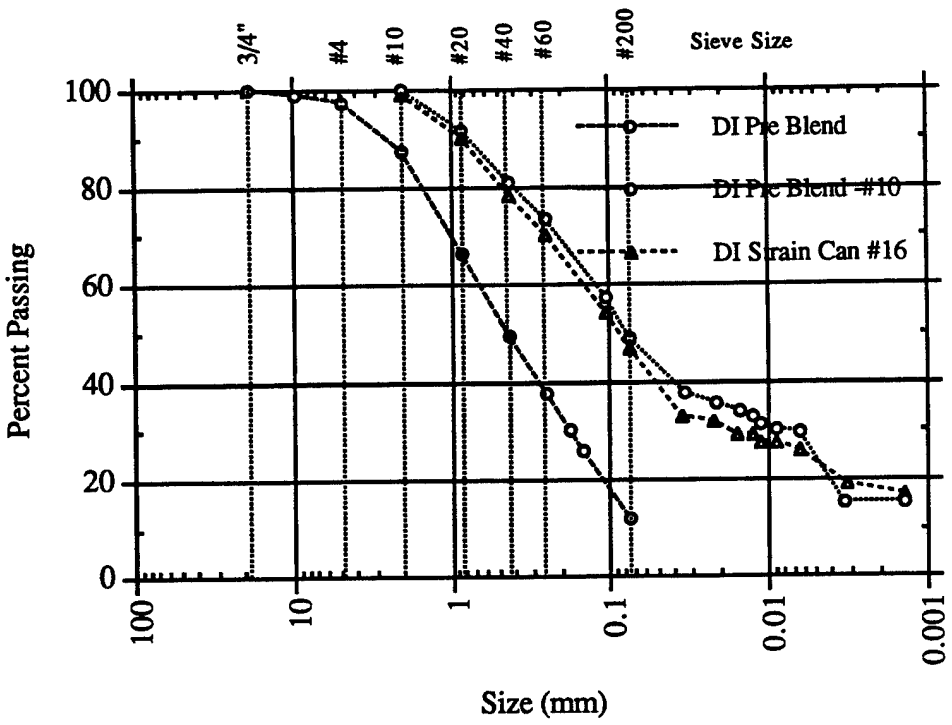

Figure A-7. DISTANT IMAGE pre blend and Strain Can 16 gradations.

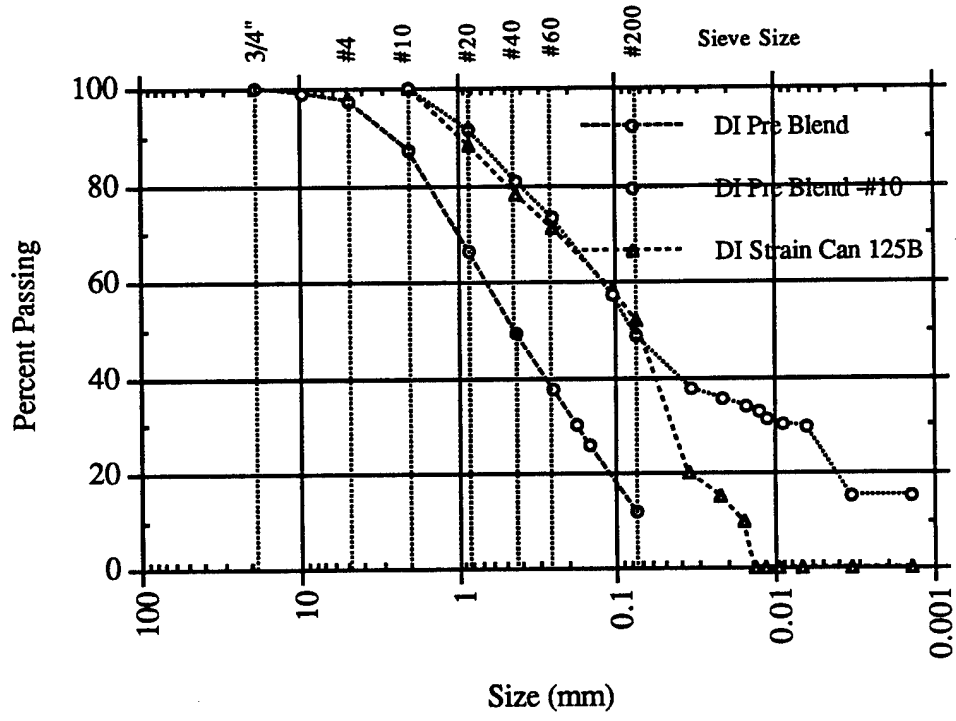

Figure A-8. DISTANT IMAGE pre blend and Strain Can 125B gradations.

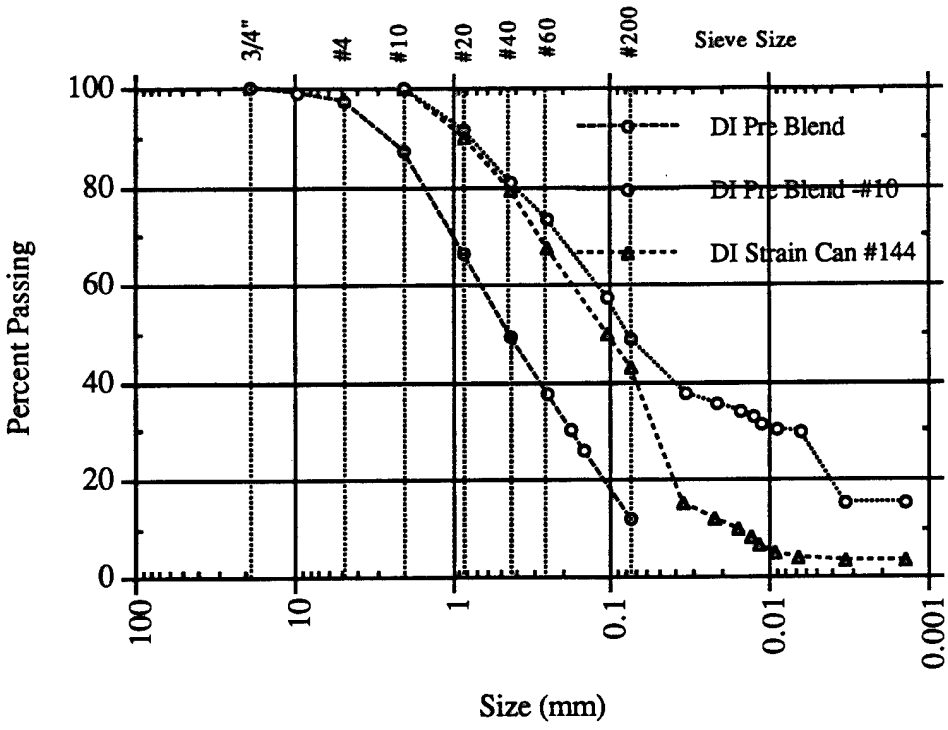

Figure A-9. DISTANT IMAGE pre blend and Strain Can 144 gradations.

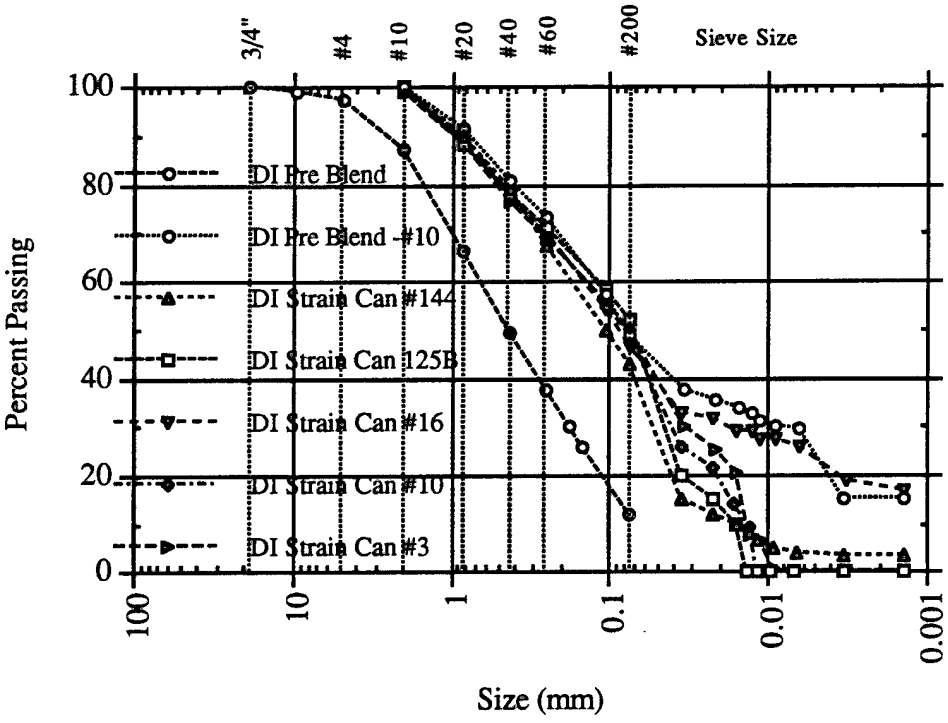

Figure A-10. DISTANT IMAGE all strain cans and pre-test gradations.

blended sample in Figure A-3. No change in gradation as a result of the hydrostatic compression to 10,000 psi is evident in the particle size analysis data.

Figure A-4 shows the gradation of the whole blended sample and the < 2 mm (< #10 sieve) blended sample required for hydrometer testing. Figure A-5 shows the results of post-test Strain Can 3 in comparison to the pre-test data from Figure A-4. The Strain Can 3 sample is the same above the 0.074 mm (#200) sieve and coarser in the range below the 0.074 mm (#200) sieve. The particle sizes below the 0.074 mm correspond to the silt and clay particle size ranges. Figures A-6, A-7, A-8, and A-9 show similar comparisons for Strain Cans 10, 16, 125B, and 144, respectively. Figure A-10 shows all strain can data on a single graph with the pre-test gradation. The similarity of the data are apparent. All samples are coarser in the smaller size ranges except Can 16 which has a gradation very near the pre-test sample. The coarser gradation could be due to sample segregation during preparation of the strain cans or due to some loss of fines in the test. All gradations of strain can samples above the 0.074 mm (#200) sieve are very near the original gradations.

Similar gradation comparisons for the pre-test MINOR UNCLE soil samples and samples from the natural ejecta fragments Y08, Y10, Y21, Z10, and Z14 are shown in Figures A-11 through A-15. Figure A-16 shows all post-test samples and the pre-test sample. In contrast to the DISTANT IMAGE strain can data, these post-test MINOR UNCLE samples are almost all similar to the pre-test sample except Z14, which is coarser in the fine sizes.

A.2.2 Density Test Data.

The results of two sets of tests performed using a modified COLE procedure are reported here. The data shown are for the pre-test soil and the post-test ejecta fragments for MINOR UNCLE. The samples were coated with Saran resin, a liquid plastic made by dissolving the powdered resin in methyl ethyl ketone (MEK). The samples are dipped into the liquid resin to form a plastic coating. Two coats were applied for these samples. After the coating cured the sample was weighed in air and water to obtain the soil density by water displacement. The samples were then placed in a cold oven which was started and heated to 105 $^{\circ}$C. The samples remained overnight, a minimum of 16 hours. Saran resin permits water vapor to escape through the plastic coating so that it does not have to be removed to dry the sample. By starting with a cold oven and heating the sample slowly, the plastic does not separate from the soil and maintains a tight coating. Once the soil is oven dried it is again weighed in air and water to obtain data for computing a final density and water content of the sample after drying. Table A-3 gives the data for samples of pre-test MINOR UNCLE soil. Table A-4 gives the results for the ejecta samples from MINOR UNCLE. Data were obtained in the field on the day of test but the data shown in Table A-4 were obtained in June 1994 after a significant storage period. The samples lost part of the moisture and increased in density, probably in response to the drying. Similar data were obtained for the DISTANT IMAGE test and were reported previously (Benson and Henny 1992), these are discussed below.

A summary of results of pre-test and ejecta density, water content, and air porosity are shown in Table A-5. The data for DISTANT IMAGE were obtained in the field previously (Benson and Henny 1992). These data show no difference between the pre-test and the ejecta samples from DISTANT IMAGE. The MINOR UNCLE ejecta (day of test) data were obtained in the field immediately after the test. The data identified as COLE tests 6/94 were performed much later as is evident from

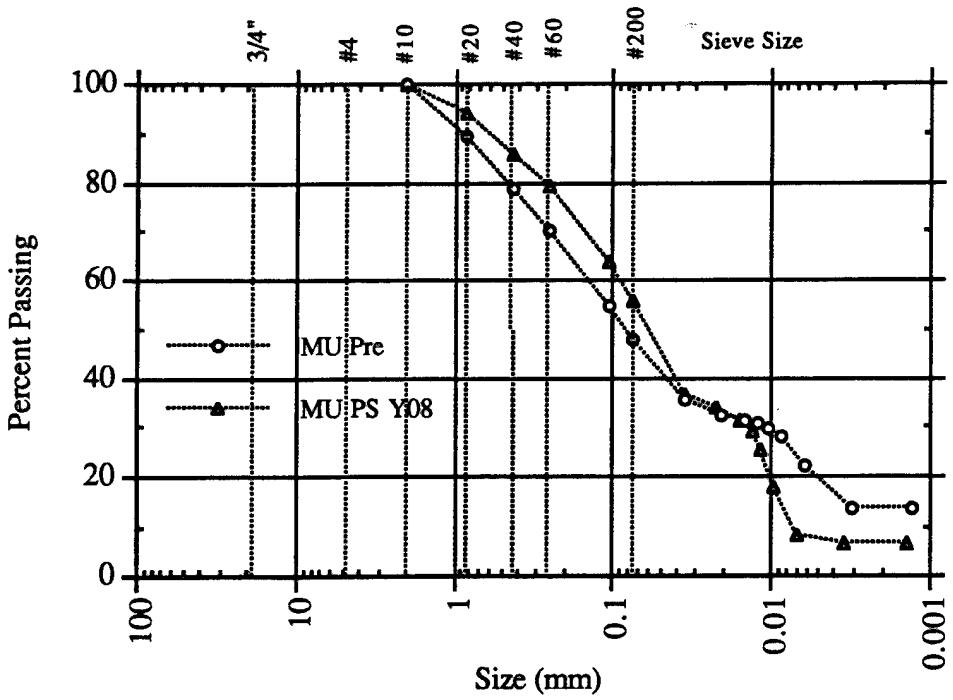

Figure A-11. MINOR UNCLE pre-test and post-test ejecta Y08 gradations.

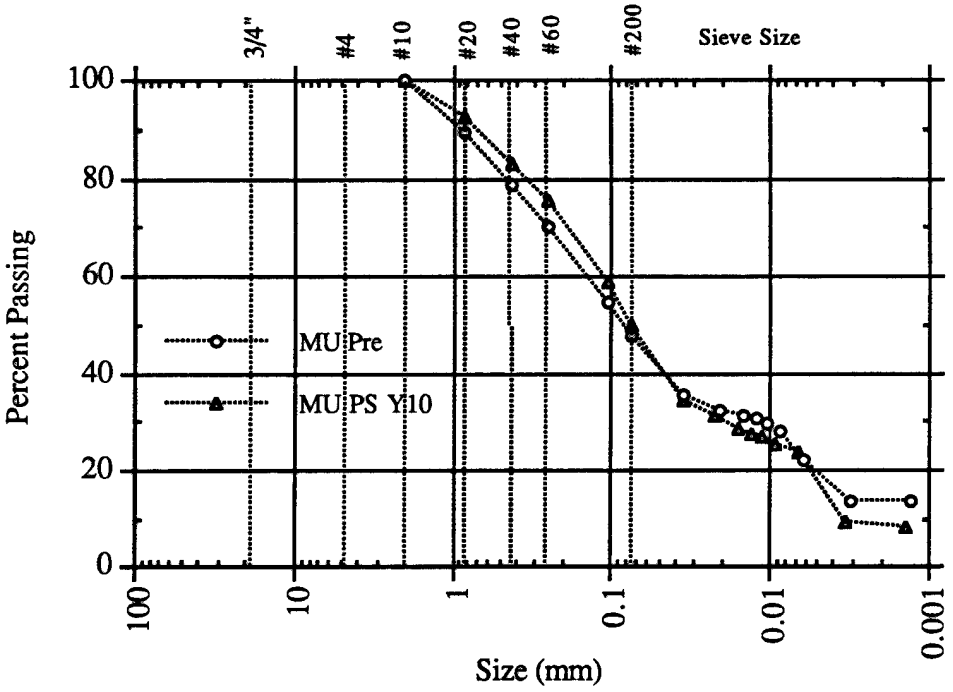

Figure A-12. MINOR UNCLE pre-test and post-test ejecta Y10 gradations.

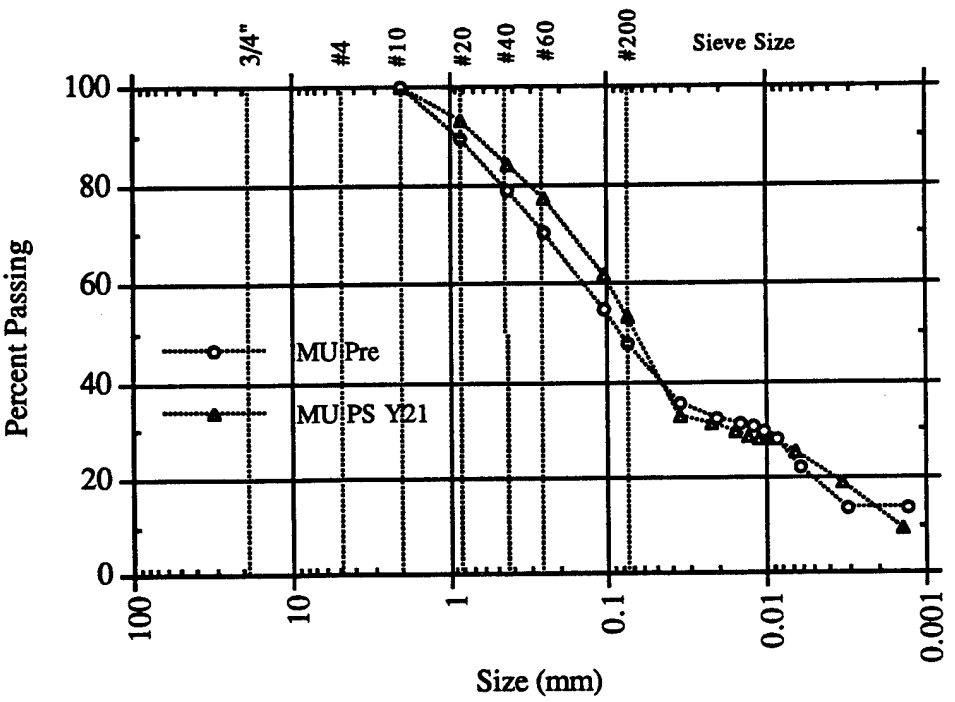

Figure A-13. MINOR UNCLE pre-test and post-test ejecta Y21 gradations.

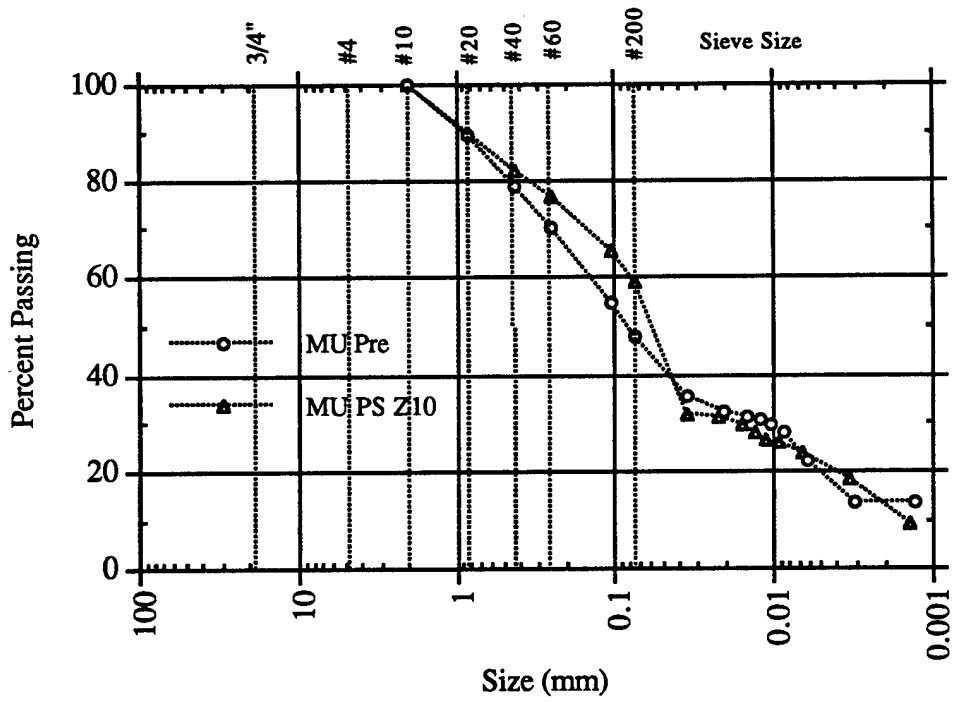

Figure A-14. MINOR UNCLE pre-test and post-test ejecta Z10 gradations.

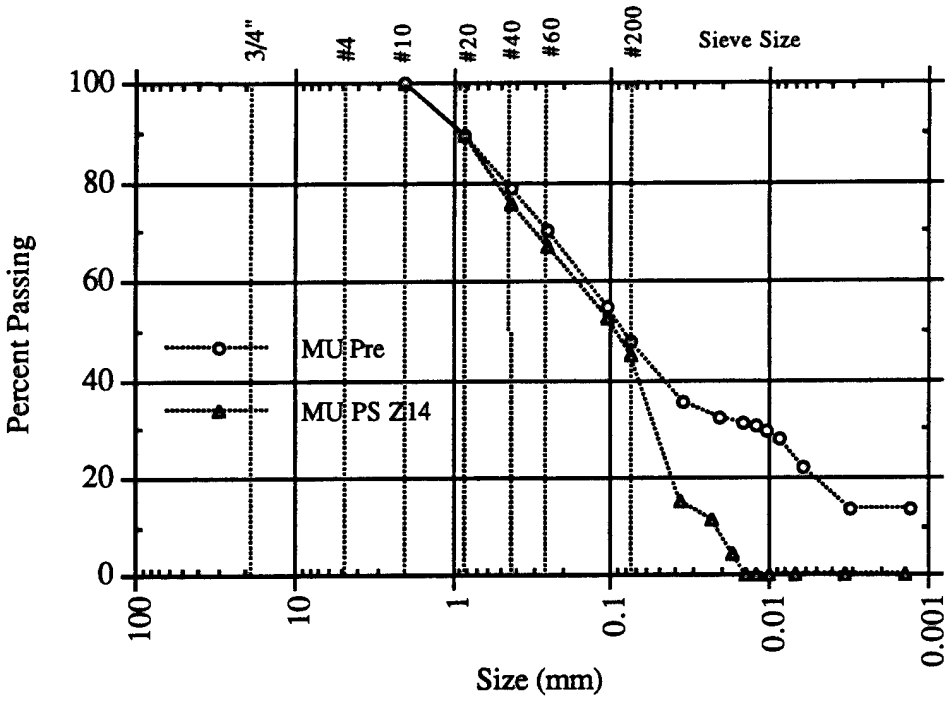

Figure A-15. MINOR UNCLE pre-test and post-test ejecta Z14 gradations.

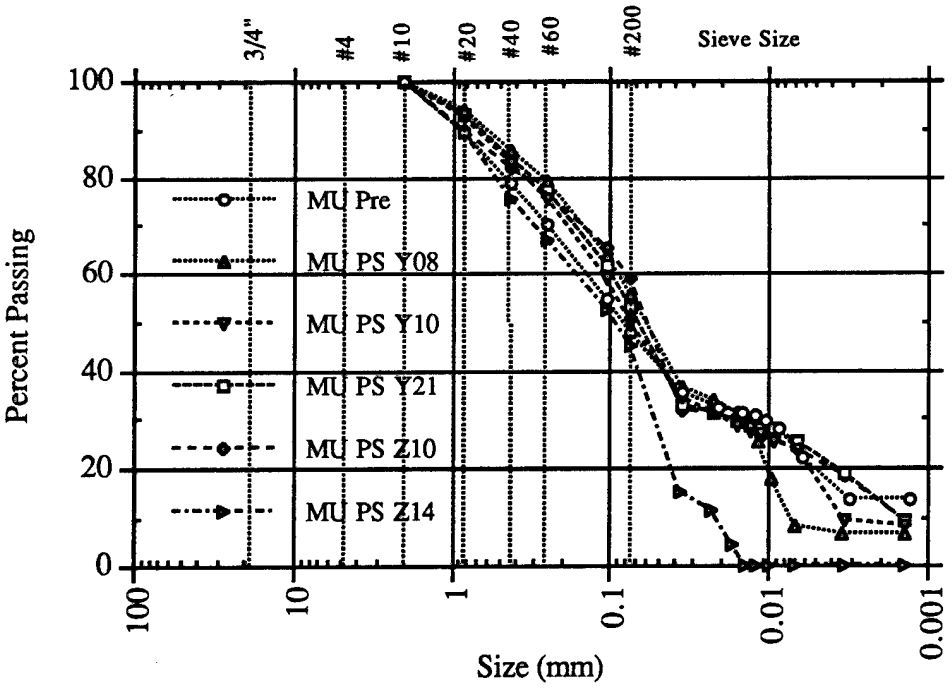

Figure A-16. MINOR UNCLE pre-test and all post-test ejecta gradations.

Table A-3. MINOR UNCLE pre-test COLE density and water content determinations.

Range ft	Sample Number	Wt. of Solids g	Water Content g/g	Dry Density g/cm^3	Dry Density lb/ft^3
75C	A1	286.76	0.07	1.86	116.2
75C	A2	221.97	0.12	1.87	116.4
75C	A3	error			
60C	A4	299.61	0.09	1.75	109.5
60C	A5	175.49	0.09	1.77	110.2
60C	A6	425.46	0.08	1.84	115.1
90C	A7	636.23	0.12	1.86	116.2
90C	A8	326.81	0.09	1.80	112.2
90C	A9	473.64	0.10	1.85	115.5
38C	A10	129.57	0.14	1.83	114.0
38C	A11	163.36	0.13	1.88	117.1
38C	A12	261.14	0.12	1.88	117.0
105C	A13	275.66	0.11	1.74	108.5
105C	A14	338.98	0.11	1.83	114.4
105C	A15	387.94	0.12	1.75	109.3
50C	A16	387.68	0.12	1.80	112.0
50C	A17	173.13	0.09	1.76	109.6
50C	A18	218.84	0.13	1.79	111.8
118C	A19	151.60	0.08	1.81	113.1
118C	A20	198.96	0.12	1.78	110.8
118C	A21	231.86	0.14	1.80	112.3
Mean			0.108	1.89	117.6

Table A-4. MINOR UNCLE ejecta COLE density and water content determinations.

Sample Number	Wt. of Solids g	Water Content g/g	Dry Density g/cm^3	Dry Density lb/ft^3
Y 01	329.97	0.036	2.02	125.87
Y 02	390.90	0.041	1.99	124.21
Y 03	423.56	0.049	1.94	121.11
Y 04	760.49	0.038	2.07	129.26
Y 05	769.71	0.046	2.07	129.44
Y 06	497.83	0.034	2.03	126.93
Y 07	465.63	0.041	2.02	125.75
Y 08	301.08	0.027	2.04	127.52
Y 09	322.86	0.023	2.07	129.38
Y 10	389.87	0.022	2.05	127.97
Y 11	515.43	0.055	2.06	128.49
Y 12	531.68	0.034	2.00	124.58
Y 13	440.82	0.031	2.07	129.08
Y 14	454.93	0.040	2.02	125.83
Y 15	538.30	0.060	1.96	122.42
Y 16	696.10	0.034	2.12	132.09
Y 17	316.18	0.031	2.08	129.94
Y 18	571.16	0.046	2.07	129.37
Y 19	372.69	0.047	2.02	126.09
Y 21	473.19	0.045	2.09	130.68
Y 23	455.97	0.033	2.13	132.68
Z 01	885.35	0.048	2.01	125.43
Z 02	error	not used		
Z 03	198.04	0.044	1.96	122.16
Z 04	868.52	0.034	2.13	133.13
Z 05	660.94	0.047	2.05	127.62
Z 06	508.59	0.045	1.96	122.44
Z 07	258.84	0.015	2.06	128.50
Z 09	262.23	0.014	2.08	129.87
Z 10	826.72	0.028	2.05	127.69
Z 12	76.52	0.005	2.13	132.90
Z 13	315.46	0.039	2.03	126.59

Table A-4. MINOR UNCLE ejecta COLE density and water content determinations (Continued).

Sample Number	Wt. of Solids g	Water Content g/g	Dry Density g/cm^3	Dry Density lb/ft^3
Z 14	113.21	0.007	2.13	132.97
Mean		0.058	2.09	130.14

Table A-5. Summary of soil properties for pre-test and natural ejecta fragments.

Sample	Dry Density (g/cc)	Water Content (%)	Air Porosity (%)	Specific Gravity
DISTANT IMAGE[1]				
Pre-test	1.89	8.4	14.8	
Ejecta	1.90	8.2	14.6	
MINOR UNCLE				
Pre-test	1.89	10.8	11.3	2.761
	1.89	10.8	7.0	2.603
Ejecta (day of test)[2]	1.97	10.3	7.3	2.603
Ejecta (COLE tests, 6/94)	2.09	5.8	7.6	2.603

(1) Data from Benson and Henny (1992).
(2) Data obtained in the field on the day of test.

the water content reduction and density increase (Table A-4). Based on a review of all the data the 2.603 specific gravity for MINOR UNCLE soil is believed to be the correct value. The high value in Table A-2, 2.76, is most likely due to a local anomaly for the sample and is not believed to be representative. The results obtained comparing pre-test and ejecta indicate an increase in density (from 1.89 to 1.97 g/cm^3) and a small change in air porosity. The air porosity is highly dependent on the soil specific gravity used in the computations.

A.2.3 Suction Testing.

Soil suction is a term used by engineers for the thermodynamic quantity Gibbs free energy which is inherently negative, as seen in Equation A.1, and generates tension in the pore water stretching between soil particles:

$$h = (RT/mg)\ln(H/100) \qquad (A.1)$$

where

h = total suction in g-cm/g, a negative number
R = the universal gas constant, 8.314 x 10^7 ergs-K/mole
T = absolute temperature, degrees K
m = gram molecular weight of water, 18.02 g/mole
g = 981, conversion from grams mass to grams force,
H = relative humidity, in percent.

Soil suction testing was performed following ASTM D 5298, Standard Test Method for Measurement of Soil Potential (Suction) Using Filter Paper. The sample water content was altered in increments of 2 percent water content. Samples were adjusted to -2, -4, and -6 percent and +2, +4, and +6 percent water contents relative to the original water content. The purpose of this procedure was to determine the suction values over a range of water contents for the soil in order to measure the slope of the suction-water content curve. The data obtained are shown in Table A-6. Suction-water content graphs are shown in Figures A-17 through A-19. An explanation of the data follows.

Total suction has two components: matrix suction due to the attraction of water to the soil particle surfaces and osmotic suction, which is due to dissolved salts or other solutes in the pore water. A complete discussion of suction and its measurement has been published (Fredlund and Raharjdo 1994).

Specific levels of suction are associated with specific physical behavior of soils as illustrated in Table A-7. Suction units are pF (logarithm to the base 10 of the pressure in centimeters of water and kPa). Suction testing, using the filter paper method (ASTM D 5298), is a straight-forward procedure suitable for use in conventional soils testing laboratories. The only unusual requirement is the need for an analytical balance capable of weight measurements to 0.0001 g.

The value of suction characterization for active soils is that the suction level of soil water correlates with the physical behavior of the soil. A soil containing water near 3.4 pF (250 kPa) will exhibit the behavior of a soil near its plastic limit (i.e., a thread rolled to 3 mm [0.125 in] diameter breaks). It is not necessary to know the water content to draw this conclusion. Whether a clay is "lean" or "fat," the behavior at each suction level is consistent, although the fat clay will hold more water at any given suction level. Since suction tests may be performed on undisturbed samples, another advantage is gained over

Table A-6. Suction water content data for DISTANT IMAGE and MINOR UNCLE soils.

Sample	Water Content, %	Suction, pF	Suction, kPa
Distant Image #1	9.5	3.951	876.0
Distant Image #1	9.3	4.331	2101.4
Distant Image #1	14.7	3.344	216.5
Distant Image #1	18.9	2.138	13.5
Distant Image #1	19.4	3.489	302.3
Distant Image #1	23.7	3.386	238.5
Distant Image #1	23.7	3.304	197.5
Distant Image #2	6.9	4.323	2063.0
Distant Image #2	6.8	4.348	2185.3
Distant Image #2	12.1	3.783	595.0
Distant Image #2	11.9	3.750	551.5
Distant Image #2	17.8	3.617	406.0
Distant Image #2	17.2	3.539	339.2
Distant Image #2	21.8	3.577	370.3
Distant Image #2	23.1	3.635	423.2
Minor Uncle #1	6.1	4.741	5401.4
Minor Uncle #1	6.9	4.648	4360.2
Minor Uncle #1	11.1	3.700	491.5
Minor Uncle #1	10.8	3.778	588.2
Minor Uncle #1	15.6	2.961	89.6
Minor Uncle #1	16.3	3.338	213.6
Minor Uncle #1	20.8	3.335	212.1
Minor Uncle #1	23.7	3.056	111.6

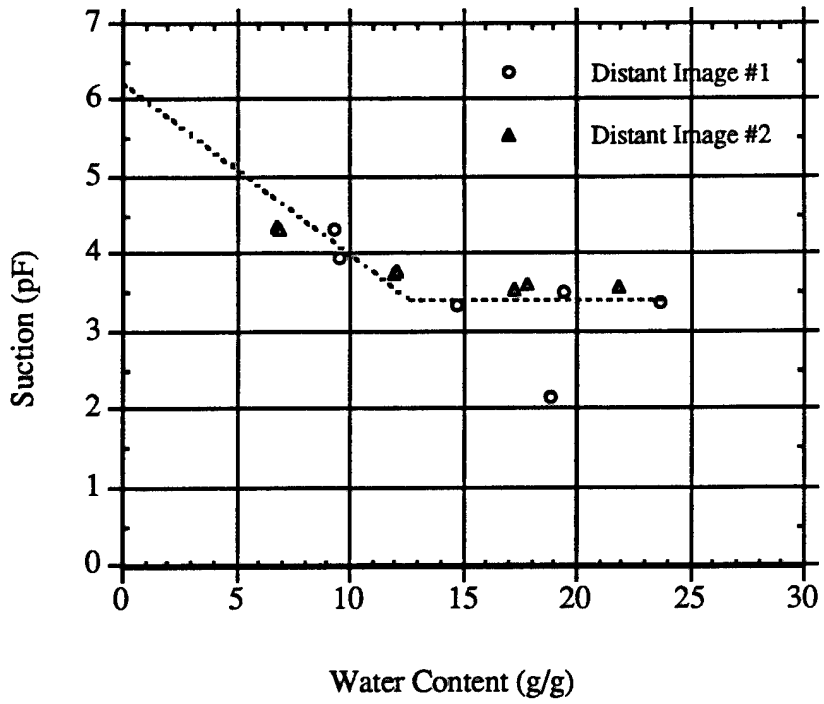

Figure A-17. Suction water content data for DISTANT IMAGE pre-test samples.

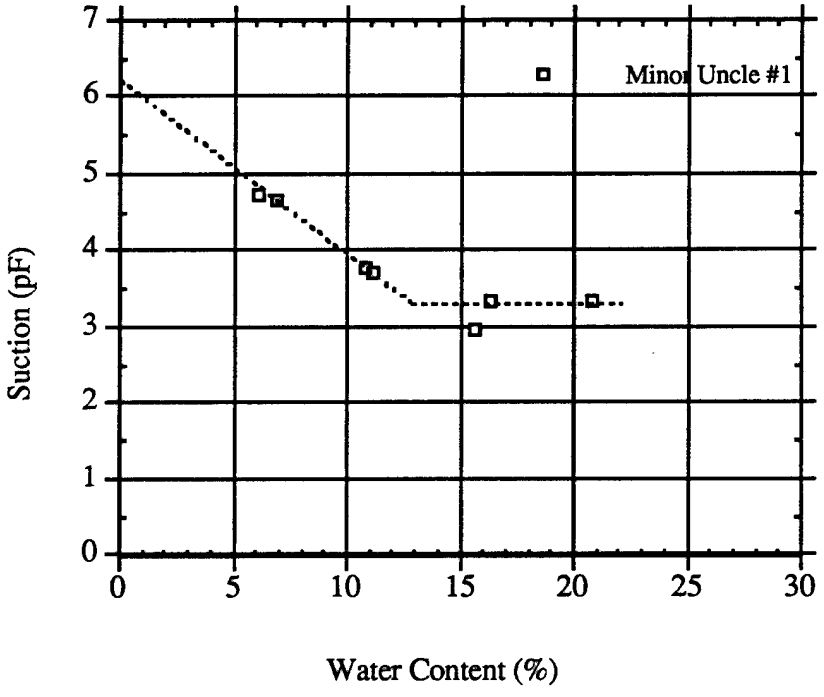

Figure A-18. Suction water content data for MINOR UNCLE pre-test sample.

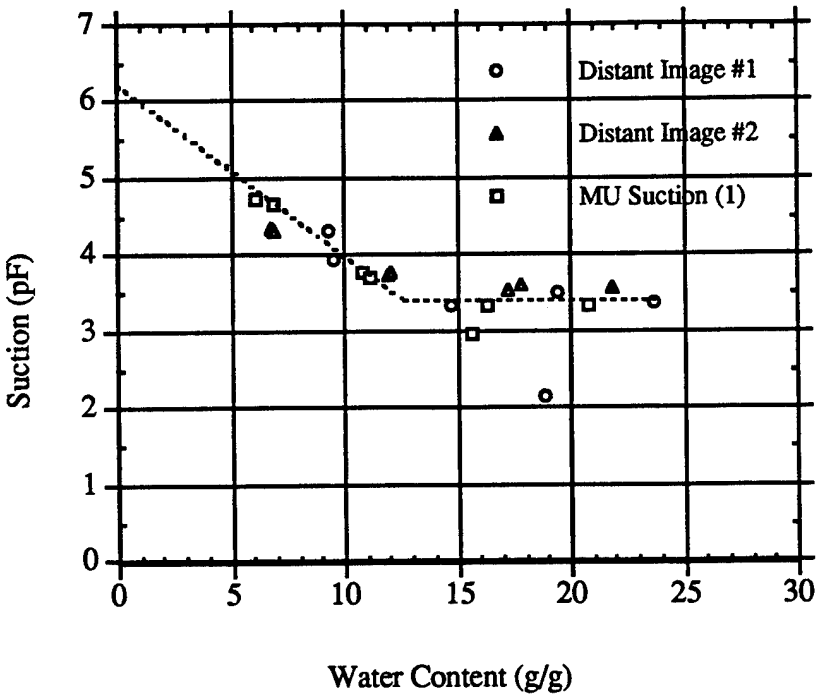

Figure A-19. All suction water content data.

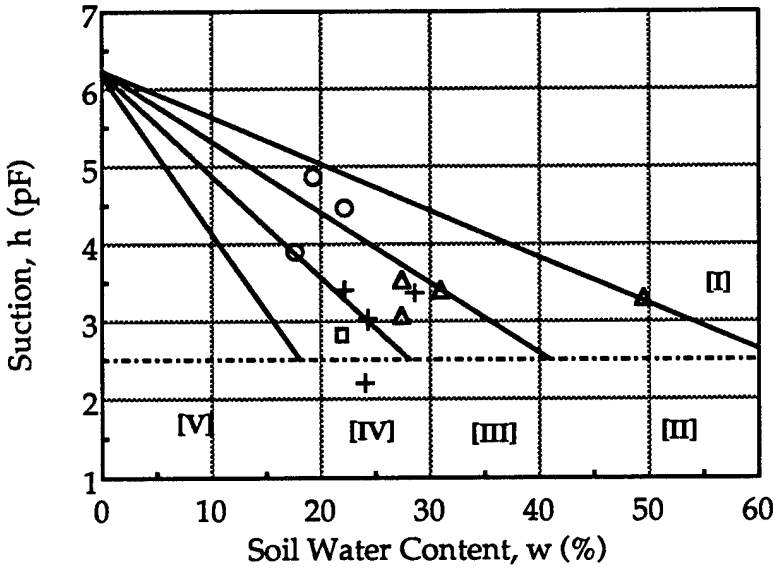

Figure A-20. Expansive soil classification system (McKeen 1992).

Table A-7. Suction correlation with physical behavior of soils.

Behavior	Suction, pF	Suction (kPa)
Saturation	0.00	0.00
Liquid Limit	1.0	0.98
Field Capacity	2 - 2.5	9.8 - 31
Plastic Limit	3.2 - 3.5	160 - 310
Plant Wilting Point	4.2 - 4.5	1,600 -3,100
Tensile Strength of Water	5.3	20,000
Shrinkage Limit/Air Dry	5.5	31,000
Oven Dry	7	980,000

properties based on disturbed soil samples. The soil behavior in the field is strongly dependent on the in-place structure as it influences moisture movement, which will also affect suction measurements.

Suction measurements in conjunction with water content of the soil are the basis for a proposed classification system for volumetrically active soils. It has the great advantage of not requiring further soil testing (McKeen 1992). Since all soil behavior is sensitive to moisture condition to some extent, the system is adaptable to all soils. Table A-8 illustrates the classes and the criteria for determining the soil classification for expansive soils. In the table "Cat." indicates the category, "$\Delta h/\Delta w$" is the slope of the suction-water content curve, "C_h" is the suction compression index, or volume change per pF change in

Table A-8. Proposed expansive soil classification system (McKeen 1992).

Cat.	$\Delta h/\Delta w$	C_h	$\Delta H^{(1)}$ cm (in)	ΔH %	Remarks
I	> -6	-0.227	15.3 (6.0)	10.0	Special Case
II	-6 to	-0.227			High
	-10	-0.120	8.1 (3.2)	5.3	
III	-10 to	-0.120			Moderate
	-13	-0.040	2.7 (1.1)	1.8	
IV	-13 to	-0.040			Low
	-20	Nonexp.	---	- - -	
V	< -20	Nonexp.	- - -	- - -	Nonexp.

(1) Calculated ΔH for f = 0.5, Z_a = 1.5 m (5 ft), Δh = 1.0 pF, s = 0.9.

suction, and "ΔH" is an estimated vertical heave for the category assuming values shown at the bottom of the table for lateral restraint factor (f), active zone depth (Z_a), and suction change (Δh). Figure A-20 is a graphical representation of the classification systems plotted on the suction water content data for an example site. The slope may also be plotted versus depth of the sample below the surface. These data are extremely valuable in assessing a site and determining how complex the behavior may be or what mechanisms are involved.

The results of the tests on samples from DISTANT IMAGE and MINOR UNCLE, Figures A-17 through A-19, indicate the soils are very similar with regard to suction-moisture content behavior. The curves shown were fit through the data points with an intercept of 6.25 pF. This intercept has been used in a model of behavior of soils in the suction-water content space. At 3.5 pF the relationship becomes horizontal, indicating no change of suction level for increasing water content. This feature results from an osmotic suction component equal to about 3.5 pF (310 kPa). The osmotic component of suction would cause the soil to be more stable at higher water contents than a similar soil without the osmotic component. The classification system previously developed for active soils is shown in Figure A-19 for reference to the data for DISTANT IMAGE and MINOR UNCLE. Most of the DISTANT IMAGE and MINOR UNCLE samples tested are on the dividing line between category IV and V, indicating that these are not volumetrically active soils. It is very likely the dynamic behavior could be related to the moisture condition as indicated by suction measurements if some research were completed to investigated this specific behavior. The reference cited (McKeen 1992) provides a more detailed discussion of the classification system. This classification system has little relevance to granular soils, other than identification of them by their low potential for volume change. However, it is anticipated that studies of the relation between suction characteristics and dynamic behavior would be a fruitful research area.

A.3 CONCLUSIONS AND RECOMMENDATIONS.

No significant differences in specific gravity, gradation, or density are apparent between the pre-test soils and ejecta samples tested from the DISTANT IMAGE and MINOR UNCLE tests.

Static compaction of the DISTANT IMAGE soil in the laboratory caused no change in the physical characteristics of the soil.

High pressure testing of the DISTANT IMAGE soil to 10,000 psi (1034 kPa) hydrostatic compression caused no changes in the soil gradation characteristics.

Soil suction testing clearly indicates that the slope of the suction water content curve is high or steep suggesting a low surface area or soil mineral composition. This is consistent with granular soils. The other notable feature is a high osmotic component equal to 3.5 pF. This is important for two reasons. First, the high osmotic suction component will cause these soils to "hold together" better than similar soils without the osmotic suction component due to the tension in the pore water. Second, the soil characteristics may dramatically change if it is subjected to leaching due to water exposure that may dissolve and remove the salts.

APPENDIX B

HYDROSTATIC COMPRESSION TESTS

B.1 INTRODUCTION.

The New Mexico Engineering Institute (NMERI) at The University of New Mexico (UNM), in Albuquerque, performed evaluations of soil characteristics and behavior using several laboratory test procedures. These included specific gravity, particle size analysis, soil density, soil suction, and high pressure hydrostatic compression. The hydrostatic compression tests were performed by Lary R. Lenke, P.E., and Thomas Escobedo in the NMERI Material Response Laboratory. The other soil index testing was performed by R. Gordon McKeen, P.E., and Ken Martinez in the NMERI Materials Laboratory, and is reported in Appendix A.

B.2 SAMPLE PREPARATION.

Hydrostatic compression tests were performed on five samples of pre-test DISTANT IMAGE soil. These samples were prepared from a single batch of soil blended using previously stored samples 1, 2, 4, 6, 7, 9, 13, and 14 (Benson and Henny 1992) as provided to NMERI by SEA. After blending the eight samples, material coarser than the #4 sieve (2 mm) was removed to reduce the potential for membrane rupture during hydrostatic loading. A particle size distribution was determined for this blended material (Appendix A).

B.3 TEST PROCEDURES AND RESULTS.

Samples of 2-in diameter and 4-in length were prepared to a dry density of 1.9 g/cm^3 and a moisture content of 8.5 percent. This density was achieved by using a press (universal testing machine) and compressing the soil in four 1-in lifts. A post-compaction particle size analysis was performed to verify that the compaction stresses had not caused discernible grain crushing (Appendix A). The specific gravity of the blended material was 2.625. For the specified density and moisture content this yields a total porosity of 0.276 (void ratio of 0.382), an air porosity of 0.115, and a degree of saturation of 0.585.

The hydrostatic compression tests were performed in a Structural Behavior Engineering Laboratories (SBEL) Rockcell Model 10 triaxial cell. An SBEL HI-1000 hydraulic pressure generating system and 547 servo controller were used to obtain total stress levels to 10 ksi. Cell pressure was monitored using a Viatran Model 11S electronic pressure transducer mounted at the pressure intensifier. Pore pressure in the sample was measured by a Sensotec Model TJE/743-11 transducer external to the cell. This pore pressure gage was connected by 1/8-in diameter by 0.035-in wall thickness stainless steel tubing to the top and bottom pore pressure ports built into the SBEL cell. An 8.5-in run of tubing was used from the Sensotec transducer to a high pressure tee, with subsequent runs of 3.5-in and 6.75-in lengths to the external ports at the base of the cell. An SBEL DJC deformation jacket was used for measuring the longitudinal and radial deformations of the sample during compression. This deformation jacket incorporates six linear variable differential transformers (LVDTs), three in the longitudinal direction and three in the radial direction. The nominal gage lengths for the radial and longitudinal directions were 1 in and 2.25 in, respectively. Lucas-Schaevitz Model 250 MHR (+/- 0.25 in) LVDTs were used for this test series. An SBEL Model 250 LVDT signal conditioner was used with the

six LVDTs. A PC based digital data acquisition system was used for data recording for each test.

Five samples were tested yielding varying amounts of information regarding the bulk stress-strain and pore pressure response. These five tests were designated DISTIMG1 through DISTIMG5. Data from all five tests are presented in the figures; the graphs show stress (both total and effective), pore pressure, displacement, and strain time histories as well as the bulk stress-strain response and pore pressure versus total stress (see, for example, Figures B-1 through B-6). The displacement graphs show a relative displacement because the LVDTs were not zeroed prior to test; the strains were calculated and zeroed.

The slope of the pore pressure versus total stress is the B parameter, defined as (Skempton 1954)

$$B = \Delta u/\Delta\sigma = 1/(1 + nB_S/B_W) \qquad (B.1)$$

where n is the total porosity of the soil sample, Δu is the change in pore pressure caused by a total stress increment $\Delta\sigma$, and B_S and B_W are the bulk modulus of the soil skeleton and the pore water, respectively. The bulk modulus of water is 300,000 psi and, from the data discussed below, the bulk modulus of the DISTANT IMAGE soil is nominally 30,000 psi. For the above cited porosity of 0.28, the theoretical B value upon complete saturation is 0.973 (Equation B.1). The above equation does not account for the compressibility of the soil grains. If this were included, the B value would be basically the same because of the high modulus of the soil grains.

Tests DISTIMG1 (Figures B-1 through B-6) and DISTIMG2 (Figures B-7 through B-12) used double latex membranes and hose clamps for sealing the sample from the cell pressure. These membranes ruptured prematurely during both tests at approximately 1,300 psi (Figure B-1) and 1,700 psi (Figure B-7), respectively. Both of these samples appeared to be exhibiting significant pore pressure increases just prior to rupture. After rupture, expansion (dilation) of the samples was noted, consistent with a decrease in effective stress. The samples were fairly isotropic when one compares the longitudinal and radial strain response (this was observed for all five tests). The effective bulk secant moduli were calculated as 20,000 psi for both of these tests. The pore pressure versus total stress graphs clearly indicate the rupture of the membranes (Figures B-6 and B-12); also, during unload the slope of these curves is unity (B parameter = 1).

Because of the incomplete saturation upon rupture of the latex membrane, polyolefin heat shrink tubing was used for the remaining tests. The shrink tubing was placed over the entire sample length. Two short sections of additional shrink tubing were placed at the upper and lower caps to protect the underlying tubing from damage from the tightened hose clamps. The DISTIMG3 sample was loaded to 3,500 psi before membrane rupture using this approach (Figures B-13 through B-18). After rupture it was noted that the pore pressure never equaled the applied total pressure. After an hour of successive stress increments, a leak was noted in the pore pressure measurement system at the Sensotec pressure gage (Figure B-13). Upon tightening of a fitting at the pressure gage, the pore pressure and total pressure eventually equalized. The radial and longitudinal strains were virtually identical for this test. The effective bulk secant modulus at peak stress was 30,000 psi. The pore pressure graph shows the existence of the membrane rupture and the measurement system leak (Figure B-18). During unload the slope is again unity (B=1).

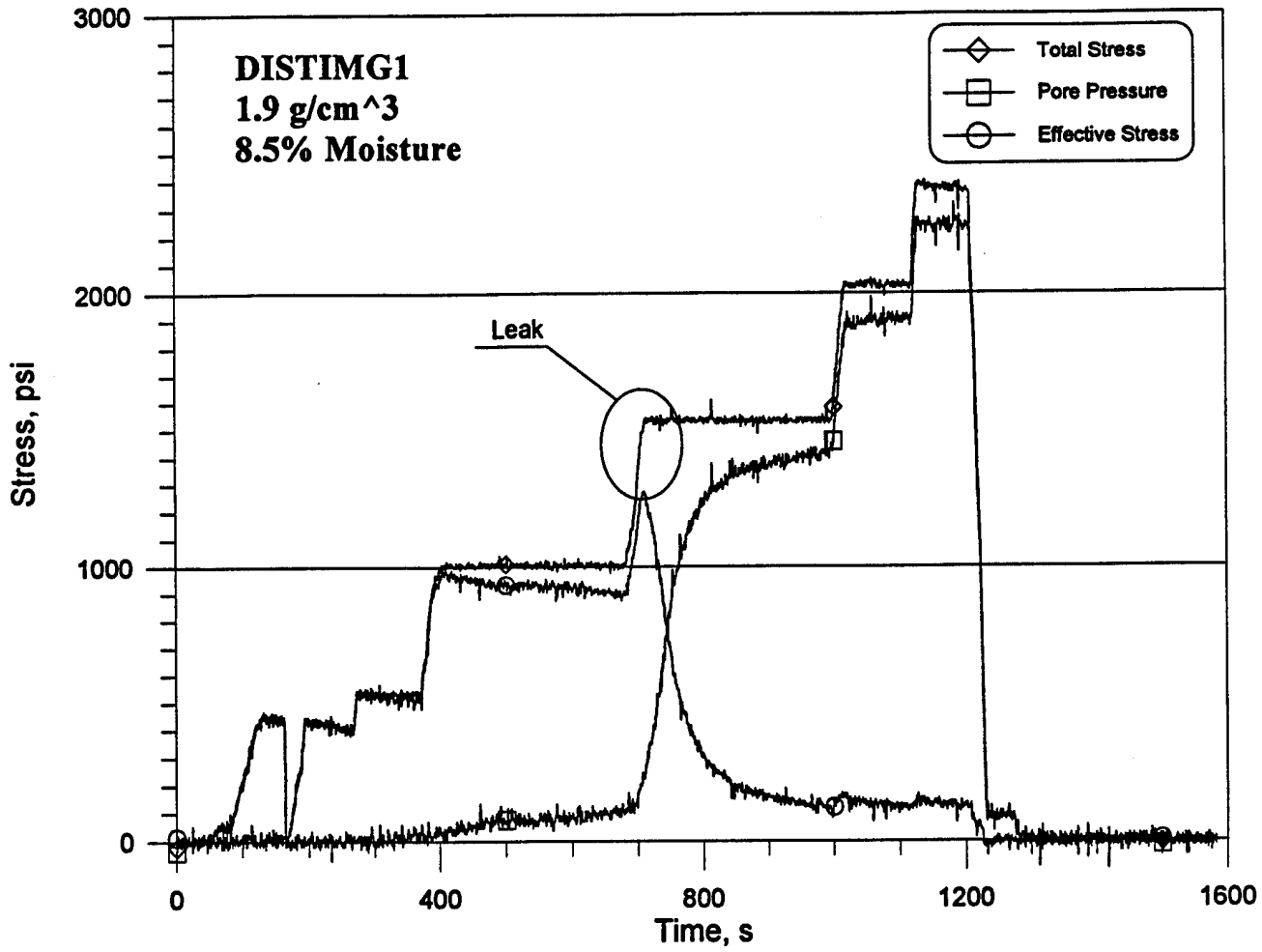

Figure B-1. Total stress, pore pressure, and effective stress time histories for test DISTIMG1.

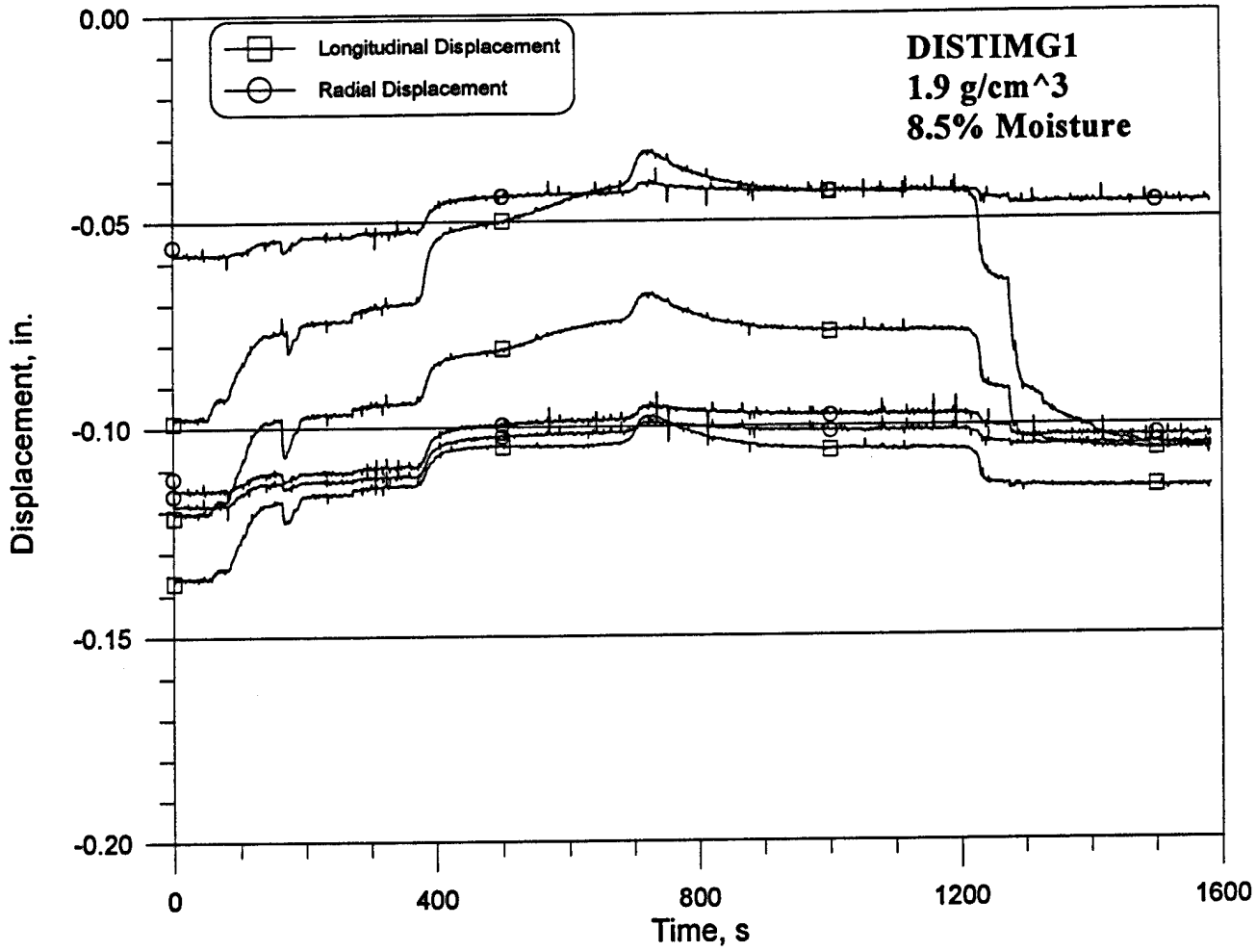

Figure B-2. Displacement time histories for test DISTIMG1.

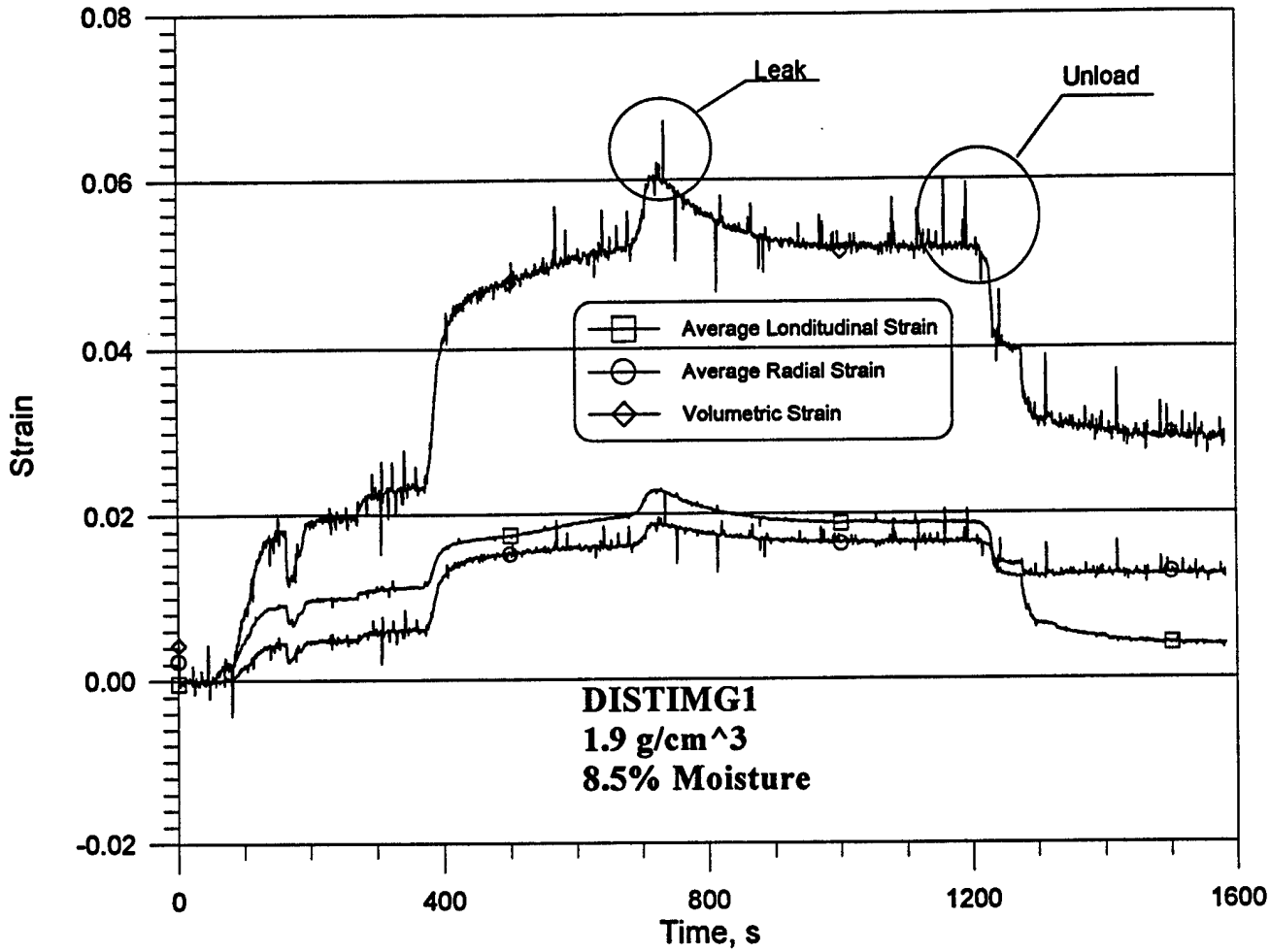

Figure B-3. Strain time histories for test DISTIMG1.

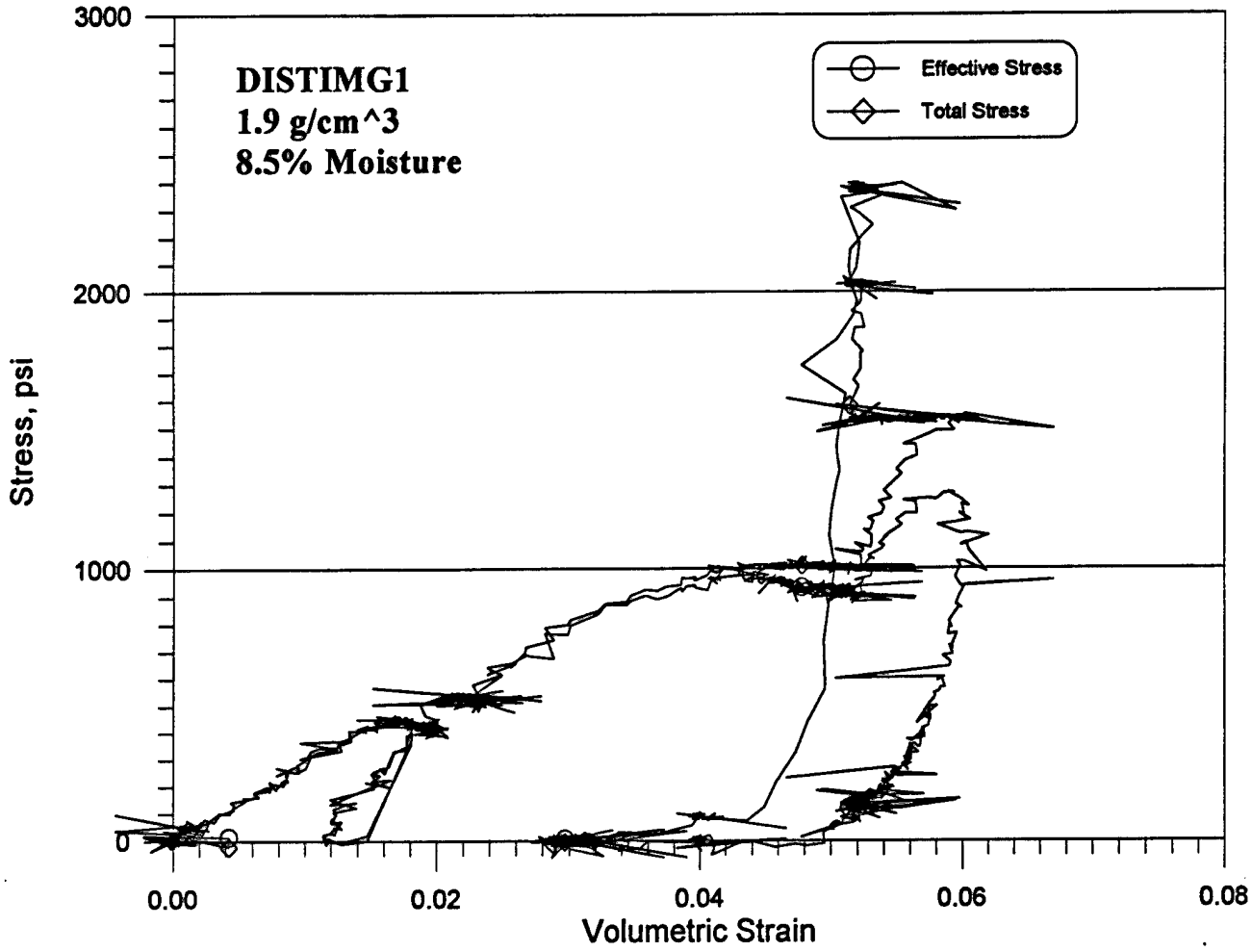

Figure B-4. Stress versus volumetric strain for test DISTIMG1.

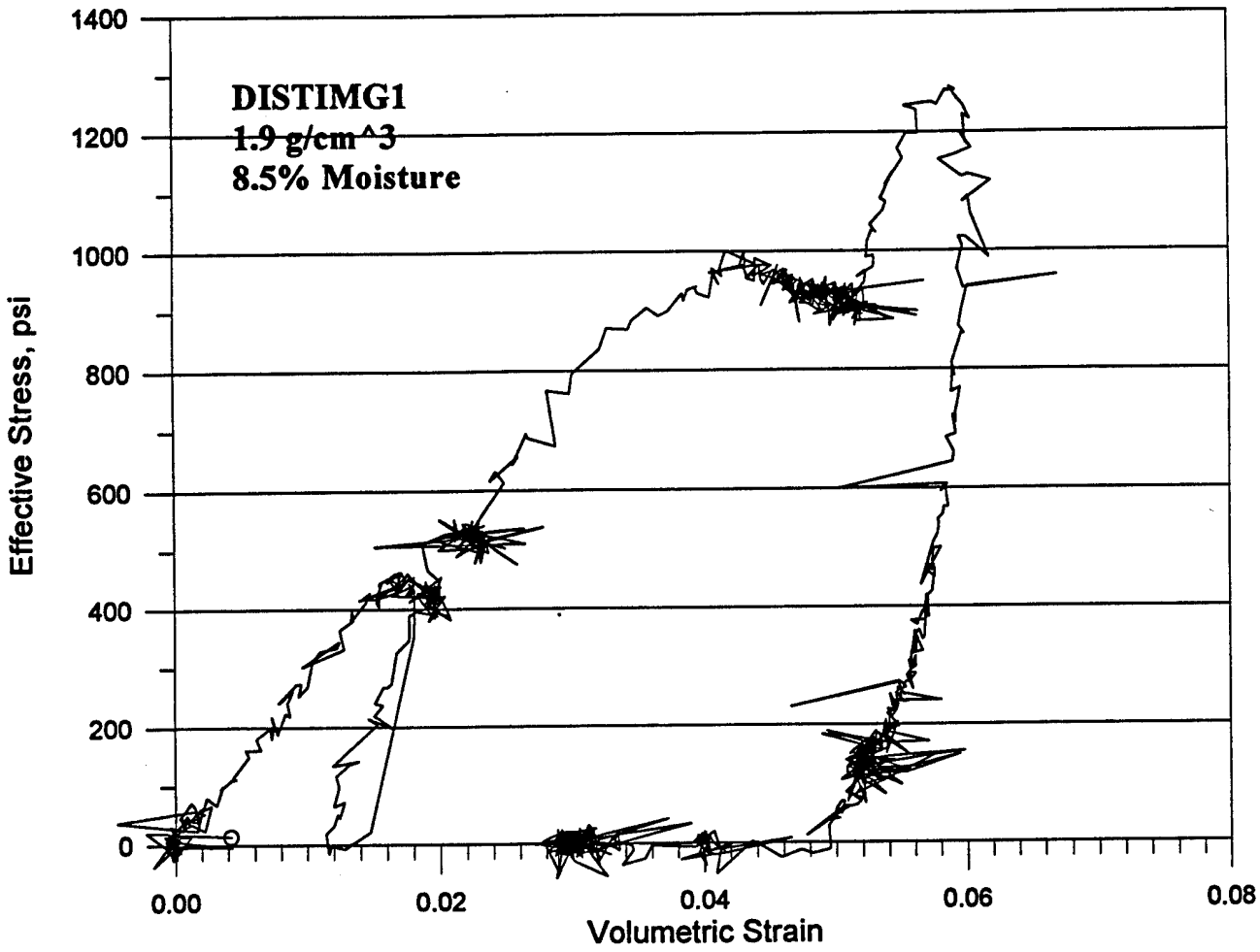

Figure B-5. Effective stress versus volumetric strain for test DISTIMG1.

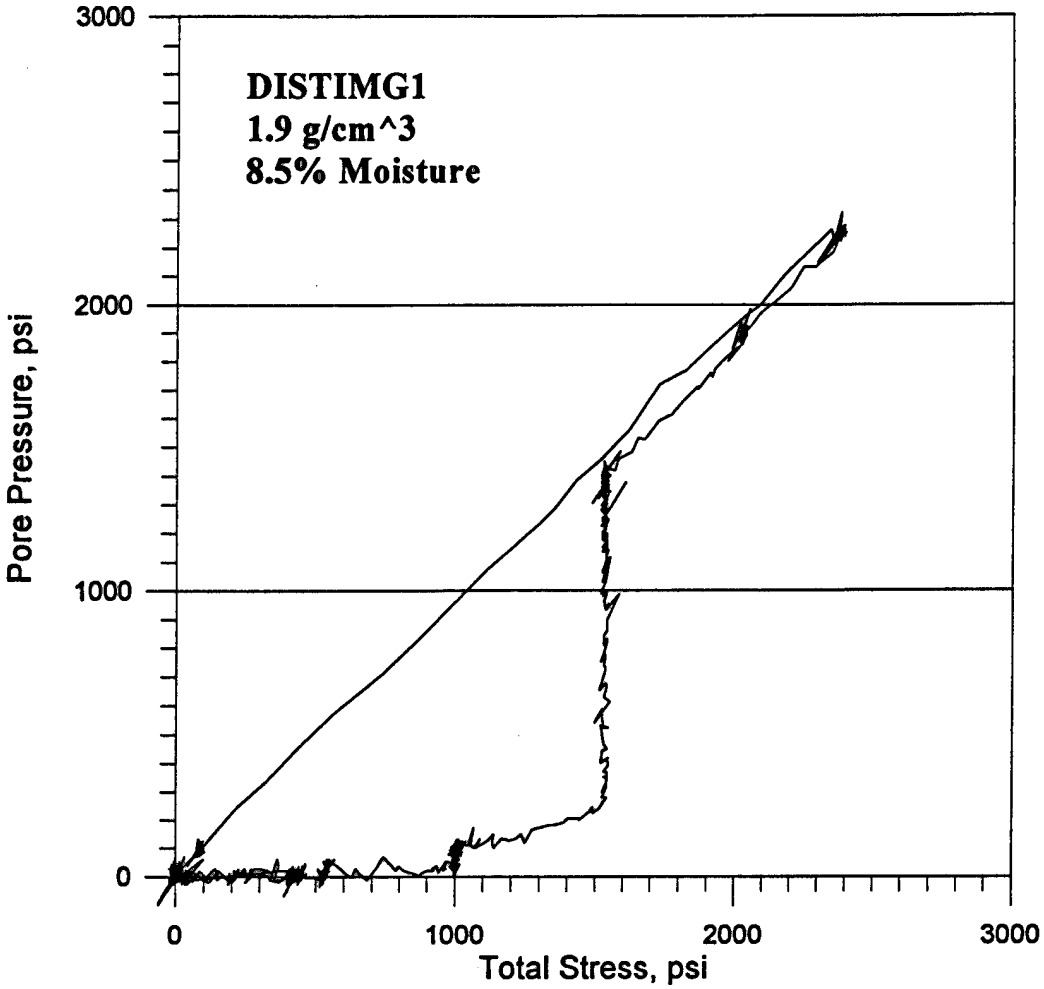

Figure B-6. Pore pressure versus total stress for test DISTIMG1.

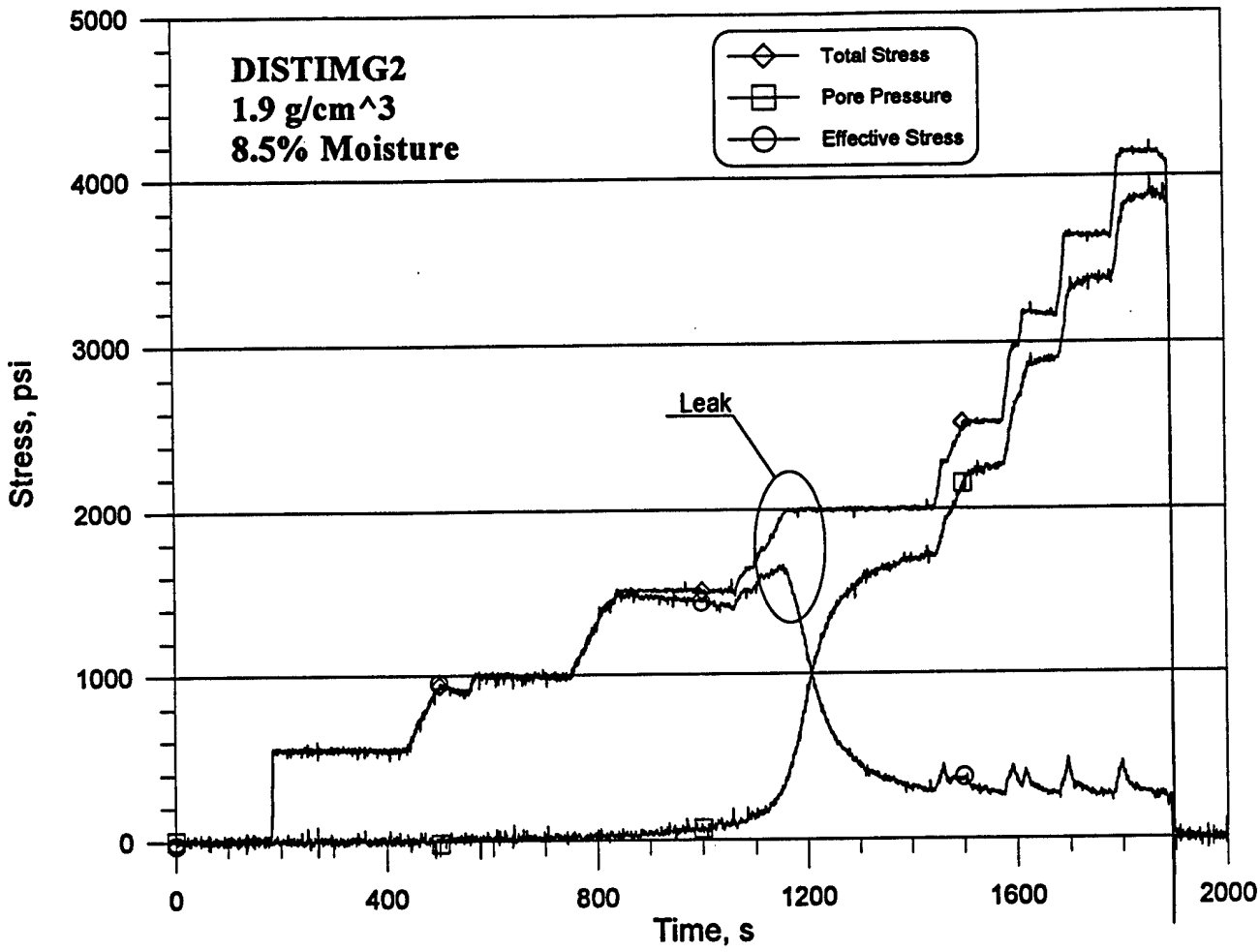

Figure B-7. Total stress, pore pressure, and effective stress time histories for test DISTIMG2.

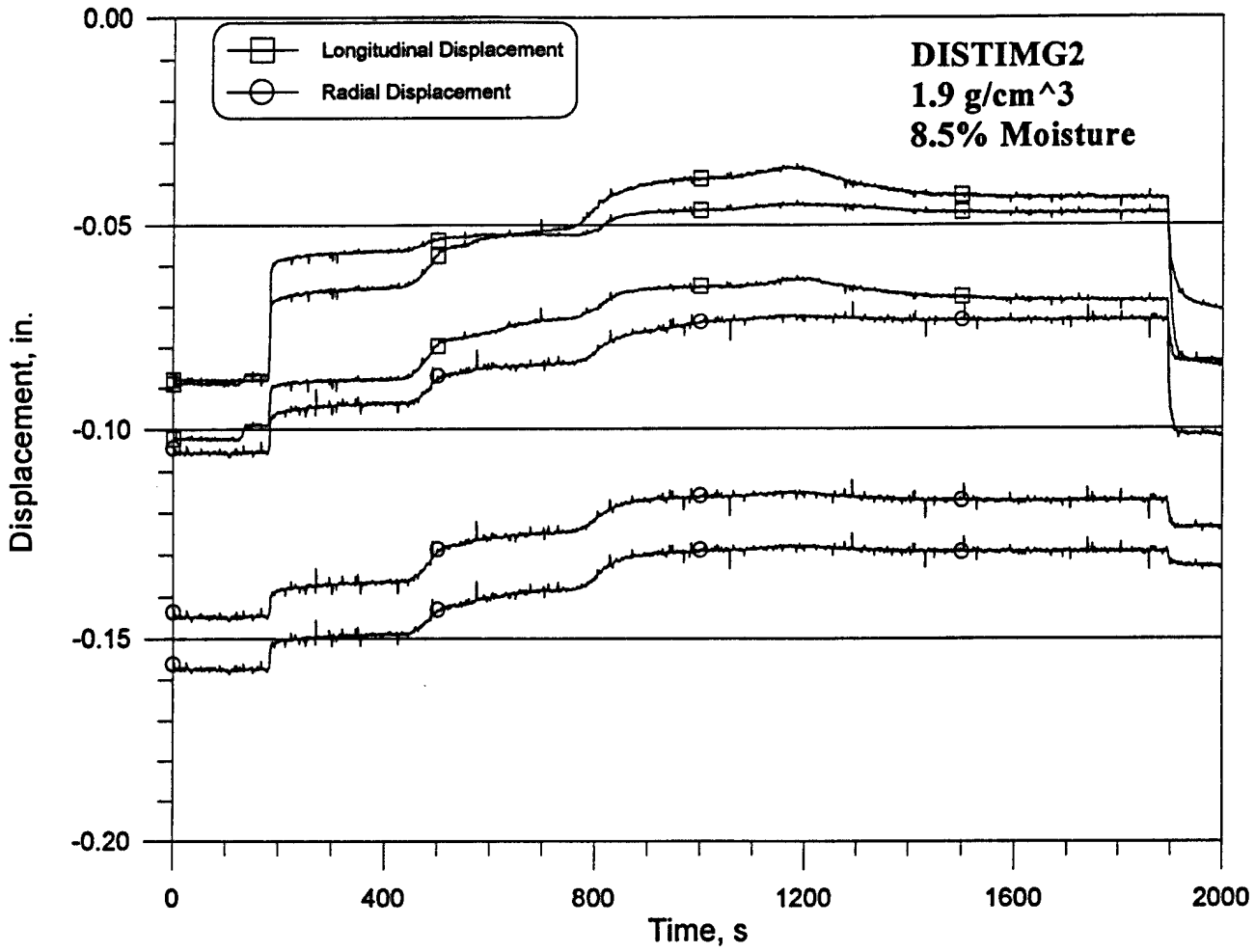

Figure B-8. Displacement time histories for test DISTIMG2.

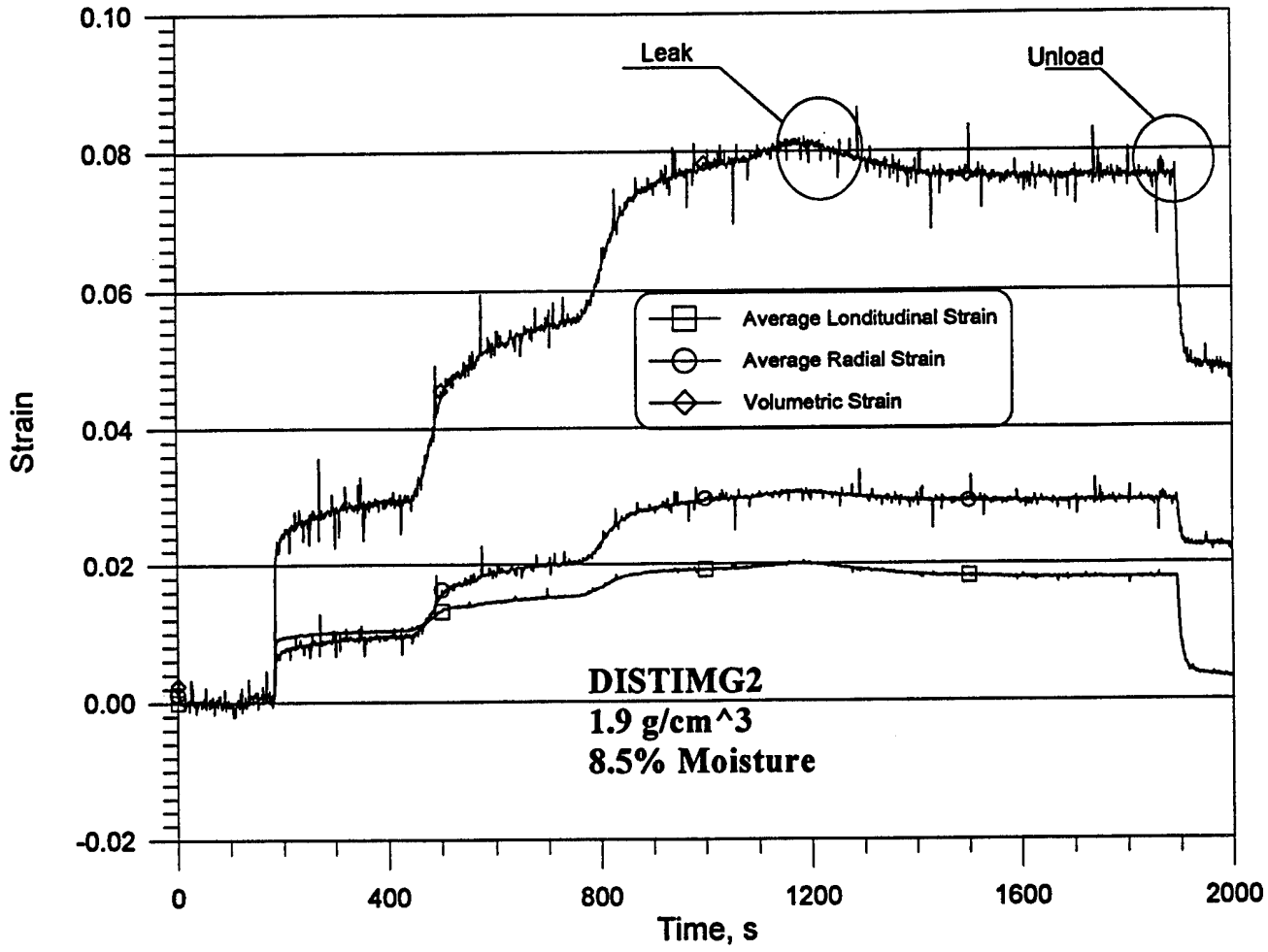

Figure B-9. Strain time histories for test DISTIMG2.

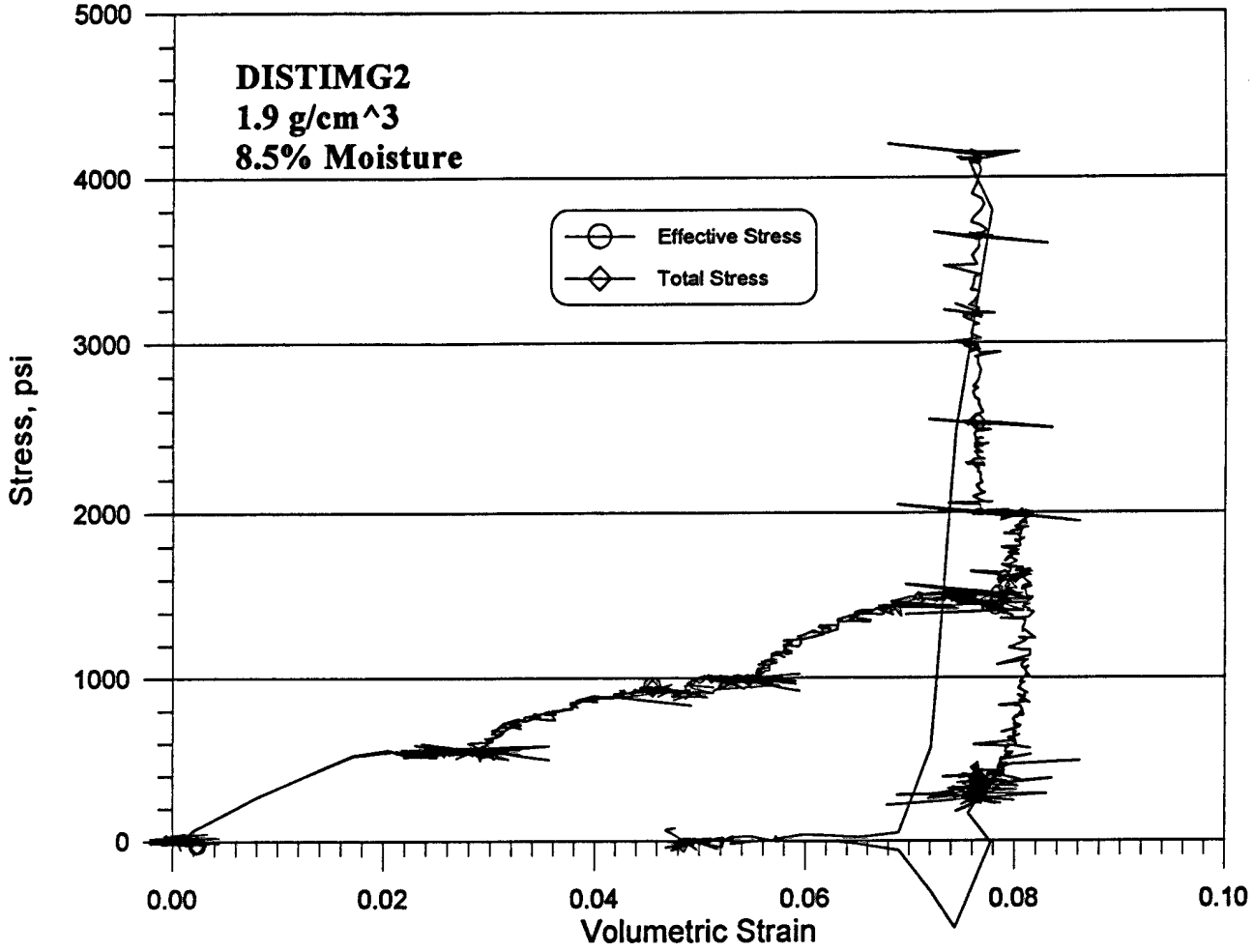

Figure B-10. Stress versus volumetric strain for test DISTIMG2.

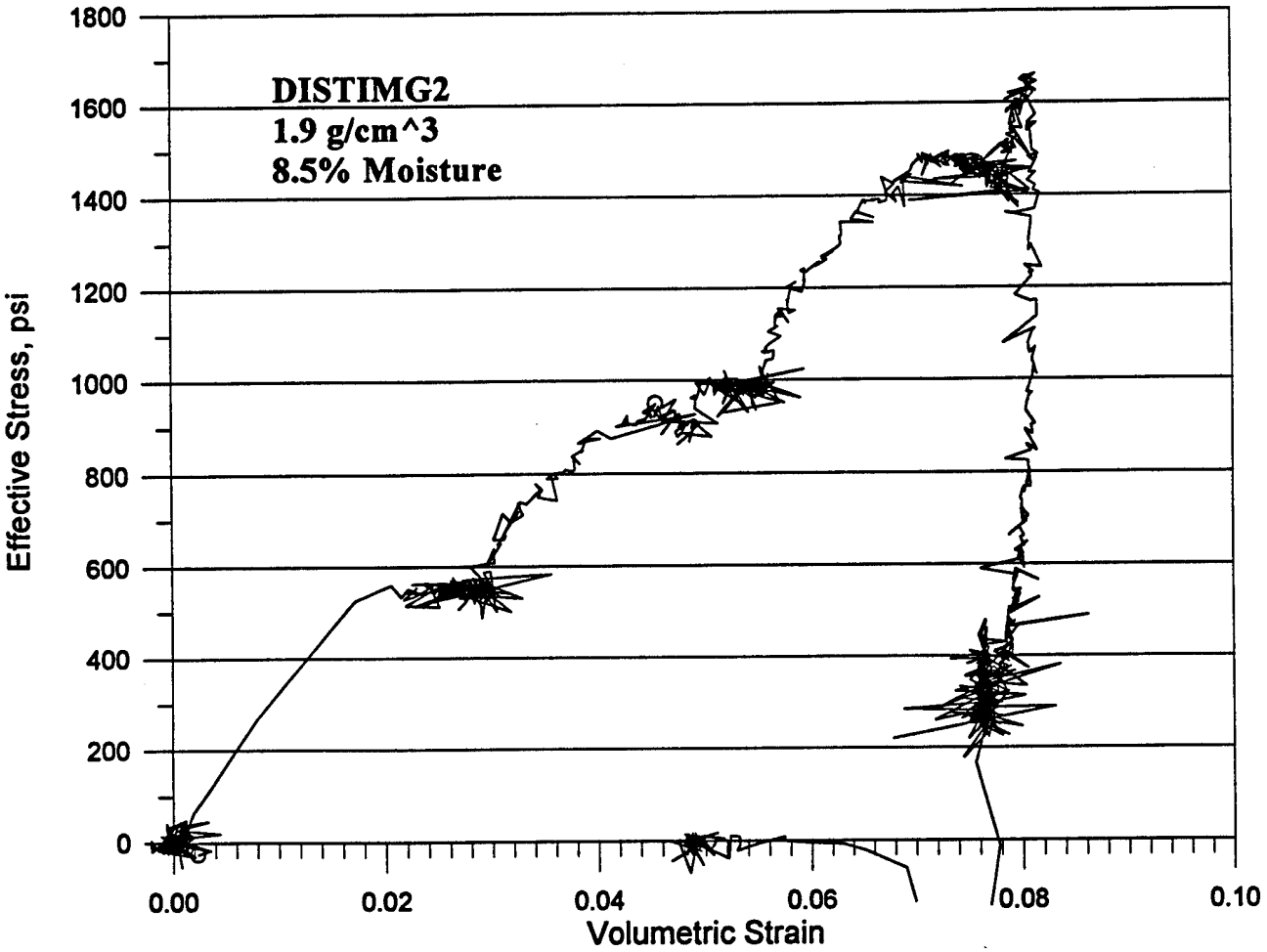

Figure B-11. Effective stress versus volumetric strain for test DISTIMG2.

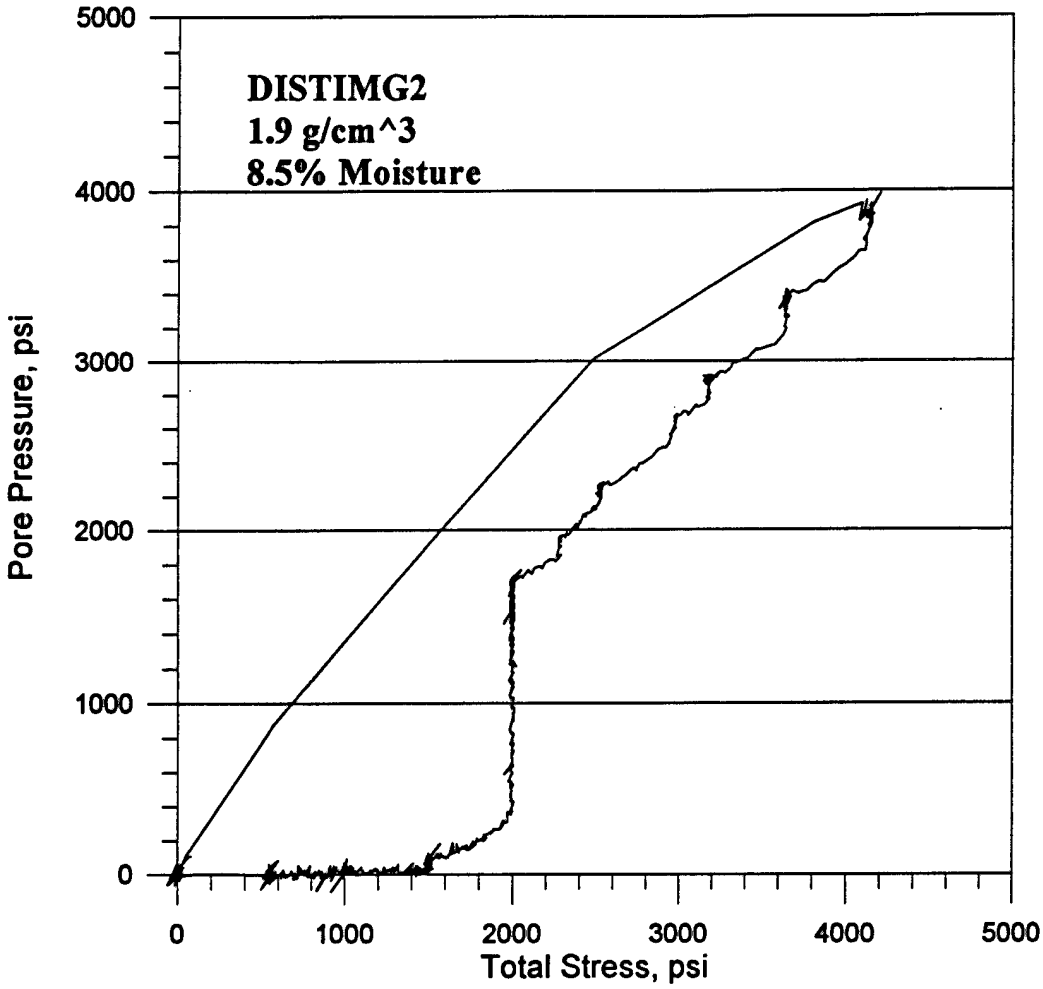

Figure B-12. Pore pressure versus total stress for test DISTIMG2.

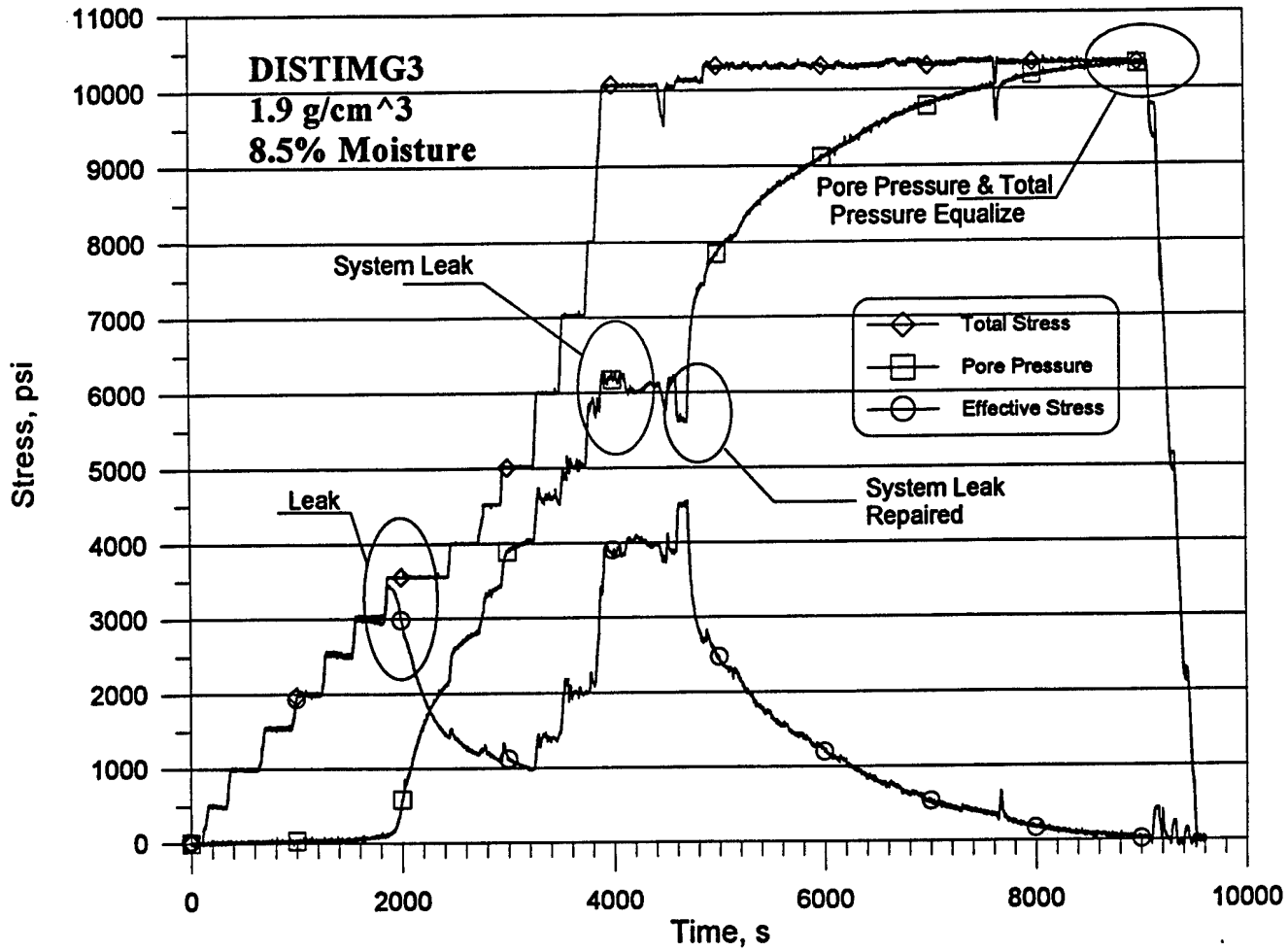

Figure B-13. Total stress, pore pressure, and effective stress time histories for test DISTIMG3.

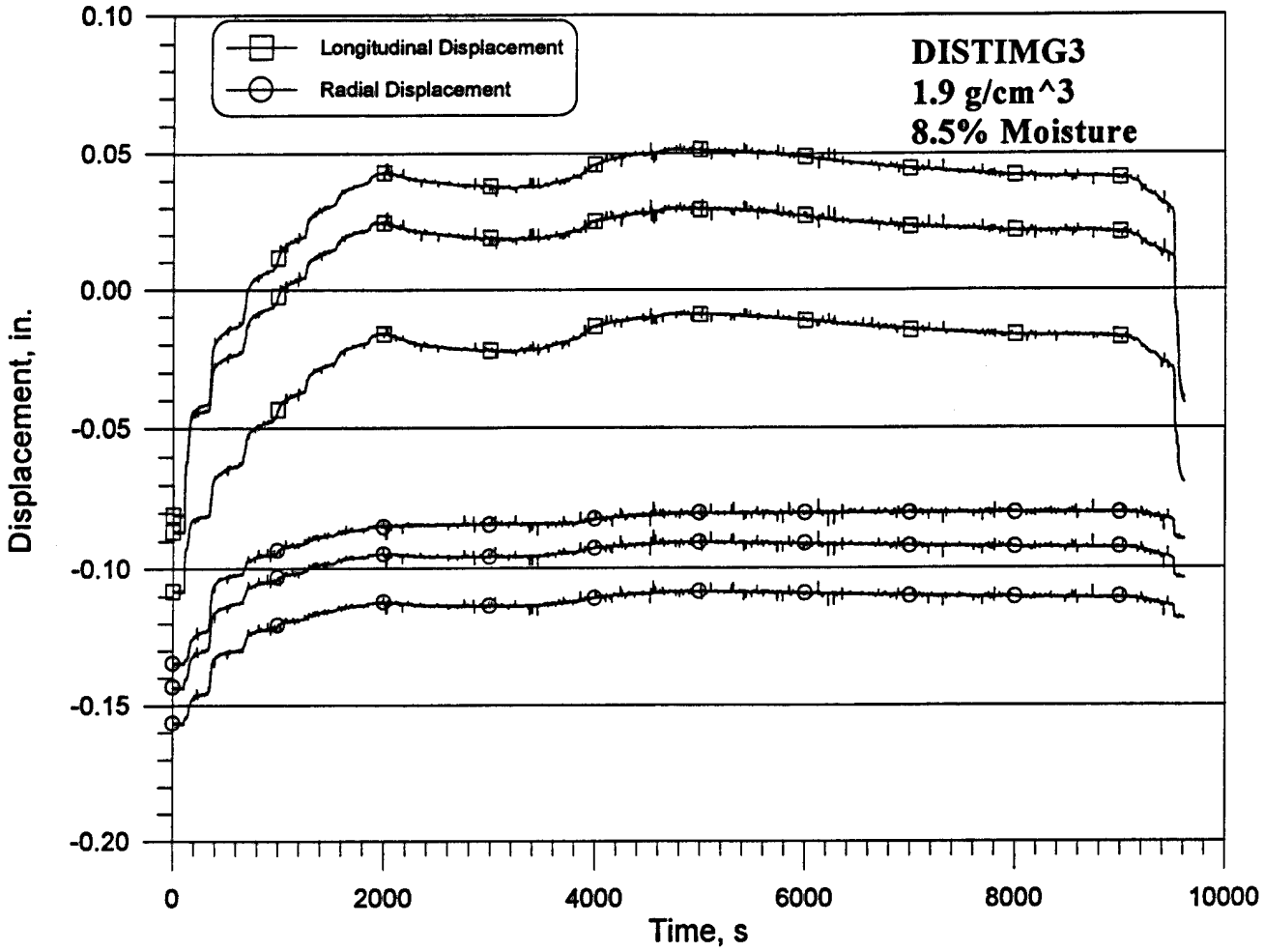

Figure B-14. Displacement time histories for test DISTIMG3.

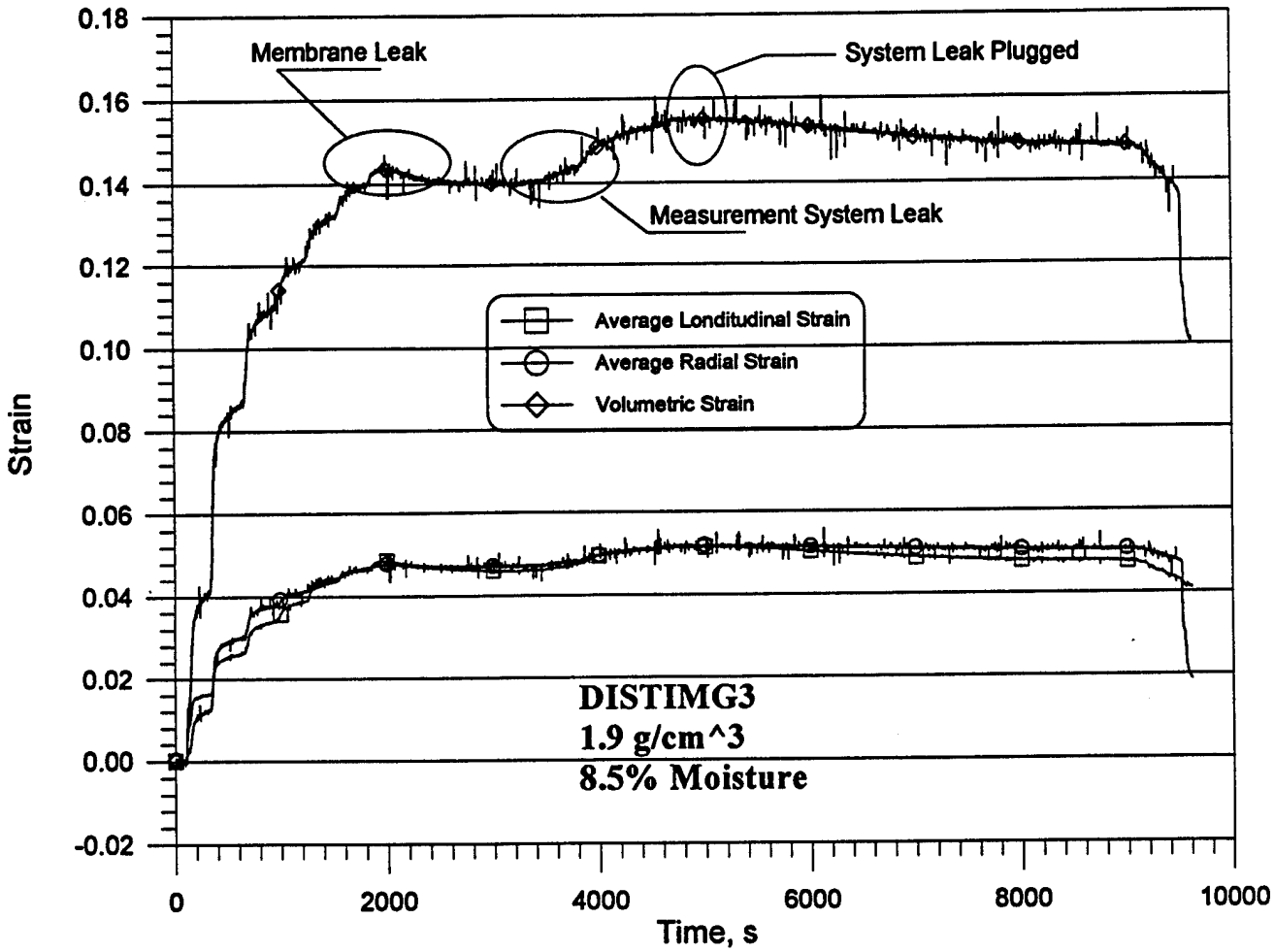

Figure B-15. Strain time histories for test DISTIMG3.

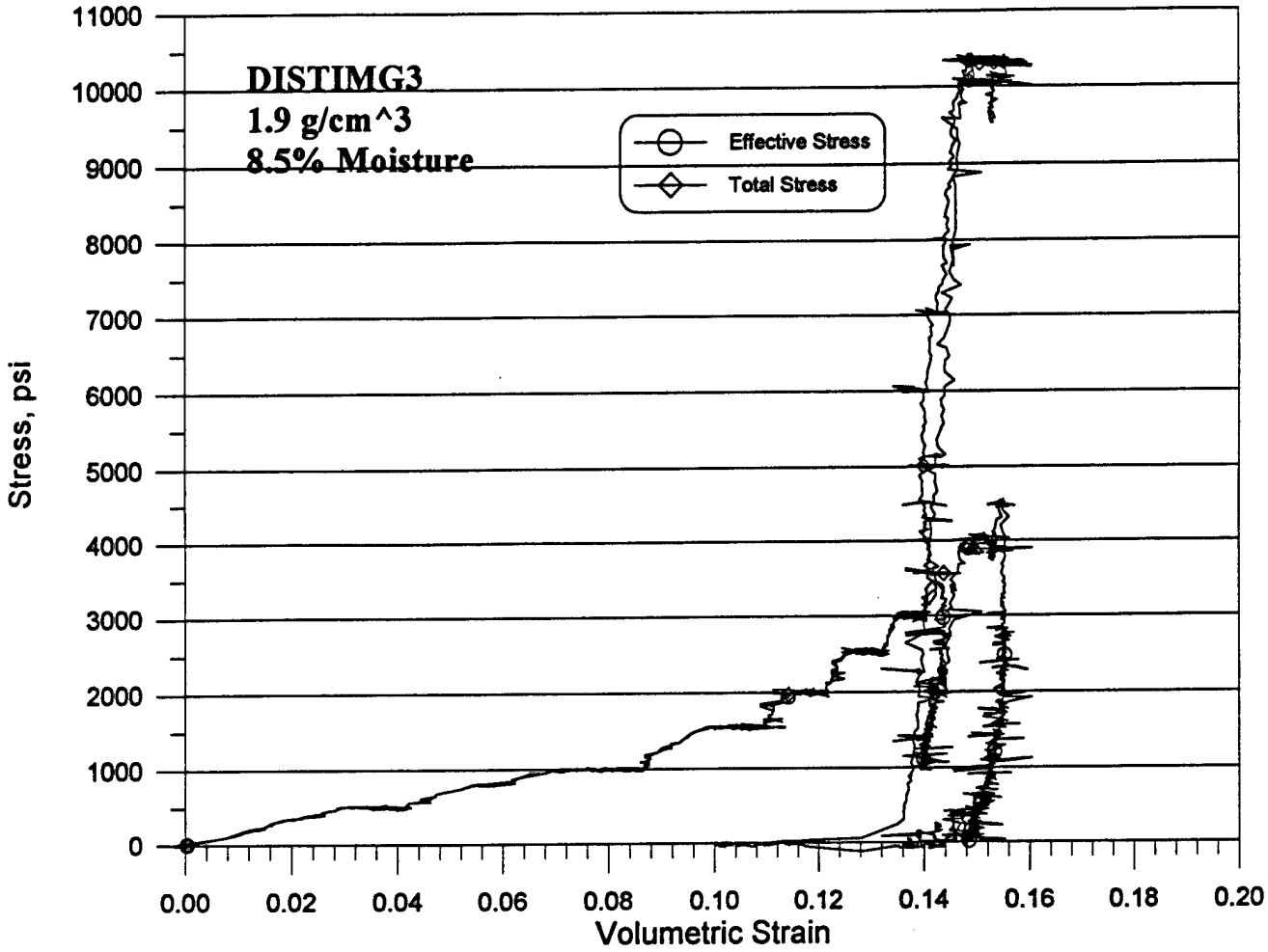

Figure B-16. Stress versus volumetric strain for test DISTIMG3.

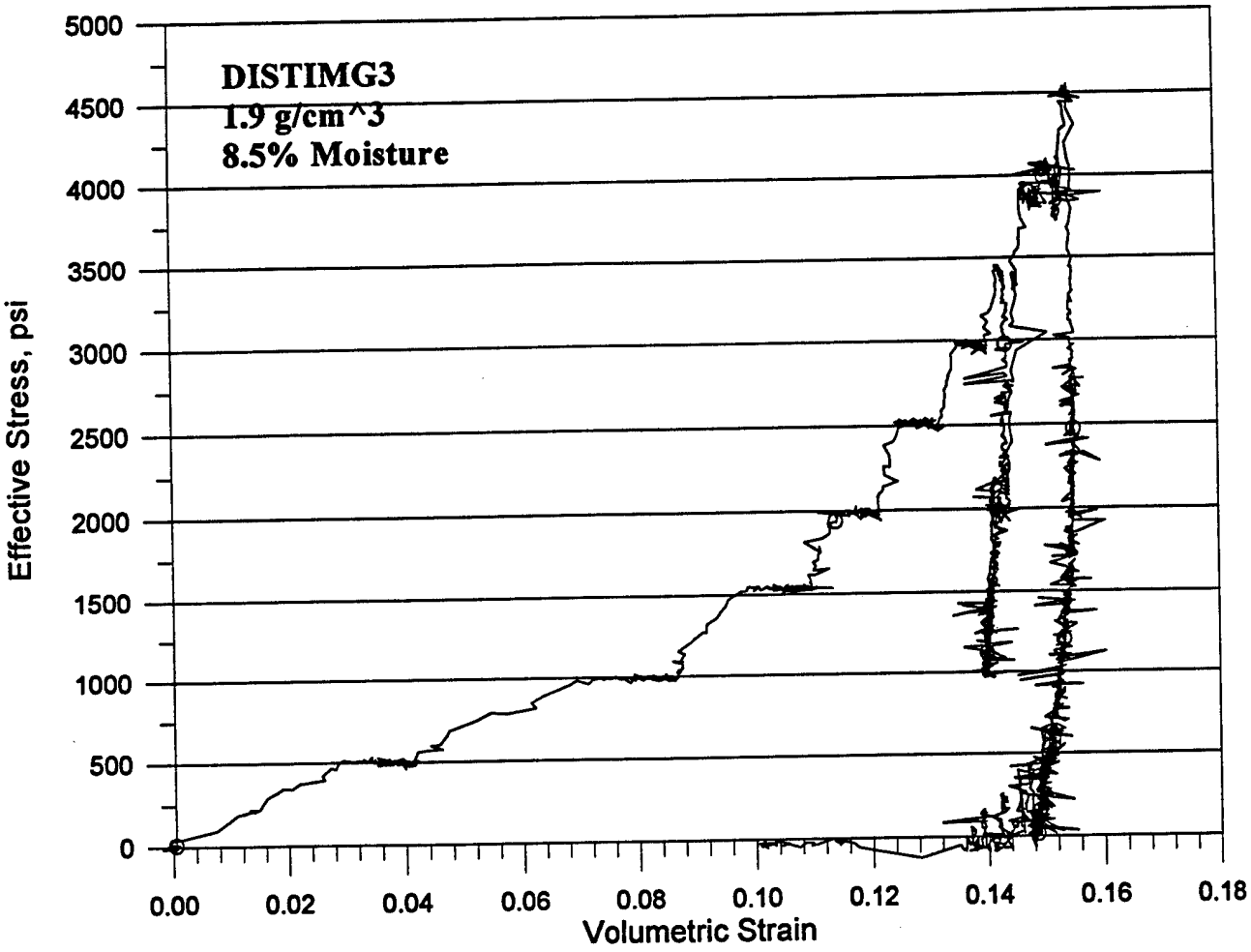

Figure B-17. Effective stress versus volumetric strain for test DISTIMG3.

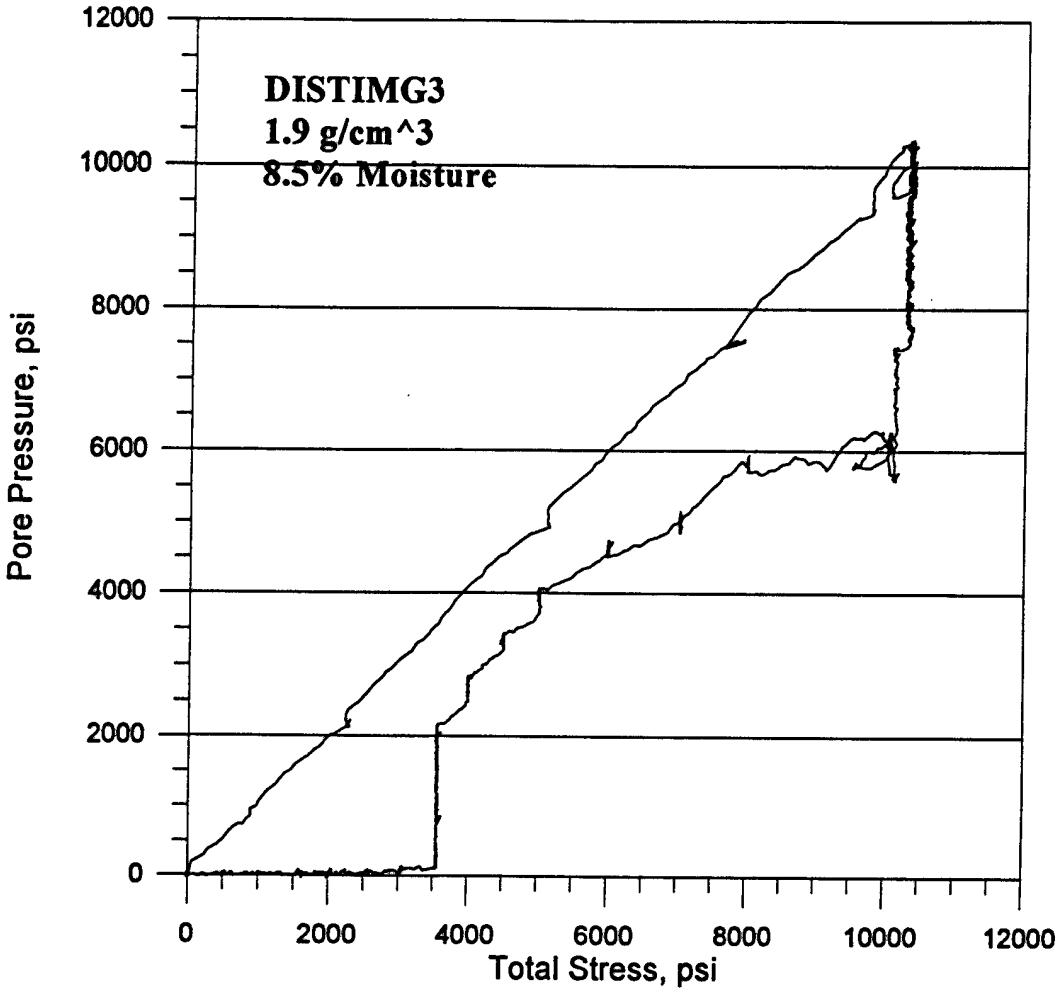

Figure B-18. Pore pressure versus total stress for test DISTIMG3.

Upon post-test examination of the DISTIMG3 sample, it was clear that the membrane had ruptured at the interface between the sample and the steel end cap. A large displacement discontinuity between the soil and the steel appears to have caused high stress concentrations in the shrink tubing at this point. In order to rectify this problem, a thin thread or bead of modeling clay was wrapped around the sample at these interfaces prior to sealing with the shrink tubing. This procedure proved completely successful for the final two tests, DISTIMG4 and DISTIMG5. At the completion of these tests, there was absolutely no evidence of hydraulic oil in the samples, only moist soil.

Tests DISTIMG4 (Figures B-19 through B-26) and DISTIMG5 (Figures B-27 through B-34) were taken successfully to 10,000 psi total stress levels without leakage. During test DISTIMG4 the pore pressure transducer malfunctioned during the early portion of the test (before 2,500 seconds). Therefore, estimates of the pore pressure response and calculated effective stress are shown as dashed lines for this test (Figure B-19). Significant pore pressures started developing after a total stress of 2,500 psi was achieved, with subsequent lockup by 3,000 psi. The effective bulk modulus was 24,000 psi. Test DISTIMG5 started developing signif-icant pore pressure at approximately 4,000 psi total stress, with subsequent lockup by 6,000 psi (Figure B-26). The calculated effective bulk modulus was approximately 32,250 psi. Stresses above lockup gave a total bulk response of 1.0×10^6 psi for both samples; this appears to be the bulk response of the soil grains. Post-test particle size analysis of the samples from DISTIMG4 and DISTIMG5 suggested that the effective stresses achieved did not produce crushing of individual soil grains (Appendix A). From the data for DISTIMG4 and DISTIMG5 the B parameter is close to unity (Equation B.1) once saturation occurs (Figures B-26 and B-34, respectively). The effective stress results for all five tests are compared in Figure B-35.

The response of three phase porous media (solids, pore fluid, and pore gas) to loading is rather complex, coupling the theories of solid mechanics and ideal gases. The time for saturation to occur is of concern, especially when rapid loading occurs. The theoretical backpressure (P) required to bring a soil sample from an initial degree of saturation (S_i) to a final degree of saturation (S) by dissolution and compression of the pore gas is given by the equation (Lowe and Johnson 1960)

$$P = P_i[(S - S_i)(1 - H)]/[1 - S(1 - H)] \qquad (B.2)$$

where P_i is the initial absolute gas pressure corresponding to S_i and H is Henry's constant of solubility of the pore gas. For air at room temperature Henry's constant is equal to 0.02 cm^3 of air per 1 cm^3 of water. The degree of saturation of the DISTANT IMAGE samples prior to test was 0.585, while the initial gas pressure was the atmospheric pressure (12.2 psia). Hence the pressure required for complete saturation is 248 psia. For the testing program cited herein, the pressures imposed in the pore fluid are a result of applied total stresses and are not caused by backpressure saturation. It seems that the soil skeleton must collapse under total stress in order to develop sufficient pore pressure to cause dissolution of the pore air into the pore water. Therefore, the above estimate may be considered as a lower bound at which pore air will dissolve in the pore water.

The immediate degree of saturation upon application of a backpressure (P_{app}) can be calculated using Boyle's Law (Black and Lee 1973) as

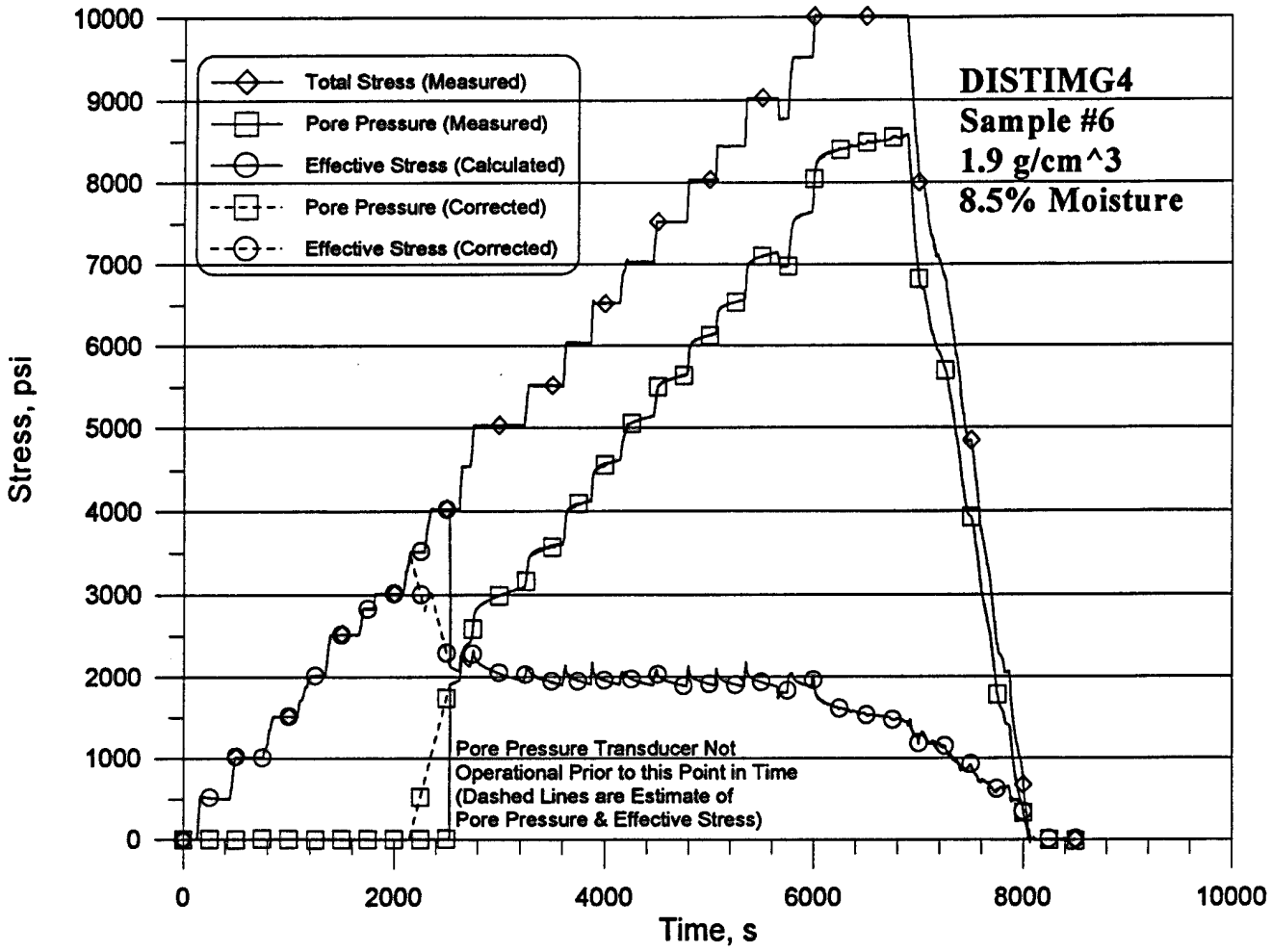

Figure B-19. Total stress, pore pressure, and effective stress time histories for test DISTIMG4.

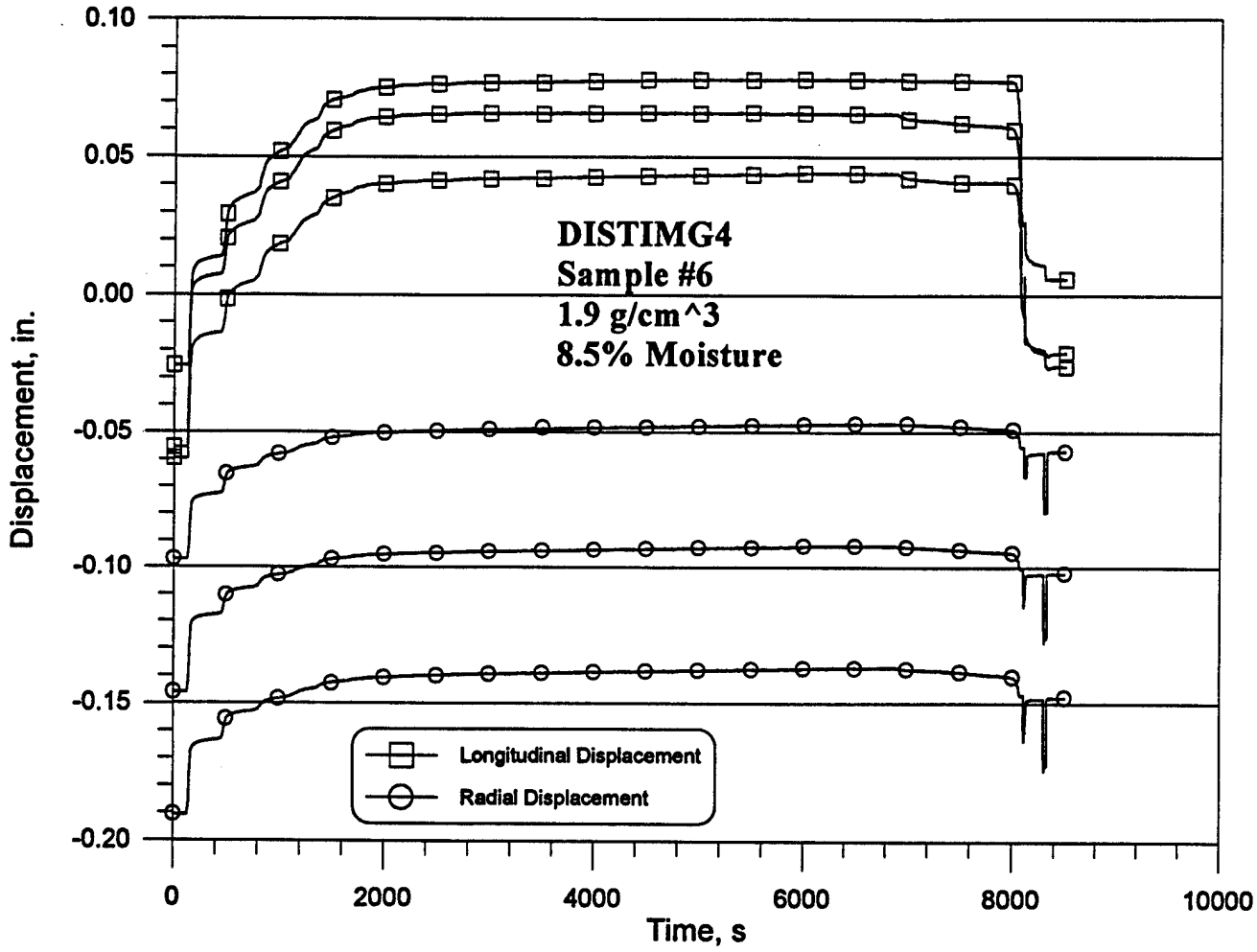

Figure B-20. Displacement time histories for test DISTIMG4.

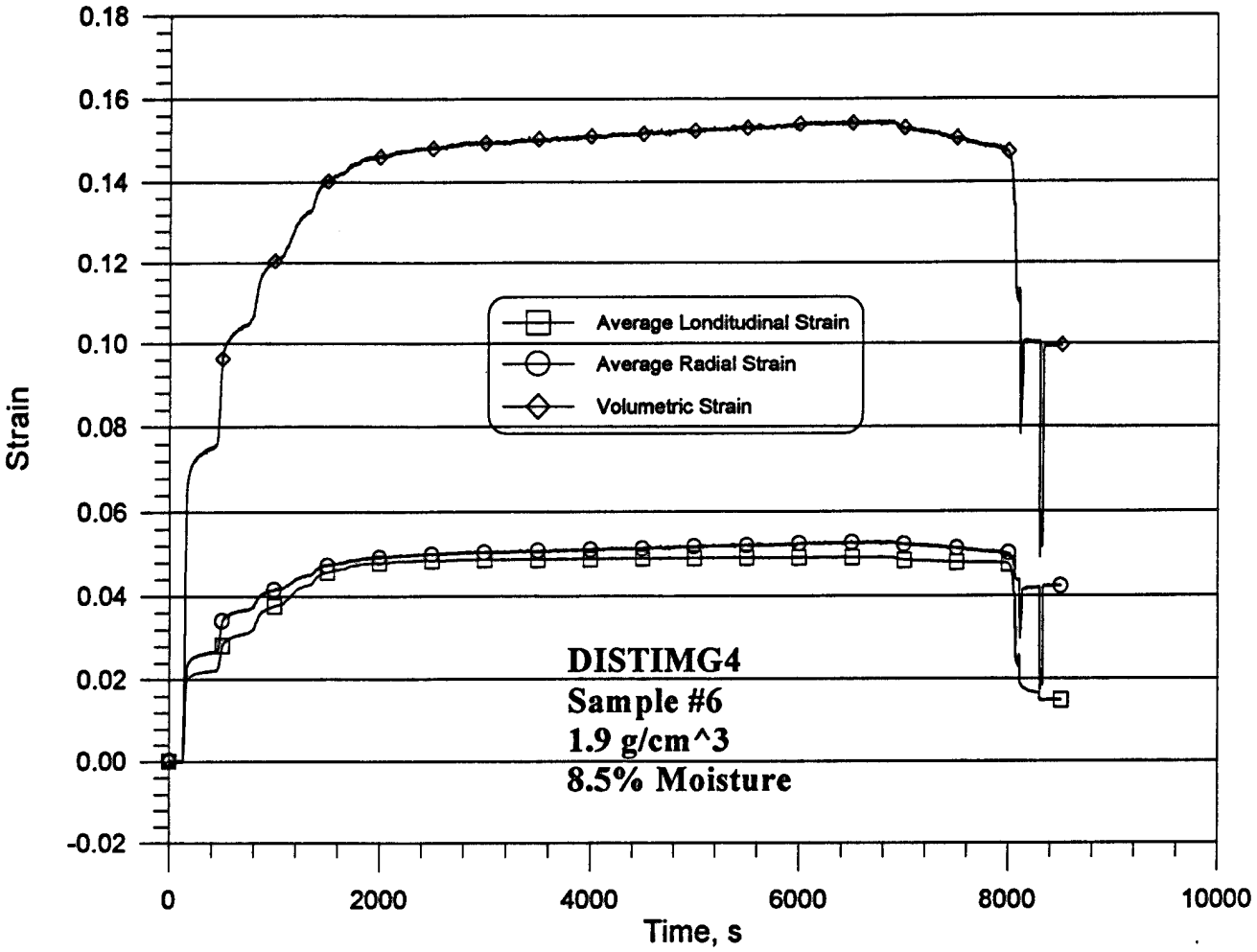

Figure B-21. Strain time histories for test DISTIMG4.

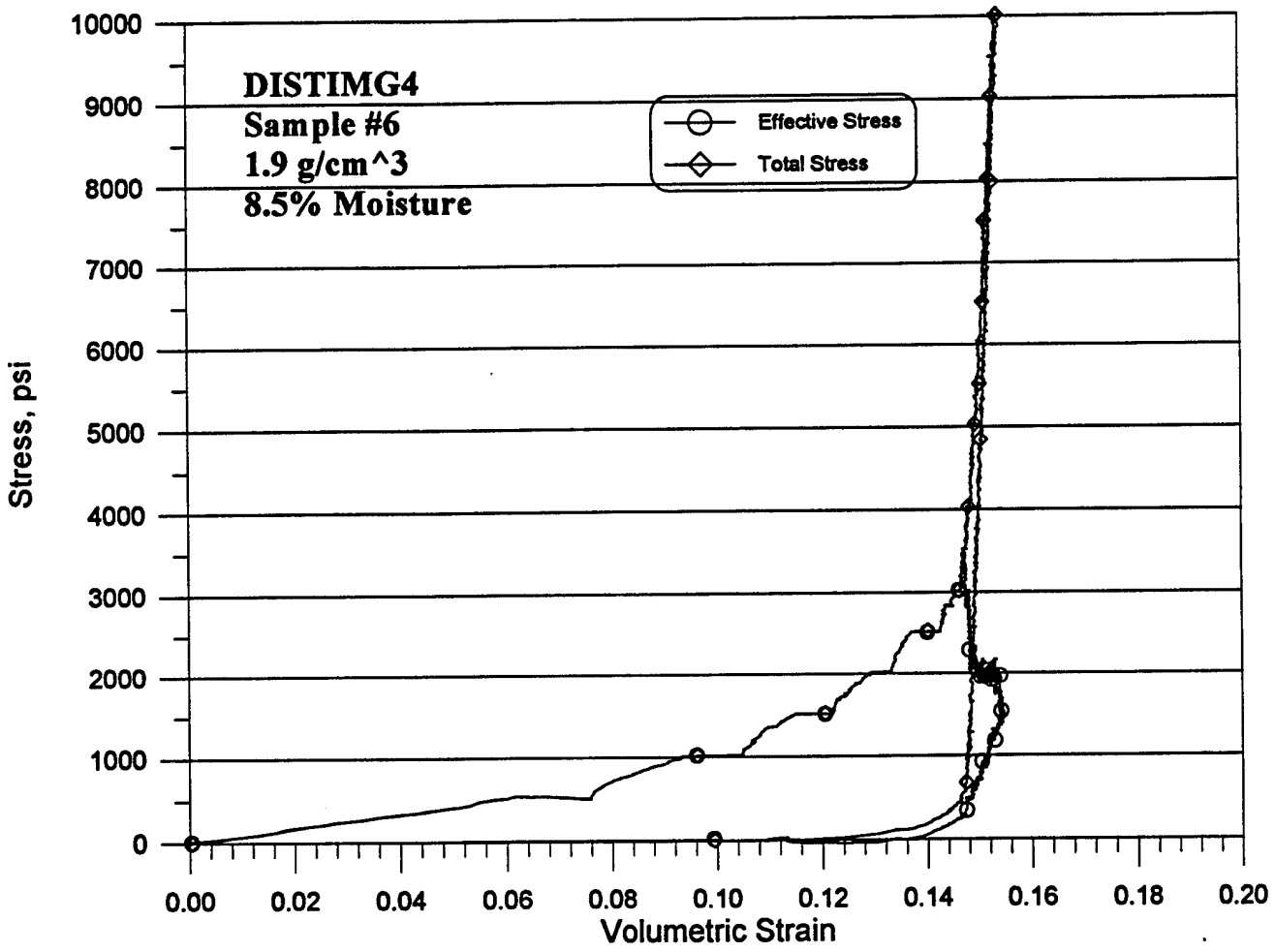

Figure B-22. Stress versus volumetric strain for test DISTIMG4.

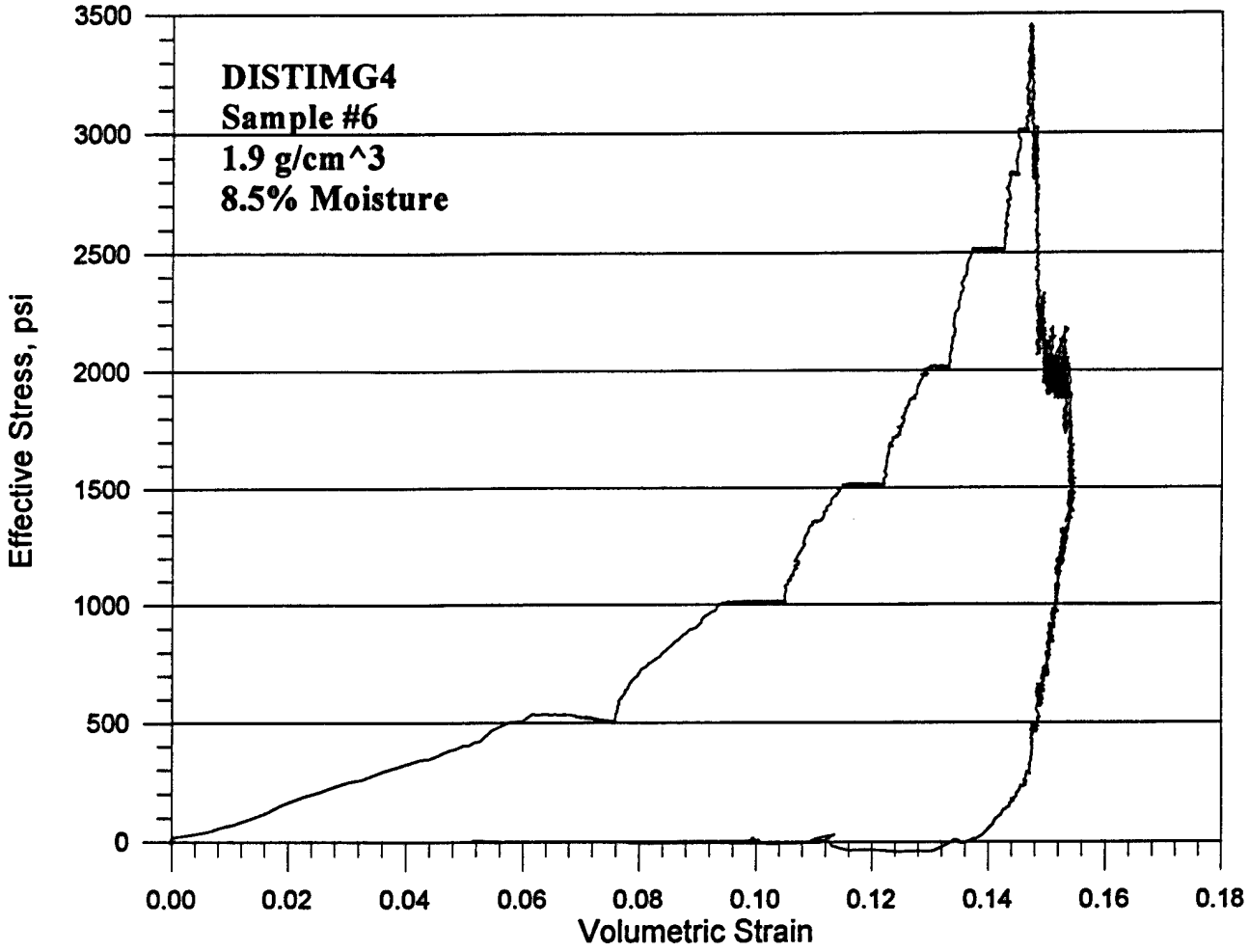

Figure B-23. Effective stress versus volumetric strain for test DISTIMG4.

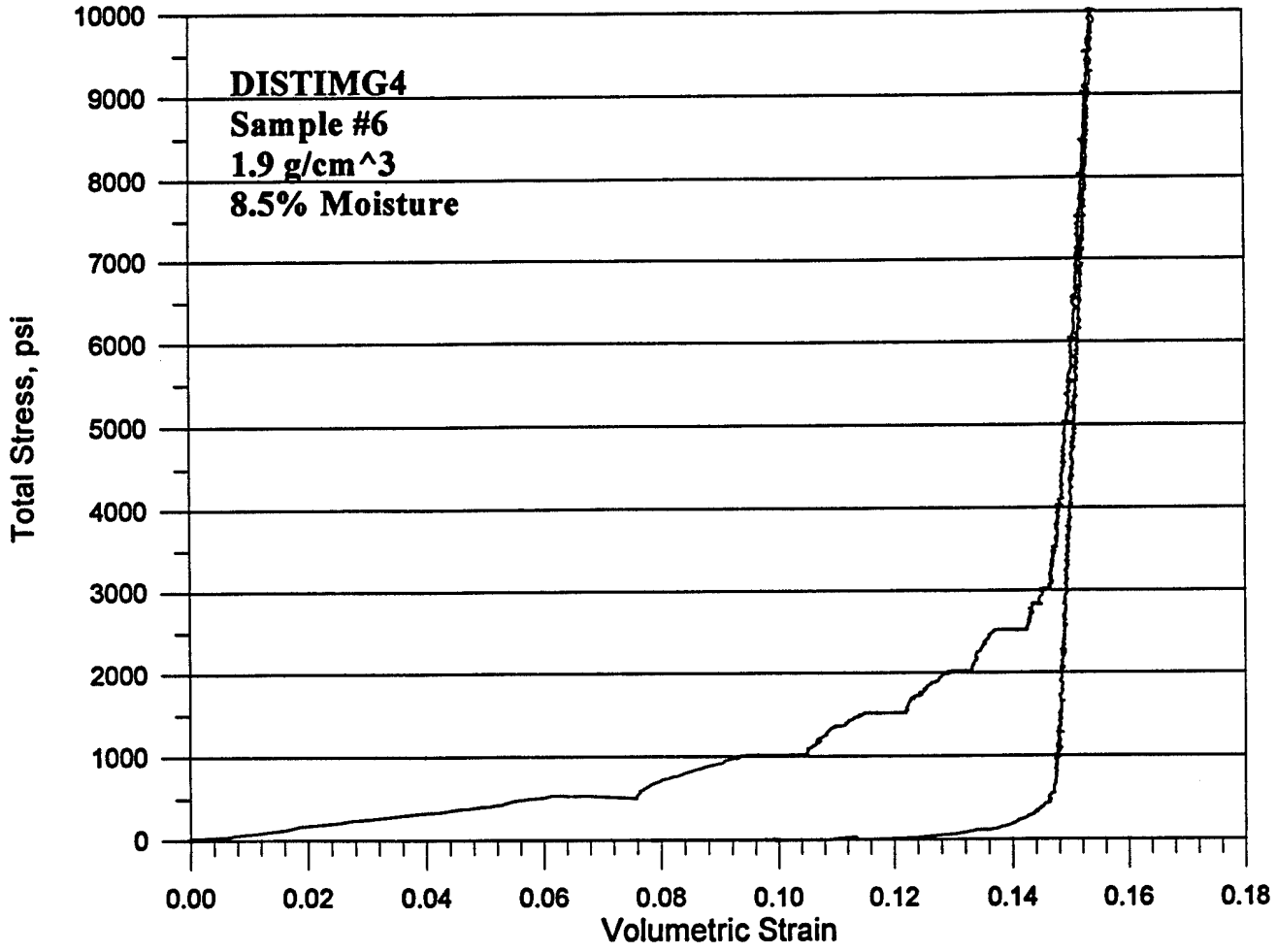

Figure B-24. Total stress versus volumetric strain for test DISTIMG4.

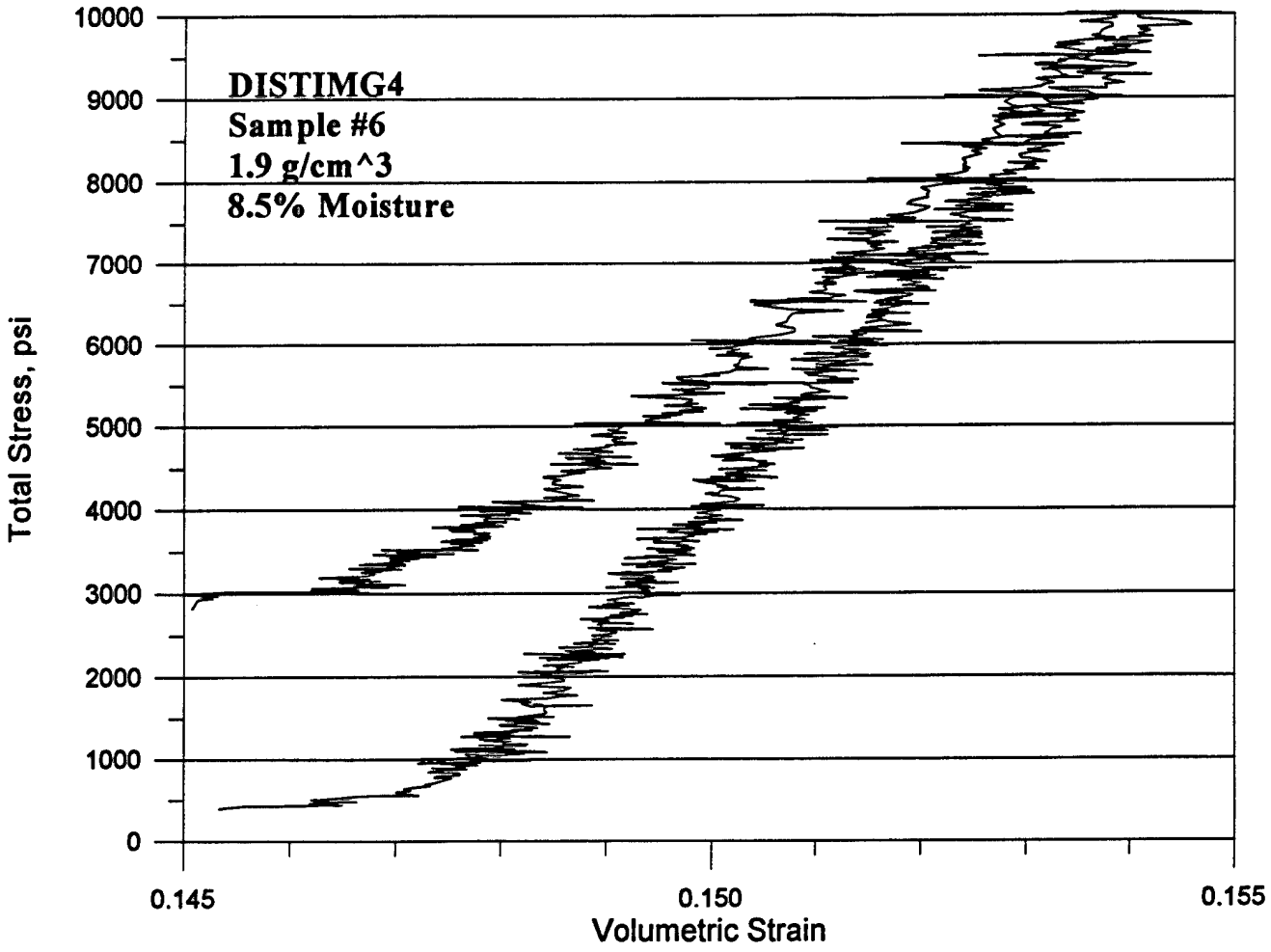

Figure B-25. Total stress versus volumetric strain for test DISTIMG4 (detail).

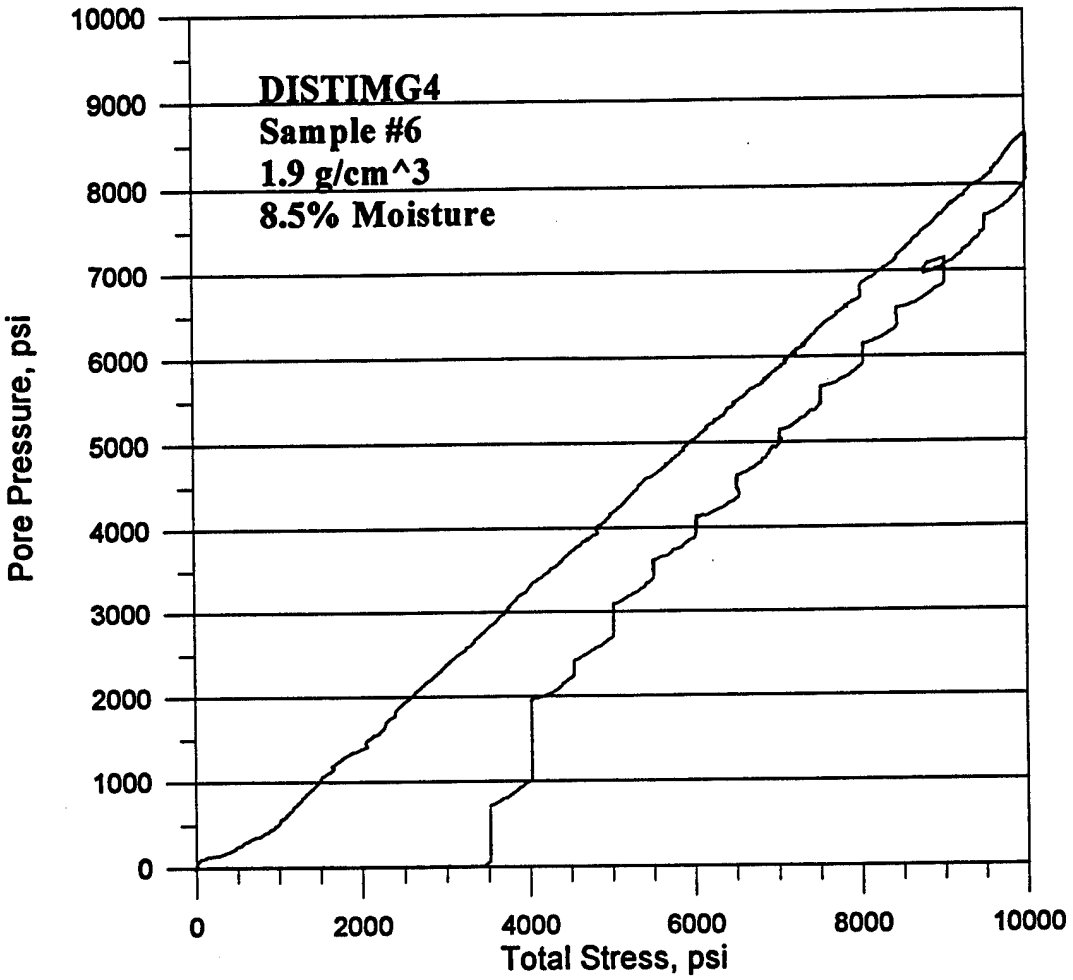

Figure B-26. Pore pressure versus total stress for test DISTIMG4.

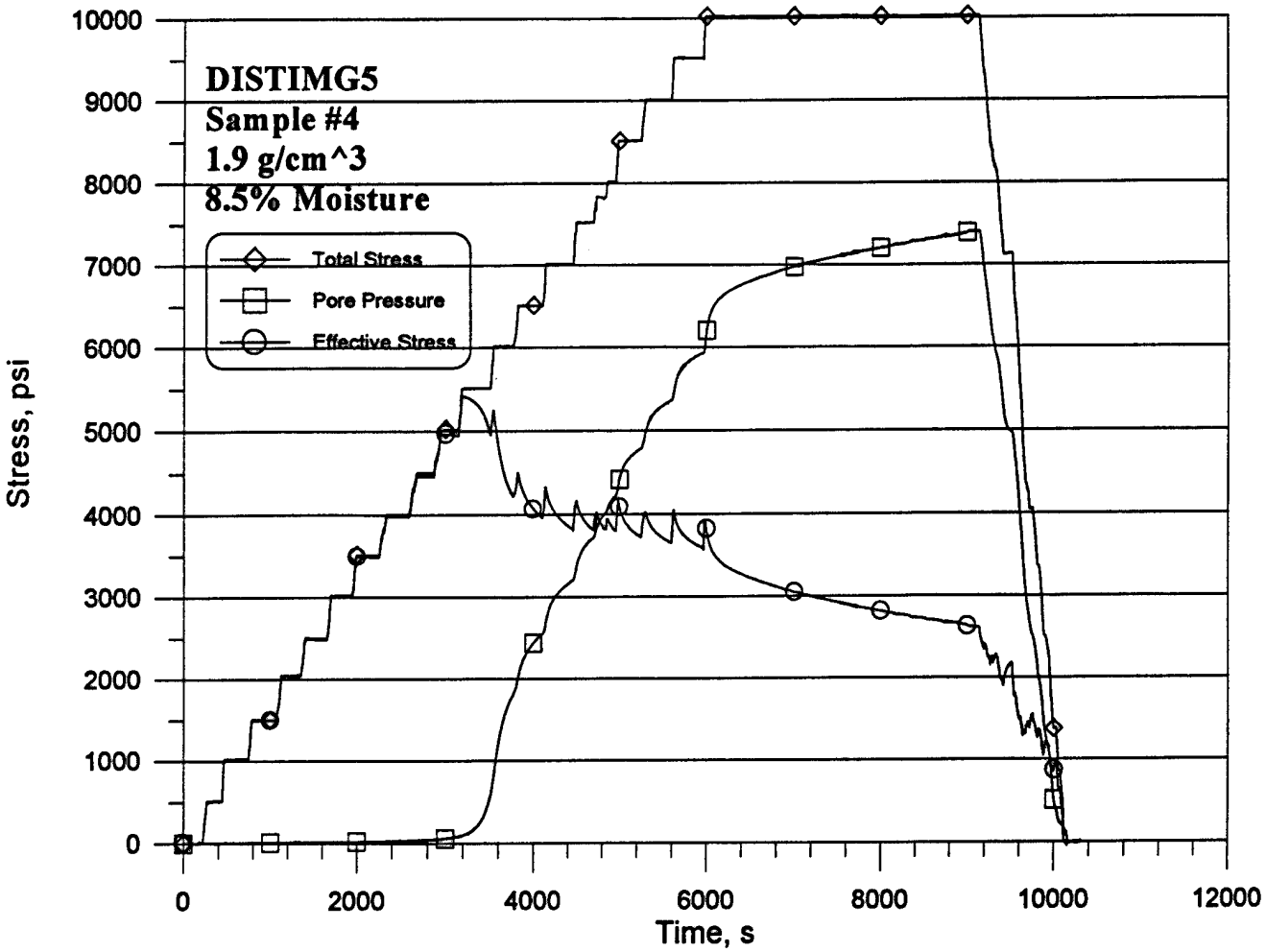

Figure B-27. Total stress, pore pressure, and effective stress time histories for test DISTIMG5.

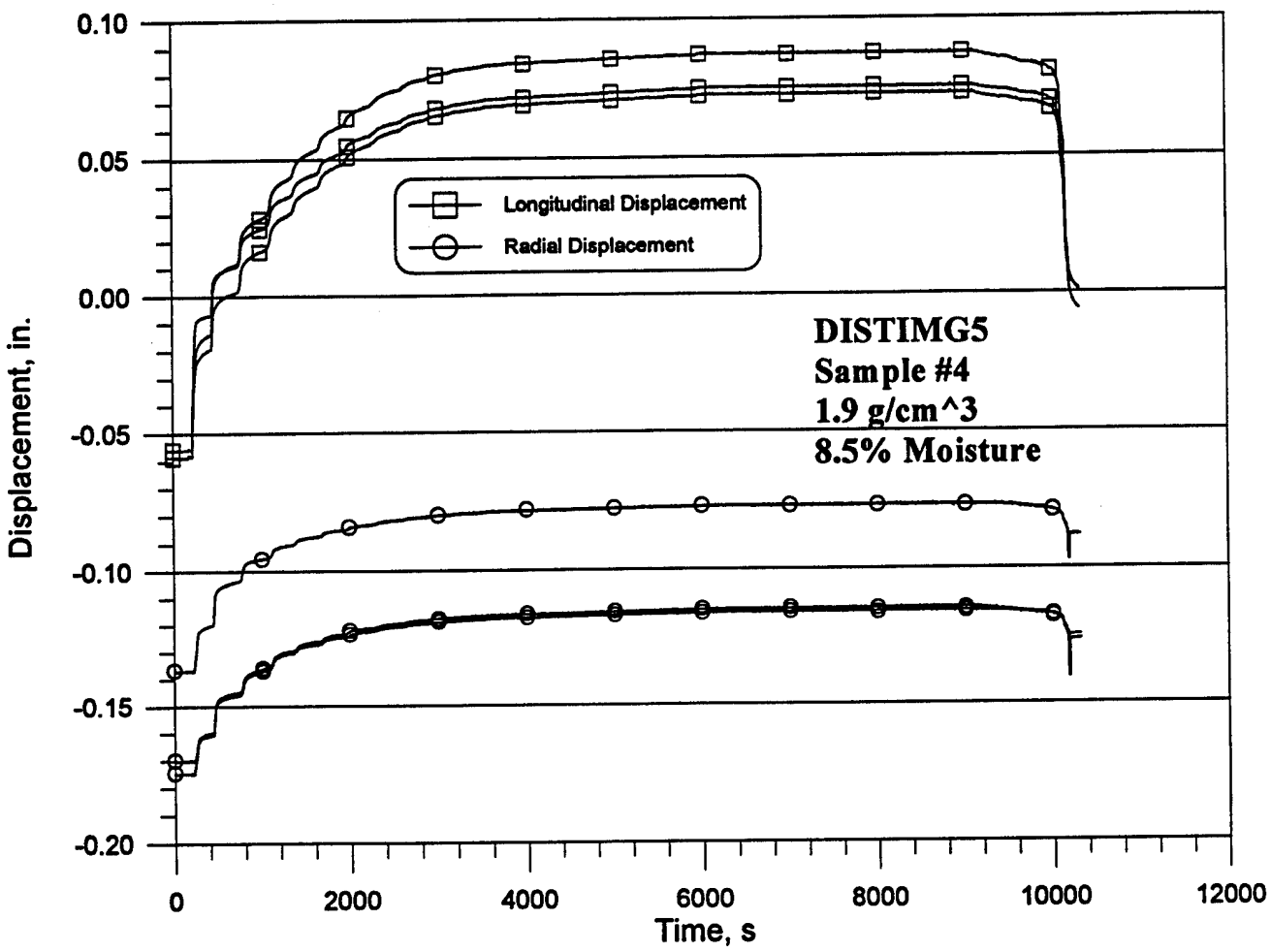

Figure B-28. Displacement time histories for test DISTIMG5.

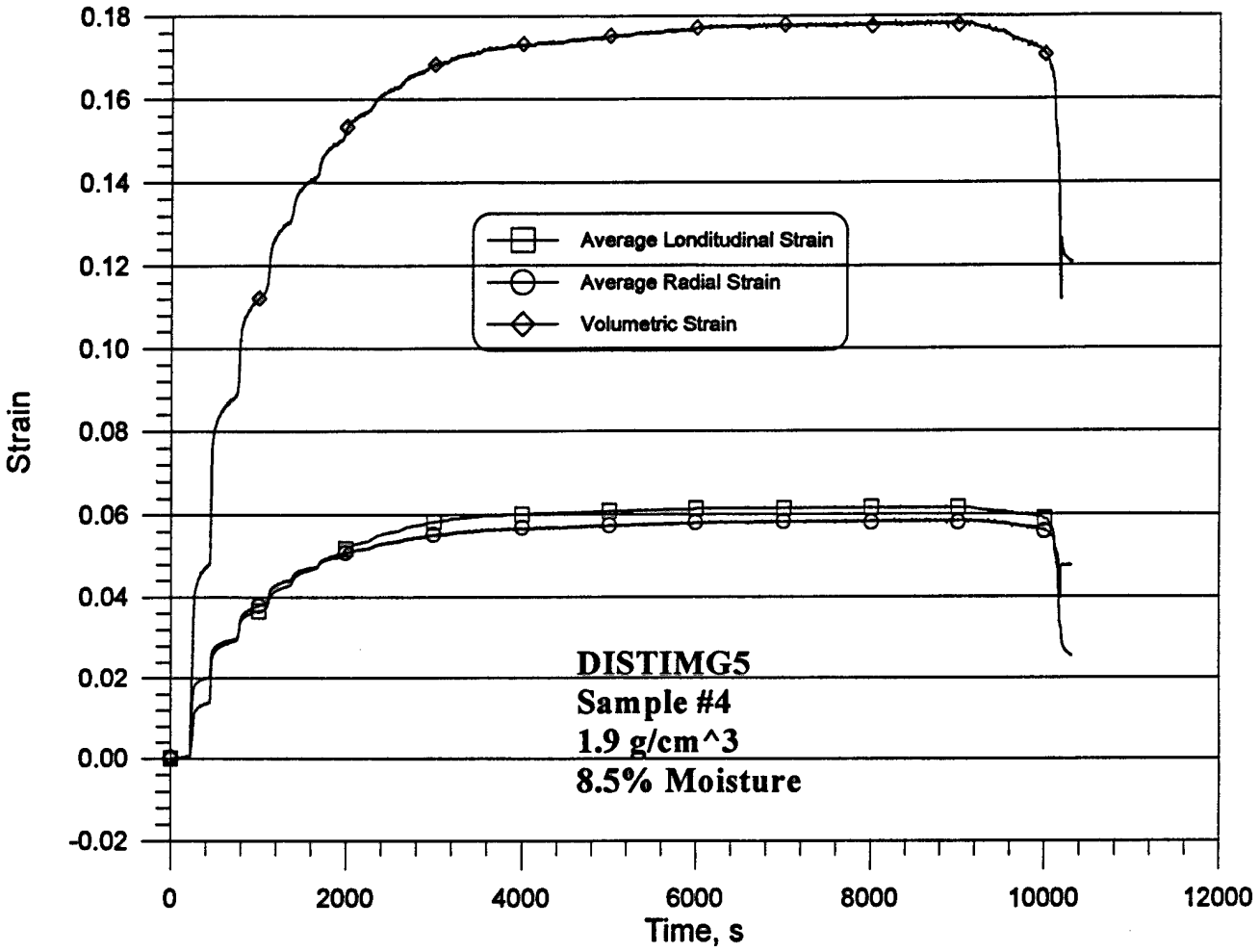

Figure B-29. Strain time histories for test DISTIMG5.

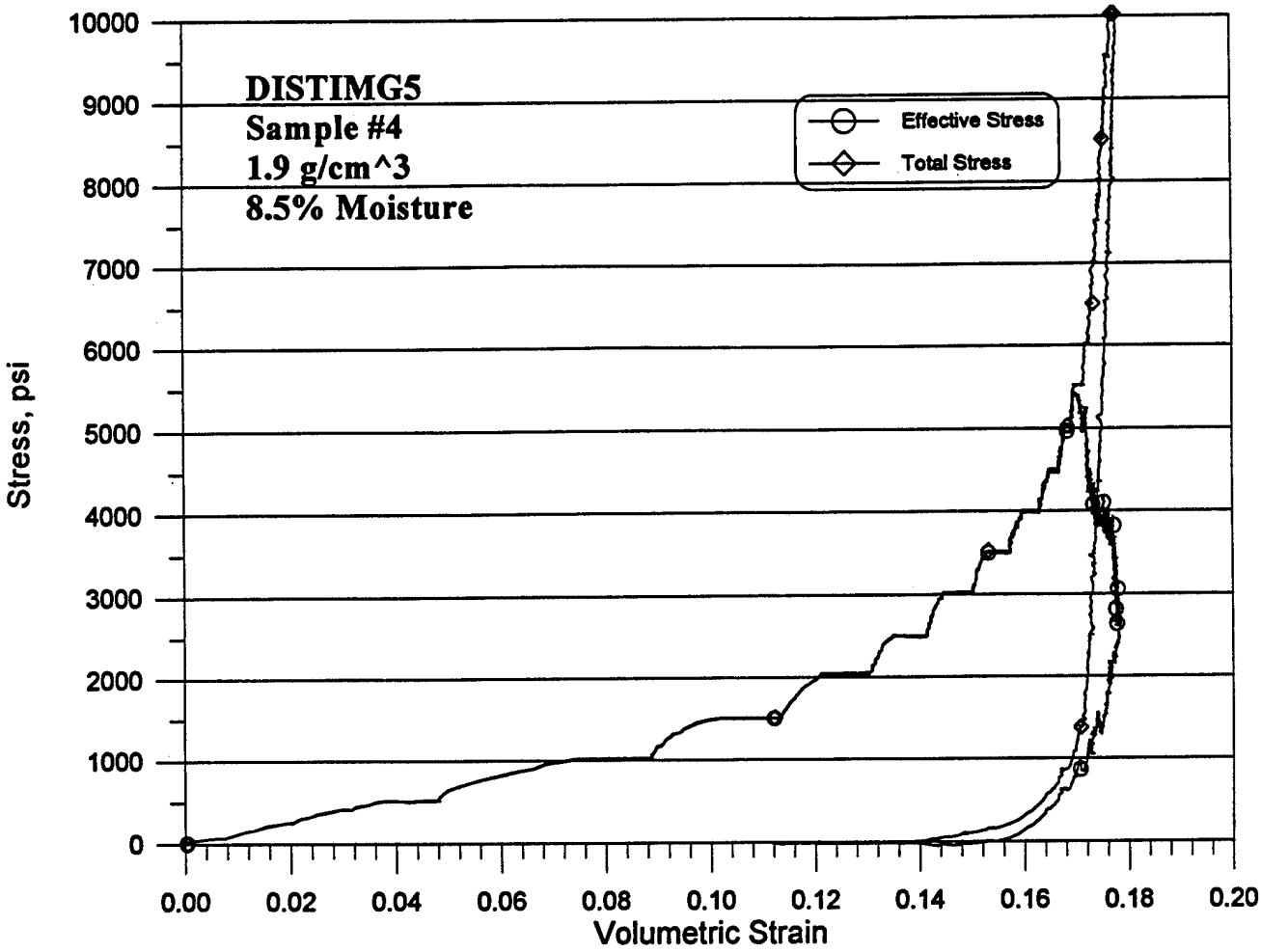

Figure B-30. Stress versus volumetric strain for test DISTIMG5.

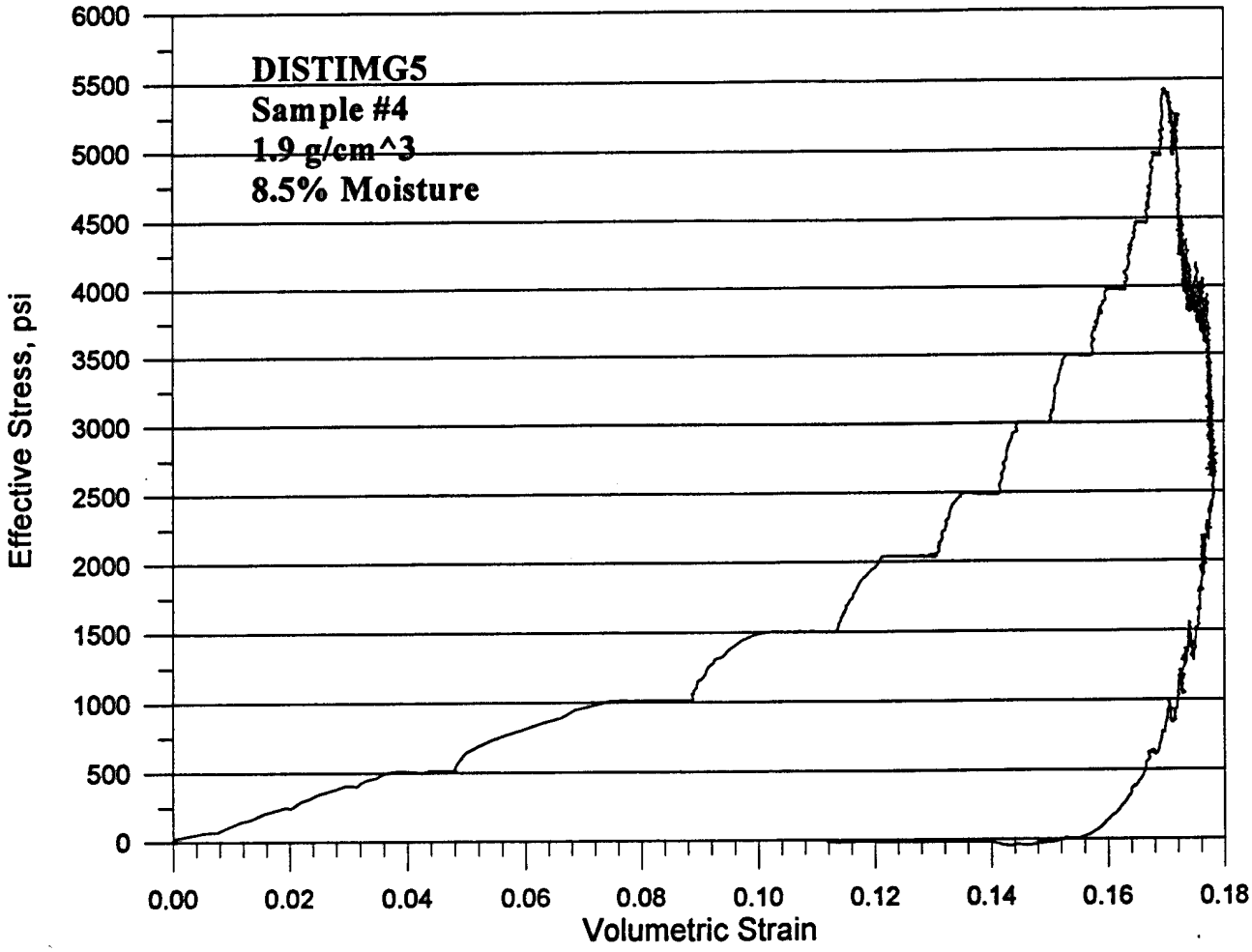

Figure B-31. Effective stress versus volumetric strain for test DISTIMG5.

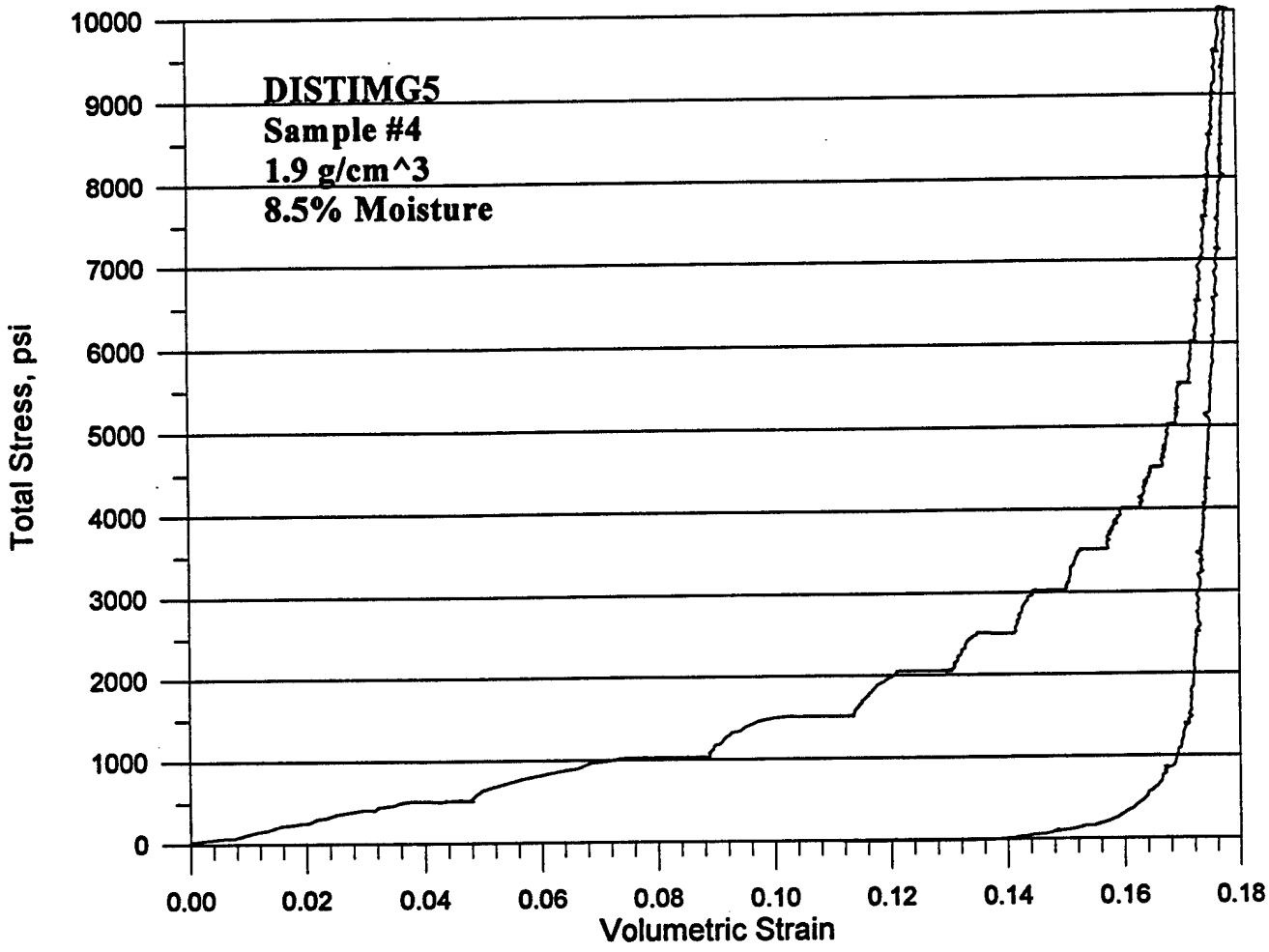

Figure B-32. Total stress versus volumetric strain for test DISTIMG5.

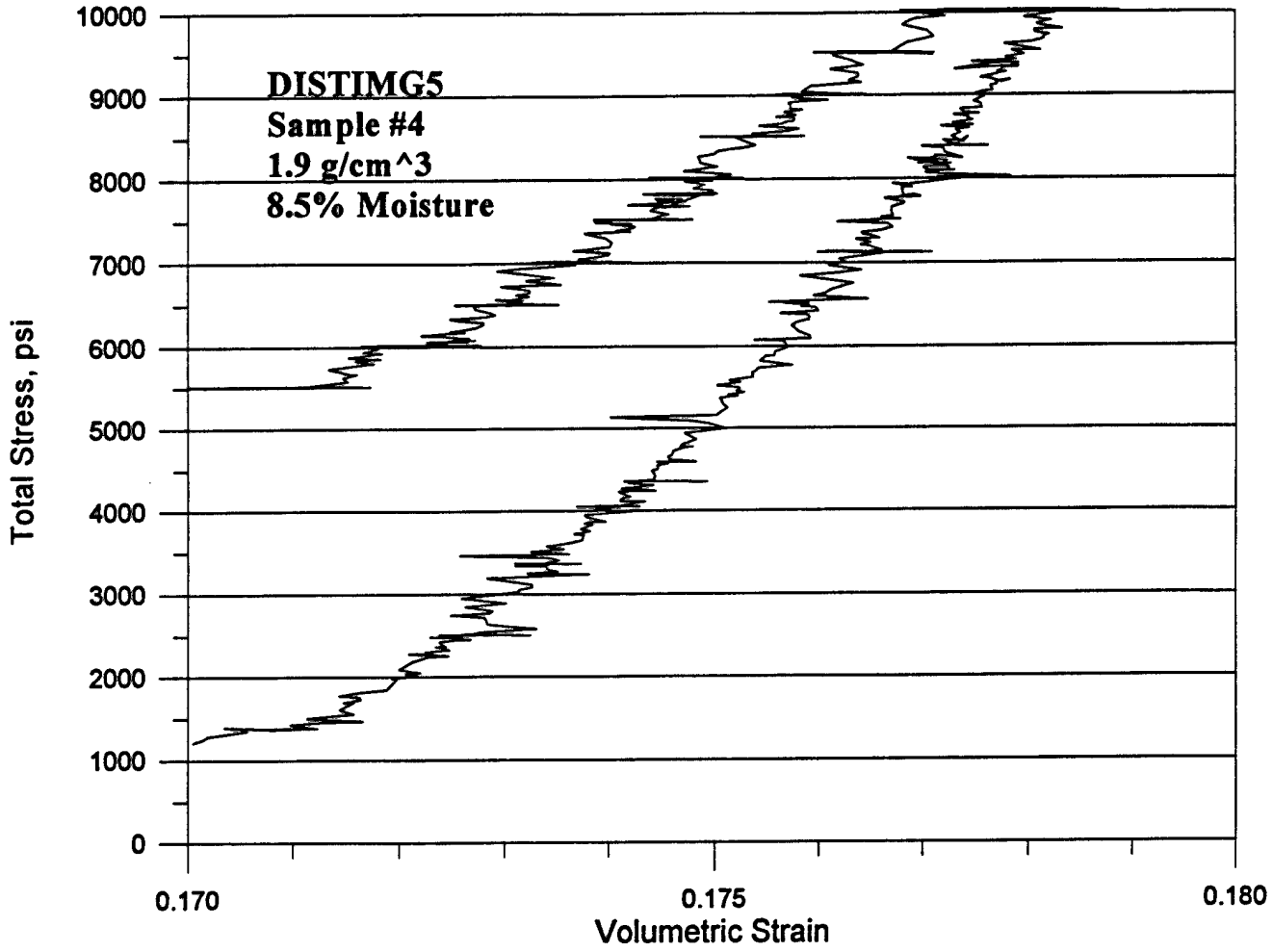

Figure B-33. Total stress versus volumetric strain for test DISTIMG4 (detail).

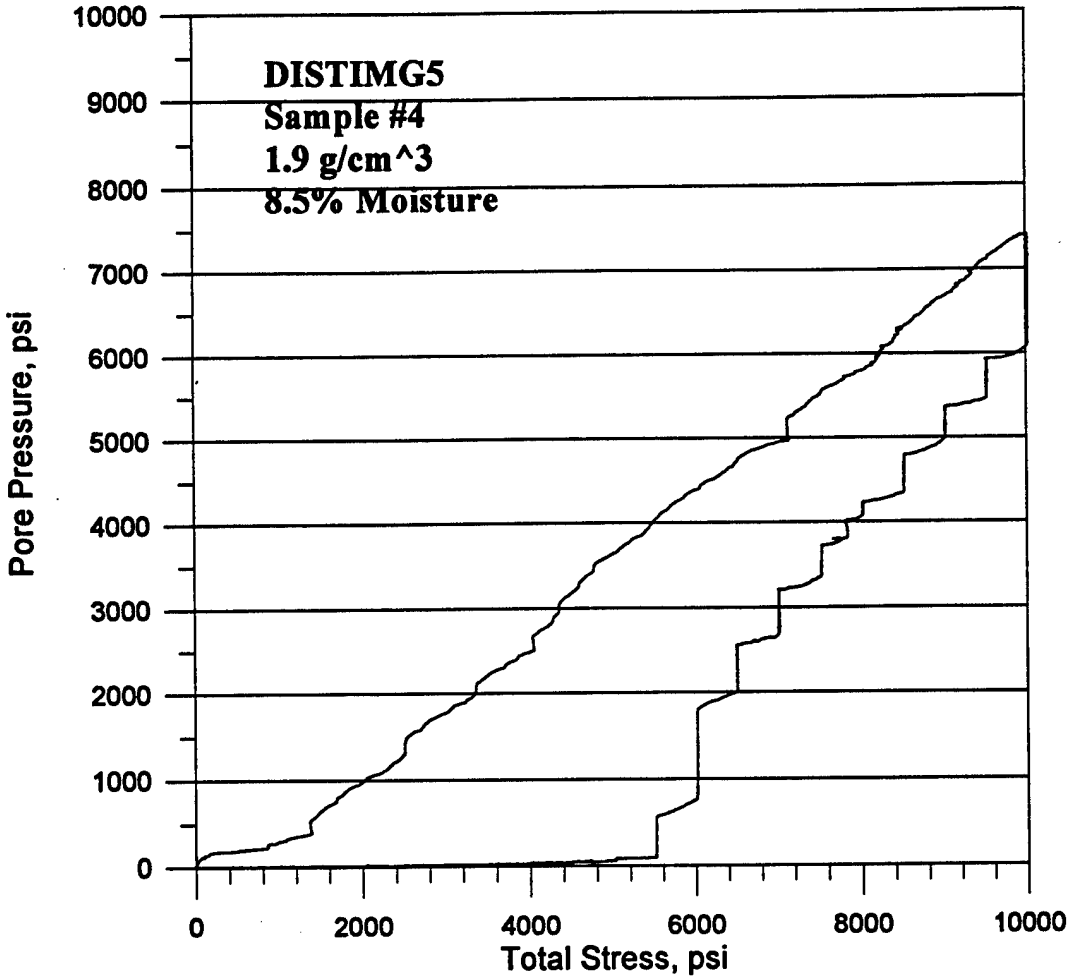

Figure B-34. Pore pressure versus total stress for test DISTIMG5.

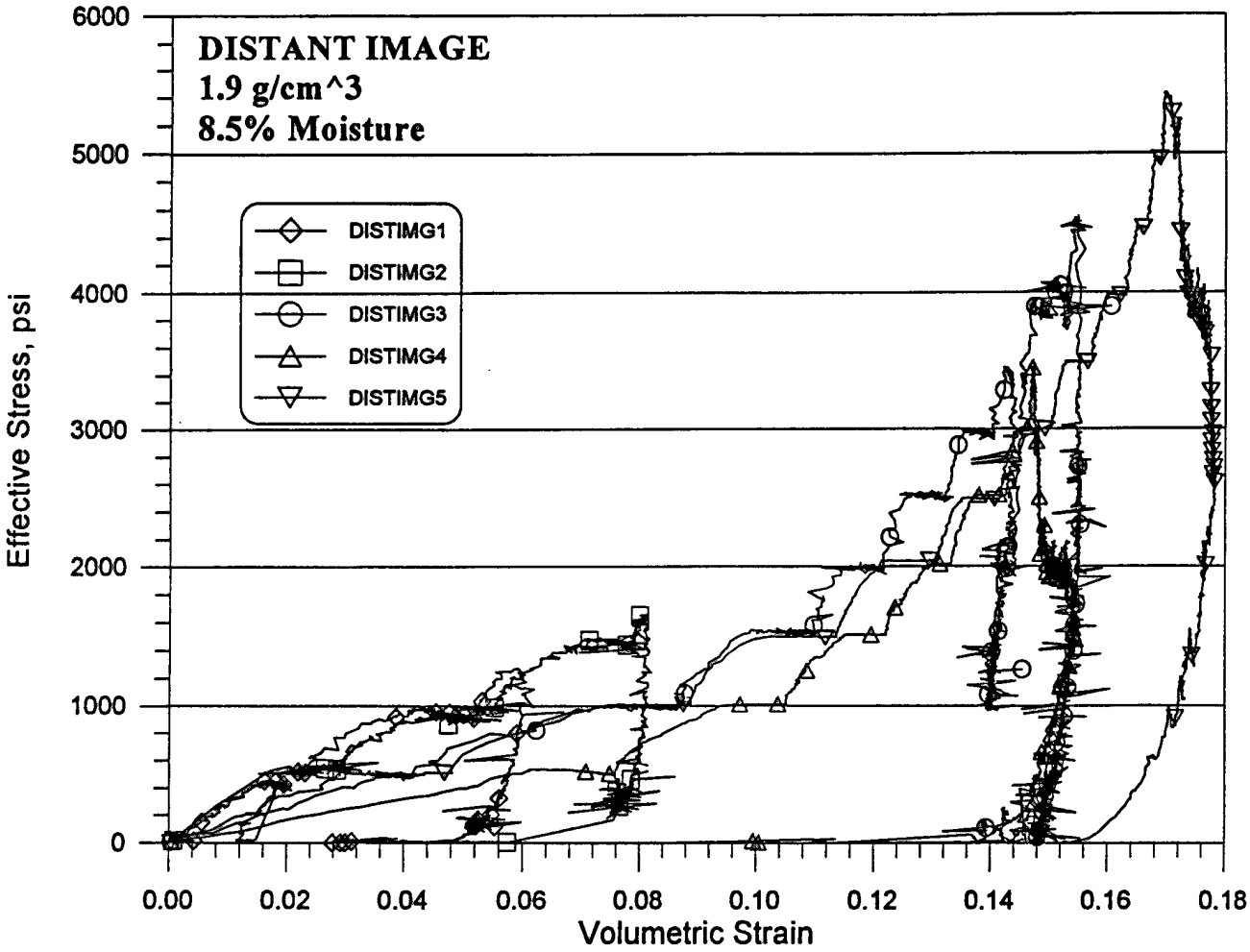

Figure B-35. Summary of effective stress versus volumetric strain for five tests.

$$S_{im} = 1 - 1/[49R + 1/(1 - S_i)] \quad (B.3)$$

where $R = P_{app}/P$, the ratio of the applied backpressure to the theoretical pressure of Equation B.2. For example, if a backpressure of 248 psia is applied for an initial saturation of 0.585, then the immediate degree of saturation would be 0.981 since R = 1.

Black and Lee (1973) also developed an empirical relation describing the time required for the diffusion of the pore gas into the pore water under a given backpressure. The time for 100 percent saturation in minutes is

$$t = \{[1 - S_{im}]/[K(1 + 49R(1 - S_{im}))]\}^{1/x} \quad (B.4)$$

where $K = 0.0094 - 0.01(S_{im})$ for $S_{im} < 0.8$, $K = 0.0014$ for $S_{im} > 0.8$, and $x = 0.085 + 0.133(S_{im})$. For the case of $S_{im} = 0.981$ and R = 1, 100 percent saturation is achieved after 8,515 minutes. A quasi-static loading was used for the test results reported herein (nominal 500 psi stress increments at five minute intervals). Saturation can only be achieved after the pore space collapses causing sufficient pressure to dissolve the pore gas phase.

For the DISTANT IMAGE explosive test event, the predicted pressures at the range from ground zero where the long range ejecta fragments originate were from 0.5 to 2.0 kbar. If one assumes that these pressures act throughout the porous soil medium (there is no membrane isolating the applied total stress from the pore fluid), then Equations B.2 through B.4 may be assumed valid. For the 0.5 kbar (7,250 psi) case, R = 29.3, and S_{im}=0.9993. This results in a time for total dissolution of the pore air of 103 ms. For the 2 kbar case, R = 116.9, S_{im} = 99,983, and the required time for saturation is 0.2 ms.

The above paragraph suggests that dissolution of the pore air occurs very quickly. It is important to bear in mind that the equations developed by Black and Lee (1973) were for more conventional geotechnical stress levels (on the order of 1 MPa) with corresponding times for saturation of minutes, hours, or even days. It also may be possible that if the pore gas goes into solution in such minimal time that it may very well come back out with comparable speed. Also, temperature effects may be important in such a blast environment.

In order to better comprehend this phenomena, it would be prudent to perform hydrostatic or uniaxial stress tests under dynamic loading conditions (to pressures of 0.5 to 4.0 kbar). Attempts should be made to measure the induced dynamic pore pressures in such a laboratory device. At such higher pressures, the importance of grain crushing could be observed and quantified. Equations similar to those developed by Black and Lee (1973) could be developed for rapid loading and unloading conditions.

DISTRIBUTION LIST

DNA-TR-94-83

DEPARTMENT OF DEFENSE

DEFENSE INTELLIGENCE AGENCY
ATTN: PGI-4

DEFENSE NUCLEAR AGENCY
ATTN: OPNA
ATTN: RAEM
ATTN: RAST W SUMMA
ATTN: SPWE LTC JIM HODGE
2 CY ATTN: SPWE LTC MARK BYERS
ATTN: SPWE MAJ DAVE MYERS
2 CY ATTN: SPWE E TREMBA
2 CY ATTN: SSTL

DEFENSE TECHNICAL INFORMATION CENTER
2 CY ATTN: DTIC/OC

FIELD COMMAND DEFENSE NUCLEAR AGENCY
ATTN: FCPR

DEPARTMENT OF THE ARMY

U S ARMY ATMOSPHERIC SCIENCES LAB
ATTN: SLCAS-AR-M

U S ARMY NUCLEAR & CHEMICAL AGENCY
ATTN: MONA-NU DR D BASH

U S ARMY TRAINING AND DOCTRINE COMD
ATTN: ATCD-N

US ARMY CHEMICAL SCHOOL
ATTN: ATZN-CM-CC-003

DEPARTMENT OF THE NAVY

NAVAL SURFACE WARFARE CENTER
ATTN: CODE H-21

DEPARTMENT OF THE AIR FORCE

AIR UNIVERSITY LIBRARY
ATTN: AUL-LSE

ASSISTANT CHIEF OF STAFF
ATTN: AFSAA/SAK

DEPARTMENT OF ENERGY

LAWRENCE LIVERMORE NATIONAL LAB
ATTN: TECH LIBRARY

LOS ALAMOS NATIONAL LABORATORY
ATTN: TECH LIBRARY

SANDIA NATIONAL LABORATORIES
ATTN: TECH LIB 3141

DEPARTMENT OF DEFENSE CONTRACTORS

HORIZONS TECHNOLOGY, INC
ATTN: B LEE

JAYCOR
2 CY ATTN: CYRUS P KNOWLES

KAMAN SCIENCES CORP
ATTN: D MOFFETT
ATTN: DASIAC

KAMAN SCIENCES CORPORATION
ATTN: DASIAC

S-CUBED
ATTN: J NORTHROP

SCIENCE & ENGRG ASSOCIATES, INC
2 CY ATTN: W R SEEBAUGH

SCIENCE APPLICATIONS INTL CORP
ATTN: E SWICK

SCIENCE APPLICATIONS INTL CORP
ATTN: J MCGAHAN